A rigorous analysis of cascaded step discontinuities in open waveguides

Chang, C. S.

Award date:
1993

Awarding institution:
University of Bath

A RIGOROUS ANALYSIS OF CASCADED STEP DISCONTINUITIES IN OPEN WAVEGUIDES.

Submitted by C.S.Chang, B.Eng.(Hons)
for the degree of
Doctor of Philosophy
of the University of Bath
1993

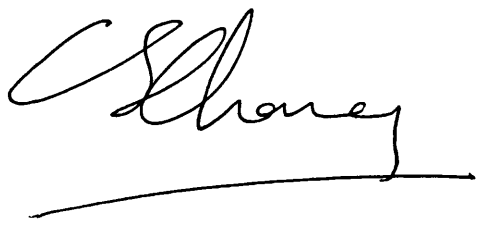

ProQuest LLC
789 East Eisenhower Parkway
P.O. Box 1346
Ann Arbor, MI 48106-1346

TO MY PARENTS

Abstract

The objective of this thesis is the development of a rigorous analytical technique for solving the problem of field scattering by cascaded step discontinuities. An improved Ritz-Galerkin variational technique based on the *Methods of moment* has been developed for this purpose. The development of this technique is done in three stages. Firstly the scattering formulation for a single step discontinuity is formally derived. The known effect of field singularity at the edges of the dielectric step for a TM polarised field is considered and solved. Convergence of the variational solution with different sets of expanding functions were investigated at this stage. Then the theory is extended to solve the problem of guided and radiation mode coupling caused by a second step in closed proximity to the first. This problem is solved by using an analogous network representation of the double step. Finally, the extension to the case of multiple cascaded steps is developed. By adopting a canonical form of representation for the transmission matrix of each cascaded step, it is shown that structures of finite and infinite extent can be analysed without the problem numerical ill-conditioning. The technique is then demonstrated by analysing two novel structures, namely a High Q bragg reflection grating resonator and a Log-Periodic grating filter.

This method shows very rapid convergence on it solutions and results obtained from it are in good agreement with some experimental measurements as well as with other published work.

Acknowledgements

First and foremost, I would like to express my sincere gratitude to Professor T Rozzi for his excellent supervision. Without his unstinting patience and expert guidance this work would not have been possible.

Thanks are also due to Dr.J Sarma and Dr.J.S Kot for many interesting and helpful discussions and Mr.D Hatten for his technical expertise and constant moral support and encouragement.

To all at the School Office, a special big thank you for all the support and help given to me all these years.

Finally I would like to thank the Universities of Bath and Liverpool for providing their financial support, facilities and resources needed for this work.

Contents

Chapter 1

Introduction

1.1 A brief History

The possibility of designing millimeter-wave systems using conventional printed-circuit technology was first investigated in the 1950's [1]-[4]. These new circuits offer the many attractive attributes of the conventional printed circuits, such as light weight, low cost, ease of manufacture, miniaturisation and the ability to design highly complex circuitry.

Unfortunately, developments during the early years were impeded by a lack of dielectric materials with good uniformity and low loss and also because practical sources of millimeter wave power were not available. Within the past decade, however, both sources and greatly improved materials have become readily available and have resulted in an intense revival in the field of microwave integrated circuits ; with the microstrip [3] being the favoured transmission structure. The principal advantages of the microstrip are that it can be easily manufactured with current technology and the design of microwave components [8] such as filters,

couplers, etc using microstrip is relatively easy.

However, there remains one main disadvantage with microstrip, and that is, that it is relatively lossy compared to hollow metallic guides. Generally the loss in dB/cm in microstrip is about ten times as high for an equivalent metallic waveguide operating at the same frequency [9]. Hence the Q obtainable from a microstrip circuit is generally low (500) at 90 GHz. Moreover, the increasing demand on tolerances in manufacture for frequencies above 20GHz have led many to consider alternative waveguide structures. Some of these alternative guides such as the H-guide, groove guide and dielectric image guide [4] are not new but were invented at about the same time that microstrip was, about 30 years ago. Other more recent guide structures such as the insular [7] and the inverted strip guide [10] are like the image guide - "open" type waveguides - i.e, they are unbounded in the plane transverse to the direction of propagation of the field. Both the insular and the inverted strip guide have low loss with loss comparable to that of hollow metallic waveguides. Conductor loss in these structures are reduced by concentrating the field in the low loss dielectric medium. In the case of the H-guide and groove guide, metal wall losses are reduced by having the modal electric field to be essentially parallel to the metal walls. With this arrangement, metal wall losses actually decreases as frequency is increased.

Besides being low loss, the open nature of various dielectric waveguides have a significant virtue in that fields are accessible externally. This makes them convenient for the introduction of attenuating or phase shifting media [29]. For instance thin film attenuators can be deposited or glued to the dielectric interface to give very effective attenuation with virtually no field perturbation. These forms of attenuators are extremely useful as end terminations.

The disadvantage of such open waveguides are also clear. Since the field is only loosely bound to most dielectric waveguides, sharp bends will radiate strongly and typical microwave configuration like T-junctions are not possible. In order to achieve small circuit dimensions and avoid radiation loss, dielectric waveguides are often made of alumina or semiconductor materials which have high dielectric constants (of the order of 10-15 or higher). This results in better field confinement, allowing guides to have tighter bends. Although the open nature of dielectric guides poses considerable problems when radiation loss is undesirable, they can be a considerable virtue when radiation is sought, such as in the design of low-cost frequency scanning antennas.

Some of the early passive dielectric waveguide components however tend to suffer from bandwidth limitations. An early example was the parallel waveguide directional coupler [30]. The parallel line couplers were narrow band because the coupling results from the interference of two waveguide modes propagating at different velocities. Another early design was the dielectric ring resonators. These filters have the obvious drawback that they must have very sizeable radii as compared to wavelength in order to reduce radiation. The advent of the non-radiative dielectric waveguide [30][31] seems to solve the problem of unwanted radiation. The non-radiative guides are essentially H-guides operated at below cut-off frequency of the parallel metal plates. Unfortunately this means they are bandwidth limited.

These problems are gradually being resolved and better designs have emerged. Recently, a parallel grating coupler [32] was proposed which is capable of broadband coupling. The same gratings can also be used to achieve broadband filters. Indeed a log-periodic grating has been proposed here for just such a purpose.

Another weighty issue was the mounting of active devices on dielectric waveguides. It has been difficult to mount an active device directly in the waveguide without causing conversion to higher order and radiation modes. But even in this area, progress have been made. Direct mounting of active devices in image waveguides has been demonstrated in a module consisting of an oscillator, modulator and detector [33]. A radial ring was thin film deposited on the top surface of the silicon image guide and a package diode was mounted in a hole in the dielectric image guide. Bias was supplied through a thin-film line also deposited on the guide.

However the development and design of microwave systems based on dielectric waveguides are still in its infancy. The requirements and complexity of any given system still do not permit the full realization of the potential circuit volume reduction due to dielectric waveguide circuit integration. In this respect, microstrip is still superior in terms of ease of active component integration and smaller cross-sectional dimensions.

As component development continues, the number of system types which can be covered will increase. At present the technique is most appropriately applied to systems having modest bandwidths. This is not a severe limitation since many of the systems in the sub-millimeter wavelength are of this type.

All in all, an accurate theoretical treatment and an understanding of the scattering properties of an abrupt discontinuity are essential for the proper design of complex dielectric waveguide components.

1.2 Objective of thesis

The electromagnetic field guided by an open dielectric waveguide structure is known to have a set of discrete modes and a continuous mode spectrum. Yet few techniques are known which take fully into account the contribution from the continuous mode spectrum in their treatment of the problem of abrupt discontinuities. Moreover, only Rozzi [11] and Shigesawa [27] have considered the field coupling or interaction caused by two discontinuities which are close together.

The aim of this thesis is to provide a rigorous analytical technique of general validity for solving the problem of arbitrarily large step discontinuities in planar open dielectric waveguides and to use this technique in the investigation of finite cascaded step structures. The technique is considered rigorous in that it provides a means of determining the appropriate solutions to arbitrarily defined precision. The problem of TE and TM mode scattering by an arbitrarily large step in both single and multimoded dielectric slab guides which may include loss in the material is first considered. Convergence and accuracy of the solutions are discussed and the results are compared with other published work and validated by means of experimental measurements whenever possible. The extension to the case of a double *interacting* step is then solved, and the limiting cases of coupling between two abruptly ended slabs are also resolved. Finally, the theory of the interacting double step is extended to treat the problem of finite cascaded steps which may be periodic or aperiodic in nature. Two novel structures, namely the High Q quarter wave transmission resonator, and a 20 element Log-Periodic filter are analysed using this technique. A detailed discussion of these structures will be given in Chapter 5. It is appropriate at this point to give a brief review of some of the analytical techniques that are available for solving discontinuity

problems.

1.3 Available analytical techniques

The exact solution of the discontinuity problem for open waveguides requires that the field contributions from a continuous spectrum of modes to be included. This results in highly complex spatial and spectral integrations for which exact analytical forms cannot be obtained. Consequently, previous investigations of the dielectric step discontinuity problem have been concerned with approximate solution techniques. All these techniques are limited in the scope of their applicability.

For the case of a small discontinuity between two monomode slabs, Marcuse [12] provided a very simple approximation to the solution by ignoring the backward radiation from the discontinuity.

Clarricoats and Sharpe [13] have provided an approximate solution for the case of a small step in a multi-moded guide by using a mode-matching technique. This technique was frequently employed for solving discontinuity problems in closed waveguides where the spectrum of the field is composed of discrete modes. For open waveguides however, a continuous spectrum of radiation modes is present and this method is strictly speaking, invalid. To take partial account of the continuum, they proposed analysing an alternate structure shown in Fig. 1b to that of the original discontinuity problem of Fig. 1a. The discontinuity in Fig. 1b is enclosed by an outer medium of finite transverse extent. The field is then expanded in terms of only the discrete modes of this new system, and the

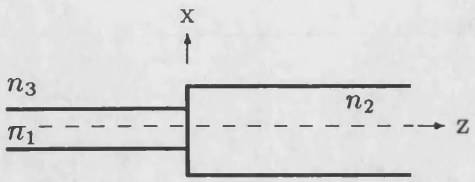

Fig 1.1a Abrupt step discontinuity.

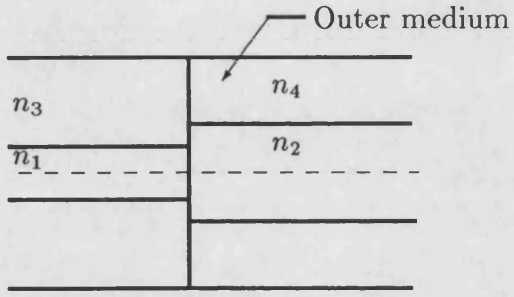

Fig 1.1b Abrupt discontinuity considered by [13,16]

discontinuity problem is solved by matching the discrete modes on either side of the junction. Radiation is assumed to be negligible and is neglected.

A more accurate method based on an integral equation formulation of the problem was later provided by Hockham and Sharpe [14]. Their method amounts to a first order variational solution which accounts exactly for the field to the right of the discontinuity (excitation from minus infinity) but only included the discrete modal fields to the left of it. The back reflected radiation modes are assumed to be negligible.

Recently more rigorous procedures have been developed to take better account of the continuous spectrum. A scheme to discretize the continuous spectrum by employing a complete set of Laguerre polynomials (defined in the interval $(0, \infty)$ was proposed by Mahmoud and Beal [15]. They pointed out that the set of expanding functions used need not be orthogonal, only to be complete. This discretization was performed in the spectral domain with the amplitude coefficient

of the continuous modes expanded into an infinite series. Errors lower than 3 percent was claimed by using just 2 or 3 terms of the series. However proper convergence was not demonstrated. Moreover it has been pointed out in [25] that the spectral profile of the continuum has a weak singularity at k_o (the free space wavenumber) which will adversely effect the accuracy of the approximation made by using a finite set of Laguerre functions. This difficulty could have been avoided (but was not) by the usual trigonometric variable transformation. More essential is a certain propensity of the technique to give relative convergence problem.

As an extension to the above method, Morishita and Inagaki [24] adopted a *Least Square Boundary Residual* matching of the fields at the discontinuity as opposed to the normal mode-matching. That is, instead of satisfying the condition

$$E^I = E^{II} \tag{1.1}$$

$$H^I = H^{II} \tag{1.2}$$

the minimum of

$$F = \frac{\int_s \left\{ \left| E^I - E^{II} \right|^2 + Z_o^2 \left| H^I - H^{II} \right|^2 \right\} ds}{\int_s \left\{ \left| e_{in} \right|^2 + Z_o^2 \left| h_{in} \right|^2 \right\} ds} \tag{1.3}$$

is sought. E^I *and* E^{II} being the total electric fields on either side of the discontinuity. H^I *and* H^{II} are the corresponding total magnetic fields. e_{in} *and* h_{in} are the incident electric and magnetic fields and Z_o is an arbitrary impedance parameter usually taken as the free space impedance. S is the discontinuity plane. For this added complexity, a faster and ensured convergence is achieved. The ensured convergence is a property of the least square matching method [26].

Alternatively, Brooke and Kharadly [16] proposed the introduction of a metallic enclosure to change the continuum of modes into an infinite series of discrete modes. They had argued that since the surface wave modes decay rapidly in the transverse direction away from the slab, the presence of a metallic wall placed far enough away from the slab should not effect the field appreciably. They had further shown that the functional form of the modes for the bounded configuration tends to that of the unbounded case as the metallic wall is moved to infinity. Normal mode matching is then used to solve the problem.

However numerical results obtained shows the scattered mode amplitudes to be highly dependent on the position of the metallic wall and a very slow rate of convergence (for increasing number of modes used) was achieved. In fact the scattered mode amplitudes were shown to vary sinusoidally with a slowly decaying amplitude about their true values as the metal wall is moved gradually away from the dielectric guides.

This has prompted them to suggest a *variable bound* approach where the scattering coefficients are calculated for a range of values of d (the distance of the metal wall from the guide). The range of d was arranged to be approximately equal to a period of the sinusoidal variation of the scattering parameters, and by simple averaging, the mean value (which may not be close to the true value) is obtained. More essentially, the inclusion of a metallic wall alters the boundary condition for radiation as discussed by Schevchenko [17] and Mittra and Lee [18]. Furthermore, the mode matching technique can lead to relative convergence difficulties [19-21]. This is a problem whereby the ratio of the number of modes used to represent the field on either side of a discontinuity is critical in determining the convergence of the results to the true solutions.

In this respect, techniques based on the integral equation approach such as [14] seems to be better suited to the problem. The continuous spectrum of modes can be taken into account quite naturally and there is no relative convergence difficulty. A rigorous technique based on the Ritz-Galerkin variational approach has been proposed by Rozzi [22]. A normalised set of optimally scaled Laguerre polynomials are used to discretize the modal fields in the spatial domain where the fields are well defined. For TE mode incidence at a step discontinuity, only 5 terms of the infinite Laguerre series are usually needed to obtain a solution with error of less than 1 percent.

However, convergence is slower with TM mode incidence. This results from the singular behaviour of the field at the dielectric corner of a step discontinuity as described by Meixner [23].

Another attractive method based on an iterative scheme was presented by Gelin et al [25]. In his method the modal fields are matched at the discontinuity in the usual way. Then by using the orthogonality of the modes the coefficient of the scattered modes of both sides of the discontinuity are obtained as two coupled integral equations. An approximate value for the transmission coefficient is then obtained by neglecting both the discrete reflected modes and the continuous radiation modes (Marcuse's method). This value is then used as the initial value for substituting into the coupled integral equations to start the iteration process. Again convergence was found to be slower for the TM modes incidence for the same reason as mentioned above.

With all the aforementioned difficulties in mind, an improved method based on the Ritz-Galerkin variational approach is developed. The effect of TM field sin-

gularity at the dielectric corner of the step discontinuity is included. The basic concept of this method will now be discussed in greater detail below.

1.4 The Ritz-Galerkin variational approach

It is possible, by matching the total electromagnetic field at the plane of a step discontinuity to form a Fredholm integral equation of the first kind. This may be written as

$$\int_0^\infty K(x,x')\ f(x')\ dx' \ = \ g(x) \tag{1.4}$$

where $K(x,x')$ is the kernel, $g(x)$ is the known excitation function, and $f(x')$ is the unknown function to be determined. As will be shown later in Chapter 2, the excitation function g(x) is actually the incident electric field, and the kernel K(x,x') is the *Green's impedance* function with $f(x')$ the unknown scattered magnetic field.

A general procedure for solving linear equations like Eq. (1.3) is by application of the *method of moments* [27]. It starts by expanding f in a series of functions $\{f_1, f_2, f_3, ...\}$ as

$$f \ = \ \sum_n \alpha_n f_n \tag{1.5}$$

where α_n are constants. The f_n are called *expansion functions* or *basis* functions. The summation of Eq. (1.5) is infinite for an exact representation of f and the f_n

form a complete set of basis functions. In practice however, a finite summation is used and the solution will be approximate. Substituting Eq. (1.5) into Eq. (1.4) and using the linearity of Eq. (1.4), one has

$$\sum_n \alpha_n \int_0^\infty K(x,x')f_n(x')dx' = g(x) \tag{1.6}$$

or symbolically,

$$\sum_n \alpha_n \langle K, f_n \rangle \;=\; g \tag{1.7}$$

with,

$$\langle K, f_n \rangle \;=\; \int_0^\infty K(x,x')f(x')dx' \tag{1.8}$$

Next, we take moments (ie. perform properly defined scalar products) of the functional equation (1.7) with another linearly independent set of functions $\{w_m, m = 1,2,3,.....\}$ known variously as *weighting functions* or *testing functions.* This process reduces the integral equation (1.6) to a linear system of algebraic equations given as

$$\sum_n \alpha_n \langle w_m, K, f_n \rangle = \langle w_m, g \rangle \tag{1.9}$$

This set of equations can be written in matrix form as

$$[k_{mn}][\alpha_n] \;=\; [g_m] \tag{1.10}$$

where

$$k_{mn} \;=\; \begin{bmatrix} w_1,K,f_1 & w_1,K,f_2 & \ldots\ldots \\ w_2,K,f_1 & w_2,K,f_2 & \ldots\ldots \\ \ldots\ldots & \ldots\ldots & \ldots\ldots \end{bmatrix} \tag{1.11}$$

$$\alpha_n = \begin{bmatrix} \alpha_1 \\ \alpha_2 \\ . \\ . \\ . \end{bmatrix} \qquad [g_m] = \begin{bmatrix} w_1, g \\ w_2, g \\ . \\ . \\ . \end{bmatrix} \tag{1.12}$$

If the matrix $[k_{mn}]$ is non-singular its inverse $[k_{mn}]^{-1}$ exist and α_n are then given by

$$[\alpha_n] = [k_{mn}]^{-1} [g_m] \tag{1.13}$$

The solution for f is then given by Eq. (1.5) as

$$f = [f_n] [\alpha_n] = [f_n] [k_{mn}]^{-1} [g_m] \tag{1.14}$$

The particular choice $w_n = f_n$ is known as *Galerkin's* or *Ritz-Galerkin* method. It can be shown that the application of the moments method to the integral equation (1.4) is equivalent to the Rayleigh-Ritz procedure [28] and hence the moments method may be viewed as a variational method.

References

[1] R.M.Barett,M.H Barnes,"Microwave printed circuits", presented at IRE National Conf, on Airborne Electrics, Dayton,OH, 1951

[2] R.M.Barett "Microwave printed circuits - A historical survey",IRE Trans Microwave Theory Tech, vol MTT-3 p1, Mar 1955

[3] D.D.Greig,H.F.Englemann,"Microstrip - A new transmission technique for the kilomegacycle L range",IRE Proc, vol 40, pp1644 , Dec 1952

[4] D.D.King,"Properties of dielectric image lines",IRE Trans. Microwave Theory Tech, vol MTT-3 p75, Mar 1955

[5] A.A.Oliner,"Equivalent circuits for discontinuities in balanced strip transmission lines",IRE Trans Microwave Theory Tech, vol MTT-3 p134, Mar 1955

[6] R.A.Pucel et al,"Losses in microstrip",IEEE MTT-S Transactions, vol MTT-16, June 1968

[7] W.V.McLevige,T.Itoh,R.Mittra,"New waveguide structures for millimeter-wave and optical integrated circuits",IEEE MTT-S Transaction vol MTT-23, Oct 1975

[8] J.A.Kostriza,"Microstrip components",Proc IRE vol 40 pp 1658-1663, Dec 1952

[9] R.M.Knox,"Dielectric waveguide Microwave Integrated Circuits - An Overview",IEEE Trans Microwave Theory Tech. vol MTT-24 Nov 1976

[10] R.Mittra,Y.L.Hou,V.Jamnejad,"Analysis of Open Dielectric Waveguides using Mode-Matching Technique and Variation Methods",IEEE Trans Microwave Theory Tech vol MTT-28 pp 36-43 Jan 1980

[11] T.E.Rozzi,G.H.In't Veld,"Field and network analysis of interacting step discontinuities in planar dielectric waveguides",IEEE Trans Microwave Theory Tech vol MTT-27 pp 303-309 Apr 1979

[12] D.Marcuse,"Radiation losses in tapered dielectric slab waveguides" Bell Syst Tech. J vol 49, pp 273-290 Feb 1970

[13] P.J.B.Clarricoats,A.B.Sharpe,"Modal matching applied to a discontinuity in a planar surface waveguide",Electronics Letters vol 8,pp 28-29, Jan 1972

[14] G.A.Hockham,A.B.Sharpe,"Dielectric waveguide discontinuities", Electronic Letters, vol 8 pp 230-231 May 1972

[15] S.Mahmoud,J.Beal,"Scattering of surface waves at a dielectric discontinuity on a planar waveguide", IEEE Trans. Microwave Theory Tech. vol MTT-23 pp 193-198, Feb 1975

[16] C.Brooke,M.Kharadly,"Step discontinuities on dielectric waveguides", Electronic Letters, vol 12, pp 471-473 Sep 1976

[17] V.Schevchenko,Continuous transitions in open waveguides, Golem Press, 1971

[18] R.Mittra,S.Lee,Analytical technique in the theory of guided waves, McMillan New York, 1971

[19] P.H.Masterman,P.J.Clarricoats,"Computer field matching solution of waveguide transverse discontinuities", Proc IEE , pp 51-63, 1971

[20] S.W.Lee,W.R.Jones,J.J.Campbell,"Convergence of numerical solutions of iris-type discontinuity problems", IEEE Trans. Microwave Theory Tech. MTT-19, pp 528-536 1971

[21] G.H.Brooke,W.K.McRitchie,"Effect of dielectric edge conditions on mode-matching conditions", Electronics Letters, pp 422-423, Aug 1975

[22] T.E.Rozzi,"Rigorous analysis of the step discontinuity in a planar dielectric waveguide", IEEE Trans Microwave Theory Tech. vol MTT-26, pp 738-746, Oct 1978

[23] J.Miexner,"The behaviour of electromagnetic fields at edges", IEEE Trans Antenna Propagation vol AP-20 pp 442-446, July 1972

[24] K.Morishita,S.Inagaki,N.Kumagai,"Analysis of discontinuities in dielectric waveguides by means of the least squares boundary residual method", IEEE Trans Microwave Theory Tech, vol MTT-27, pp 310-315, Apr 1979

[25] P.Gelin,M.Petenzi,J.Citerne,"Rigorous analysis of the scattering of surface waves in an abruptly ended slab dielectric waveguide", IEEE Trans. Microwave Theory Tech. vol MTT-28, pp 61-73 Feb 1981

[26] J.B.Davies,"A least-squares boundary residual method for the numerical solution of scattering problems", IEEE Trans Microwave Theory Tech, vol MTT-21 pp 99, Feb 1973

[27] L.Kontorovich,G.Krilov,"Functional Analysis in Normed Spaces", D.E.BROWN, trans. Oxford: Pergamon, 1964 pp 586-587

[28] R.Mittra (ed.),Computer Techniques for Electromagnetics, Oxford: Pergamon, 1973

[29] B.J.Levin,G.G.Weidner," A distributed PIN diode phaser for millimeter wavelengths",IEEE International Microwave symposium, Boulder, CO, June 1973.

[30] T.Yoneyama,S.Nishida,"Non-radiative dielectric waveguide for millimeter-wave integrated circuits",IEEE Trans. Microwave Theory Tech, vol. MTT-29, pp 1188-1192, Nov 1981

[31] T.Yoneyama,M.Yamaguchi,S.Nishida,"Bends in non-radiative dielectric waveguides", IEEE Trans. Microwave Theory Tech., vol MTT-30, pp 2146-2150 Dec 1982.

[32] G.L.Matthaei,D.C.Park,Y.M.Kim,D.L.Johnson,"A study of the filter properties of single and parallel-coupled dielectric waveguide gratings", IEEE Trans. Microwave Theory Tech., vol MTT-31, no.10, Oct 1983

[33] M.M.Chrepta,H.Jacobs,"Millimeter-wave integrated circuits", Microwave Journal, vol 17, Nov 1974

[34] H.Shigesawa,M.Tsuji,"A completely theoretical design method of dielectric image guide gratings in the Bragg Reflection region.", IEEE Trans, MTT, vol MTT-34, No 4, April 1986. pp 420-426

Chapter 2

Mode functions in Open Waveguides

2.1 Introduction

By open slab waveguides we shall mean structures of the type shown in Fig 2.1, which is unbounded in the x-direction and is homogeneous in the y-direction.

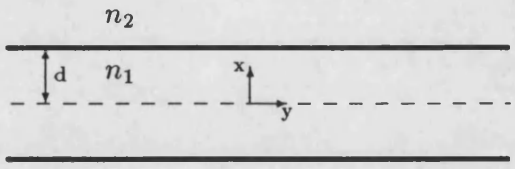

Fig 2.1 Open slab guide

The geometry of this structure (Fig 2.1) is separable and allows us to reduce the general wave equation

$$\nabla^2\psi + k^2\psi = 0 \tag{2.1}$$

to a problem of the Sturm-Liouville type [1] :

$$\left[\frac{d}{dx}\,p(x)\frac{d}{dx} - q(x) + \lambda w(x)\right]\ \psi(x)\ =\ 0 \tag{2.2}$$

The solutions of the above equation possess orthogonality and completeness properties that permit an arbitrary electric field to be represented by their superpositions [12,13]. Such solutions are termed the characteristic or eigen-solutions of the guide and they individually satisfy the field equations plus the appropriate boundary conditions.

It is generally well known that in order to construct a complete set of eigenmodes or eigen-solutions for an open waveguide, the boundary condition at infinity must be relaxed. This means that instead of the normal requirement that the field should tend to zero at infinity, a weaker condition that the field only be finite at infinity is imposed [2]. The system of eigenmodes thus derived proves to be complete and suitable for the representation of any physically realizable field in an open waveguide. The complete set of the above mentioned eigenmodes will consist of a finite number of discrete modes together with a continuous spectrum of modes.

The discrete modes are termed *proper modes* because they decay exponentially away from the guide and is zero at infinity. In contrast, the continuous modes do not individually decay to zero at infinity but remain finite. This behaviour is possible only because such modes never occur individually but always as a continuum and are defined in an integral.

The superpositions of these modes will cancel each other in such a way that the

TABLE 2.1
Transverse propagation characteristics of various modes

$e^{-\gamma x}$	discrete mode	modal solution
$e^{-j\rho' x}$	continuum mode	
$e^{\rho'' x}\ e^{-j\rho' x}$	leaky wave	non-modal solution

integral expressing them satisfy the radiation condition at infinity (ie. the field at infinity consist of outgoing waves only). Although the discrete and continuous modes together form a complete set of modal functions capable of representing an arbitrary source-free field in the system of Fig 2.1, there may also exist non-modal solutions which in distinction to the above mentioned modes grows exponentially (in the x-direction) away from the guide. Where they may not be true solutions of Eq. (2.1) in the sense that they do not satisfy the required boundary condition at infinity, they nevertheless have a physical interpretation.

These non-modal solutions or *improper modes* possess propagation constants which are complex, as opposed to those of the modal solutions which are either purely imaginary (for surface modes) or purely real (for radiation modes) for a lossless system. Their different characteristics are listed in Table 2.1 for easy comparison. We may describe these non-modal solutions by the field intensity pattern shown in Fig 2.2. In the figure, the closer the lines, the greater is the intensity. The direction of power flow is not along the guide but at an angle from it. (A consequence of the complex transverse propagation constant.) It is clear then that the exponential growth of the non-modal field in the x-direction is only a manifestation of the direction of real power flow. Since the field is constantly leaking out of the guide, it rapidly diminishes in magnitude as it travels along in the guide. Hence the term *leaky-wave.*

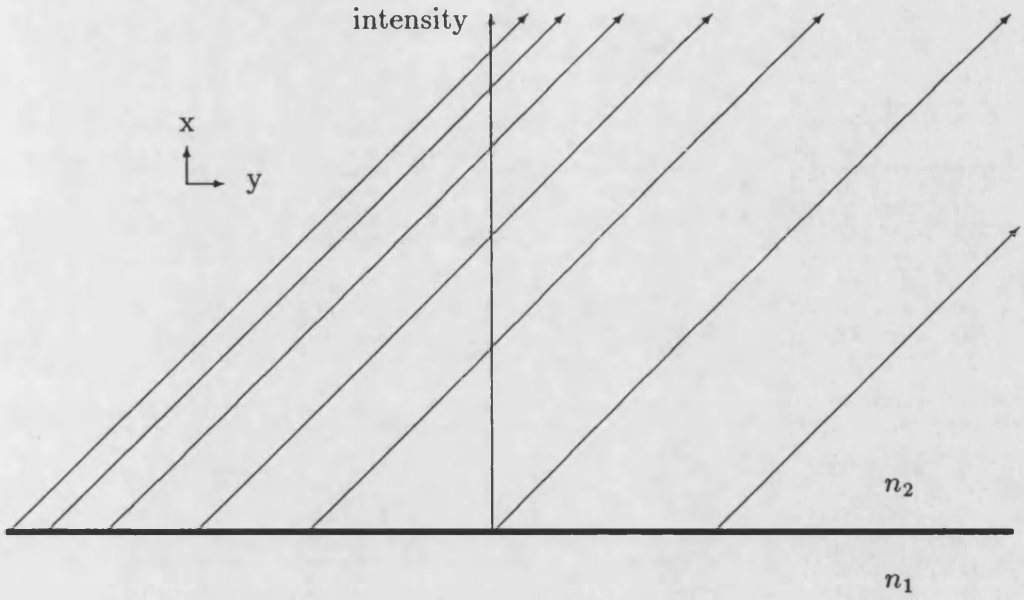

Fig 2.2 Leaky modes intensity pattern

As is indicated in Fig 2.2 these leaky-waves exist only in an angular region above the dielectric interface so that the boundary condition at infinity is irrelevant to its description.

It is noted that since these waves have a real power flow away from the guide, they could help in describing qualitatively the radiation fields caused by waveguide discontinuities.

Their contribution to the radiation field is sometimes encountered when using a steepest descent representation [4,5], which is used later in Chapter 3 to calculated the radiation pattern from a single step discontinuity.

A comprehensive discussion on leaky-waves or complex waves may be found in [2-5]. The conventional method of deriving the transverse modal function of a

slab guide involves solving the one dimensional wave equation which results in solutions of exponential form containing arbitrary constants. These arbitrary constants are related by the requirement of field continuity at the dielectric interface. Their values may then be specified by requiring the eigen-solutions to be ortho-normalised, i.e,

$$\int_0^\infty \frac{1}{w(x)} U_m(x)\, U_n(x)\, dx = \begin{cases} 1 & if \;\; m = n \\ 0 & if \;\; m \neq n \end{cases} \tag{2.3a}$$

$$\int_0^\infty \frac{1}{w(x)} \psi(x,\rho)\, \psi(x,\rho')\, dx = \delta(\rho - \rho') \tag{2.3b}$$

$$w = \begin{cases} 1 & for\ TE\ case \\ \varepsilon(x) & for\ TM\ case \end{cases}$$

where $U_p(x)$, $p = m, n$ are the discrete surface modes and $\psi(x,\rho)$ the continuous radiation modes. Normalisation by direct integration involves a considerable amount of effort and the rigorous evaluation of Eq. (2.3b) is formidable as the modal functions of the continuum are finite at infinity. These difficulties are avoided by following a procedure developed by Marcuvitz [10]. His method of construction employs the so called characteristic Green's functions. The advantage of his method over the conventional method is that the eigenmodes that are derived are automatically ortho-normalised. The great efficiency of this method when used to find the eigenmodes of general multilayer slabs will also be evident. Briefly, the above mentioned method involves establishing a relationship between the poles of the Green's function expressed in terms of two independent solutions of the homogeneous Sturm-Liouville differential equation and the poles of the eigenfunction expansion of the same Green's function.

These eigenfunctions are by their definition ortho-normal. When the two independent solutions are subsequently found, the ortho-normal eigenfunctions are easily obtain from the relationship by direct comparison. A general discussion of

this method may be found in [1,pp 832].

2.2 Eigenfunction representation of the Green's function

As mentioned earlier, the determination of the eigenfunctions f_m and the eigenvalues λ_m in the domain $x_1 \leq x \leq x_2$ poses a problem of the Sturm-Liouville type:

$$\left[\frac{d}{dx}p(x)\frac{d}{dx} - q(x) + \lambda_m w(x)\right] f_m(x) = 0, \qquad x_1 \leq x \leq x_2 \tag{2.4}$$

subject to the homogeneous boundary conditions

$$\left(p\frac{d}{dx} + \alpha_{1,2}\right) f_m(x) = 0 \quad at \; x = x_{1,2} \tag{2.5}$$

Note that this boundary condition is equivalent to the specification of the "impedance" at $x = x_{1,2}$ as it requires the ratio of the slope of the function to its value to be a constant at the boundary.(Refer to Eq. (2.29)) It can be shown [12,13] that the set of eigenfunctions f_m comprising all possible solutions of Eq. (2.4) constitutes a complete set and can be employed to represent any piecewise continuous functions F(x) in the interval $x_1 \leq x \leq x_2$ ie.

$$F(x) = \sum_m F_m f_m(x) \tag{2.6}$$

where the sum extends over all eigenfunctions. Furthermore, they have orthogonality properties with respect to the weight factor w such that

$$\int_{x_1}^{x_2} dx \; w f_m f_n = 0 \qquad m \neq n \tag{2.7}$$

and may be normalised to unity by the requirement that

$$\int_{x_1}^{x_2} dx\ w f_m^2 \ = \ 1 \tag{2.8}$$

The completeness and orthonormality of the set f_m can be expressed concisely in a symbolic manner by choosing F(x) the delta function $\delta(x - x')$. Then

$$F_m \ = \ \int_{x_1}^{x_2} dx\, w(x)\delta(x - x') f_m(x) \ = \ w(x')\, f_m(x') \tag{2.9}$$

so that from Eq. (2.6) one infers the completeness relation

$$\frac{\delta(x - x')}{w(x')} \ = \ \sum_m f_m(x) f_m(x') \qquad x_1 \leq \begin{matrix} x \\ x' \end{matrix} \leq x_2 \tag{2.10}$$

Now consider a characteristic Green's function $g(x, x', \lambda)$ satisfying the inhomogeneous Sturm-Liouville differential equation

$$\left[\frac{d}{dx} p(x) \frac{d}{dx} \ - \ q(x) \ + \ \lambda w(x)\right] \ g(x, x', \lambda) \ = \ -\delta(x - x') \tag{2.11}$$

satisfying the homogeneous boundary condition

$$(p\frac{d}{dx} \ + \ \alpha_{1,2})\ g(x, x', \lambda) \ = \ 0 \tag{2.12}$$

To relate the complete eigenmode set to the characteristic Green's function, we write

$$g(x, x', \lambda) \ = \ \sum_m g_m(x', \lambda)\, f_m(x), \qquad x_1 \leq x \leq x_2 \tag{2.13}$$

where

$$g_m(x', \lambda) \ = \ \int_{x_1}^{x_2} w(x)\, f_m(x)\, g(x, x', \lambda)\ dx \tag{2.14}$$

Upon substituting Eq. (2.13) into Eq. (2.11) and employing the delta representation of Eq. (2.10), one obtains

$$g_m(x', \lambda) \ = \ -\frac{f_m(x)}{\lambda \ - \ \lambda_m} \tag{2.15}$$

so from Eq. (2.13), we get

$$g(x, x', \lambda) \ = \ -\sum_m \frac{f_m(x) f_m(x)}{\lambda \ - \ \lambda_m} \tag{2.16}$$

Eq. (2.16) shows up clearly the pole singularities of $g(x, x', \lambda)$ in the complex λ plane at the eigenvalues λ_m. If Eq. (2.16) is now integrated in the complex λ plane, about a contour C, enclosing all singularities of $g(x, x', \lambda)$, then by Cauchy's Residue theorem,

$$-\frac{1}{2\pi j}\oint_C g(x,x',\lambda)\,d\lambda = -\sum_m f_m(x)f_m(x')\left(-\frac{1}{2\pi j}\right)\oint_C \frac{d\lambda}{\lambda-\lambda_m} \qquad (2.17)$$

$$= \sum_m f_m(x)f_m(x') = \frac{\delta(x-x')}{w(x')}$$

It will be evident later that the Green's function problem of Eq. (2.11) is equivalent to the problem of a point source excitation of a terminated transmission line which in turn is a representation of the guided wave problem of Fig 2.1. The solution of the transmission line problem is easily obtainable in network terms and Eq. (2.17) will provide us the useful relationship to the "modal" eigenfunctions of the guided waves.

2.3 Transmission line equations. (A Guided-wave representation in space)

The reduction of the general field equation to the one-dimensional transmission line equation represents an important step in our treatment of the problem. The scalarization permits a transmission-line analysis of the structure of Fig 2.1 along one of its transverse coordinates (the x-direction in this case). As is customary, the field is considered to have a time harmonic dependence of $e^{i\omega t}$. This will allow any time varying fields to be reconstructed in the sense of a Fourier series. Maxwell's equations are then

$$\begin{aligned} \nabla \times \mathbf{E} &= -j\omega\mu\mathbf{H} \\ \nabla \times \mathbf{H} &= j\omega\epsilon\mathbf{E} \end{aligned} \qquad (2.18)$$

For a wave travelling in the z-direction, we assume the fields to be of the form

$$\begin{aligned} \mathbf{E}(x,y,z,t) &= \mathbf{E}(x,y)\, e^{j\omega t-\gamma_z z} \\ \mathbf{H}(x,y,z,t) &= \mathbf{H}(x,y)\, e^{j\omega t-\gamma_z z} \end{aligned} \tag{2.19}$$

where $\gamma_z = \alpha + j\beta$ is the propagation constant of the guide (Fig 2.1) in the z-direction. Eq. (2.18) may then be expanded in separable form as

$$\nabla \times \mathbf{E} = -j\omega\mu\mathbf{H} \begin{cases} \dfrac{\partial E_z}{\partial y} + \gamma_z E_y = -j\omega\mu H_x \\ -\gamma_z E_x - \dfrac{\partial E_z}{\partial x} = -j\omega\mu H_y \\ \dfrac{\partial E_y}{\partial x} - \dfrac{\partial E_x}{\partial y} = -j\omega\mu H_z \end{cases} \tag{2.20a}$$

$$\nabla \times \mathbf{H} = j\omega\epsilon\mathbf{E} \begin{cases} \dfrac{\partial H_z}{\partial y} + \gamma_z E_y = j\omega\epsilon E_x \\ -\gamma_z H_x - \dfrac{\partial H_z}{\partial x} = j\omega\epsilon E_y \\ \dfrac{\partial H_y}{\partial x} - \dfrac{\partial H_x}{\partial y} = j\omega\epsilon E_z \end{cases} \tag{2.20b}$$

where μ is the permeability (H/m) and ϵ is the permittivity (F/m) and both may be arbitrary functions of x at this point. The factor $e^{j\omega t}$ will be understood to be present, but will not be shown for the sake of brevity.

It is clear from Eq. (2.20) that E_z and H_z are independent of each other and that the field equation describe two independent *modes*. $E_z = 0$ for a TE (Transverse Electric) mode and $H_z = 0$ for a TM (Transverse Magnetic) mode. As a further simplification, consider the guide of Fig 2.1 to be homogeneous in the y-direction, ie.

$$\frac{\partial}{\partial y} = 0$$

Using the above condition on Eq. (2.20) gives,

TE mode ($E_z = 0$)

$$\gamma_z E_y = -j\omega\mu H_x \tag{2.21a}$$

$$\frac{dE_y}{dx} = -j\omega\mu H_z \tag{2.21b}$$

$$\frac{dH_z}{dx} = \left(\frac{\gamma_z^2}{j\omega\mu} - j\omega\epsilon\right) E_y \tag{2.21c}$$

TM mode ($H_z = 0$)

$$\gamma_z H_y = j\omega\epsilon E_x \tag{2.22a}$$

$$\frac{dH_y}{dx} = j\omega\epsilon E_z \tag{2.22b}$$

$$\frac{dE_z}{dx} = \left(-\frac{\gamma_z}{j\omega\epsilon} + j\omega\mu\right) H_y \tag{2.22c}$$

Eqs. (2.21b),(2.21c) and Eqs. (2.22b),(2.22c) are recognise as the transmission line equations for the TE and TM mode respectively. More appropriately, for both the TM and TE modes, we write

$$-\frac{dV(x)}{dx} = jk_x Z(x)\, I(x) \tag{2.23}$$

$$-\frac{dI(x)}{dx} = jk_x Y(x)\, V(x), \qquad Y(x) = \frac{1}{Z}(x)$$

where

$$Z(x) = \frac{\omega\mu}{k_x} \qquad for\ TE$$

$$= -\frac{k_x}{\omega\epsilon} \qquad for\ TM$$

and $k_x^2 = \omega^2\mu\epsilon + \gamma_z$ is the propagation constant in the x direction. V(x) and I(x) are the equivalent voltage and current functions of the corresponding electric and magnetic fields respectively. The Sturm-Liouville differential form are then obtain from Eq. (2.23) as

$$\left\{\frac{d}{dx}\frac{1}{k_xZ}\frac{d}{dx} + k_xY\right\}V(x) = 0 \tag{2.24}$$

$$\left\{\frac{d}{dx}\frac{1}{k_xY}\frac{d}{dx} + k_xZ\right\}I(x) = 0$$

The solutions to Eq. (2.24) for the homogeneous case when both ϵ and μ are constant are easily obtainable and may be written as

$$\begin{aligned} V(x) &= V(x')\left[\cos k_x(x-x') - jY'(x')\sin k_x(x-x')\right] \\ I(x) &= I(x')\left[\cos k_x(x-x') - jZ'(x')\sin k_x(x-x')\right] \end{aligned} \tag{2.25}$$

where we define $Z'(x) = \frac{1}{Y'(x)} = \frac{V(x)}{ZI(x)}$ as the normalised impedance with Z (the characteristic impedance of the transmission line) as given in Eq. (2.23). $V(x')$ and $I(x')$ are arbitrary equivalent voltage and current values at the arbitrary point x' on the transmission line. The present problem (Fig 2.3) involves regions filled with different media (ie. involving different ϵ) ; therefore Eq. (2.24) must be considered for each region separately. The boundary conditions will then be applied to the solutions (of Eq. (2.25)) for each region to resolve the arbitrary constants $V(x')$ and $I(x')$. This represents the conventional and direct method of solution discussed earlier which can be found elsewhere [14,15] and so will not be discussed further.

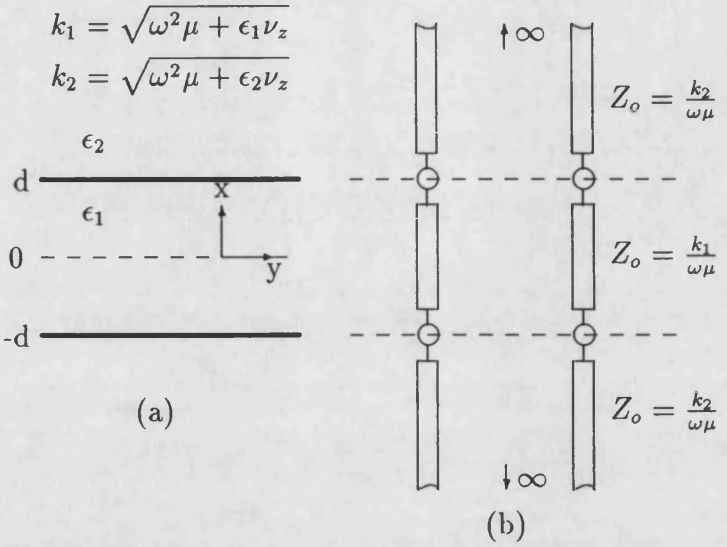

Fig 2.3 Equivalent transmission line model of a transversely viewed dielectric waveguide.

2.4 Equivalent network of the Green's function problem

As noted in Sec 2.3, the electromagnetic field solutions for a variety of closed and open stratified regions can be constructed via a guided-wave representation along a preferred z-direction. Such representations are predicated upon the separable cross-sections transverse to z. The subsequent derivation of the transmission line equations enable us to analyse the guided-wave problem in network terms. This method of solution is known as the *transverse resonance* technique. A network representation of the characteristic Green's function of Eq.(2.11) is shown in Fig 2.4(a). The voltage and current on this transmission line satisfy the non-uniform (in the x-direction) transmission line equations (2.23) with the addition of a current source term $i(x') = -\delta(x - x')$:

$$-\frac{dV(x,x')}{dx} = j\,k_x Z(x)\,I(x,x') \tag{2.26}$$

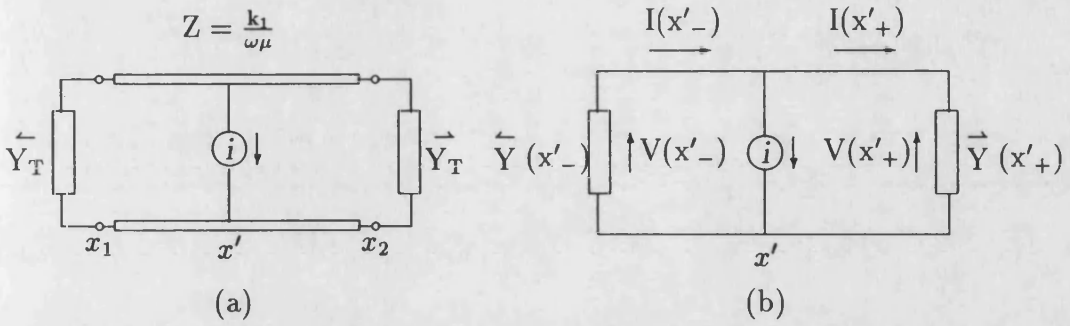

Fig 2.4 (a) Transmission line with current point source excitation
(b) and its Thevenin's equivalent

$$-\frac{dI(x,x')}{dx} = j\,k_x Y(x)\,V(x,x') - \delta(x-x')$$

For a propagating TE mode with $k_x\,Z(x) = \omega\mu(x)$, the corresponding second-order differential equation for $V(x,x')$ has the form: [See Eq. (2.24)]

$$\left\{\frac{d}{dx}\left[\frac{1}{\mu'(x)}\frac{d}{dx}\right] + k_o^2\epsilon'(x) - \frac{\gamma_z^2}{\mu'(x)}\right\} V(x,x') = -j\omega\mu_o\delta(x-x') \qquad (2.27)$$

where $k_o^2 = \omega^2\mu_o\epsilon_o$ and $\mu'(x) = \frac{\mu(x)}{\mu_o}$, $\epsilon'(x) = \frac{\epsilon(x)}{\epsilon_o}$. Upon comparing Eqs.(2.4) and (2.27) one makes the identifications:

$$p(x) = w(x) = \frac{1}{\mu'(x)} \quad , \quad q(x) = -\omega^2\epsilon(x) \quad , \quad \gamma_z^2 = -\lambda \qquad (2.28)$$

and $V(x,x') = j\omega\mu_o g(x,x',\lambda)$. The boundary conditions in Eq. (2.12) are rephrased by Eqs. (2.26) and (2.28) to give

$$\frac{I(x,x')}{V(x,x')} = \frac{jp\frac{dg}{dx}}{\omega\mu_o g} \qquad (2.29a)$$

which represents the terminating admittances $\overleftarrow{Y_T}$ and $\overrightarrow{Y_T}$ at x_1 and x_2 :

$$\overleftarrow{Y_T} = -\frac{I(x_1,x')}{V(x_1,x')} = \frac{j\alpha_1{}^{\dagger}}{\omega\mu_o} \qquad (2.29b)$$

$$\vec{Y}_T = \frac{I(x_2, x')}{V(x_2, x')} = \frac{-j\alpha_2}{\omega\mu_o}$$

For the TM mode problem, the appropriate network is dual to that shown in Fig 2.4(a). The network equations and their connection with the characteristic Green's function are obtained upon making the following duality replacements ;

$$V \Leftrightarrow I \ , \ \mu \Leftrightarrow \epsilon \ , \ Y_T \Leftrightarrow Z_T \ , \ \mu_o \Leftrightarrow \epsilon_o \tag{2.30}$$

The solution of the network problem (Fig. 2.4(a)) is accomplished by first finding the voltage at an arbitrary point x' and determining therefrom the voltages and currents anywhere in the interval $x_1 < x < x_2$ by means of the homogeneous transmission line equations (Eq.(2.25)).

This is best done by reducing the network of Fig 2.4(a) to the simpler form of Fig 2.4(b) where the admittances $\overleftarrow{Y}(x')$ and $\vec{Y}(x')$ are simply the admittances as seen looking to the left and right respectively of the source at x'.

The voltage at x' due to the current point source $i(x')$ is simply

$$V(x'_+, x) = V(x'_-, x) = -\frac{i(x')}{\overleftrightarrow{Y}(x')} \tag{2.31}$$

with $\overleftrightarrow{Y}(x') = \overleftarrow{Y}(x') + \vec{Y}(x')$

From Eqs.(2.25) and (2.31), the voltage at any point x due to a current point source at x' on a homogeneous transmission line is thus

$$V(x, x') = -\frac{i}{\overleftrightarrow{Y}(x')}\left[\cos k_x(x - x') - j\,\vec{Y}'(x')\sin k_x(x - x')\right] \ : x > x' \tag{2.32}$$

$$= -\frac{i}{\overleftrightarrow{Y}(x')}\left[\cos k_x(x - x') + j\,\overleftarrow{Y}'(x')\sin k_x(x - x')\right] \ : x < x'$$

†The positive current convention from left to right is used.

which may be written more compactly for the case of a unit current source as,

$$\begin{aligned} V(x,x') &= \left[\cos k_x(x_> - x') - j\,\vec{Y}'(x')\sin k_x(x_> - x')\right] \times \\ &\quad \left[\cos k_x(x_< - x') + j\,\vec{Y}'(x')\sin k_x(x_< - x')\right] \;/\; \overleftrightarrow{Y}(x') \\ &= \frac{\overleftarrow{V}(x_>,x')\,\vec{V}(x_<,x')}{\overleftrightarrow{Y}(x')} \end{aligned} \tag{2.33}$$

where $x_< = \begin{cases} x \text{ for } x < x' \\ x' \text{ for } x > x' \end{cases}$ and $x_> = \begin{cases} x' \text{ for } x < x' \\ x \text{ for } x > x' \end{cases}$ and $\vec{V}(x,x')$ and $\overleftarrow{V}(x,x')$ are the two solutions of the homogeneous equation (2.24) satisfying the boundary conditions at x_1 and x_2 respectively. Clearly, pole singularities for the Green's function $V(x,x')$ occur when

$$\overleftrightarrow{Y}(x') = \overleftarrow{Y}(x') + \vec{Y}(x') = 0 \tag{2.34}$$

which describe a resonance condition in the circuit of Fig 2.4(a). It can be shown that Eq.(2.34) is true not only at x' but also at all other points in the interval $x_1 < x < x_2$. Moreover, the Green's impedance function $Z(x,x')$ may be considered as that of a (normalised) voltage $V(x,x')$ for a unit current source excitation, i.e [Refer to Eq.(2.31)]

$$V(x_o,x') = Z(x_o) = \frac{\overleftarrow{V}(x_o,x')\,\vec{V}(x_o,x')}{\overleftrightarrow{Y}(x')} \tag{2.35}$$

This gives us the relation

$$\overleftrightarrow{Y}(x') = \frac{\overleftarrow{V}(x_o,x')\,\vec{V}(x_o,x')}{\overleftrightarrow{Z}(x_o)} = \overleftrightarrow{Y}(x_o)\,\overleftarrow{V}(x_o,x')\,\vec{V}(x_o,x') \tag{2.36}$$

and makes it possible to define a normalisation such that the voltage functions ($\overleftarrow{V}$ and $\vec{V}$) are unity at a convenient point x_o simply by substituting Eq.(2.36) into Eq.(2.33) to give

$$\begin{aligned} V(x,x') &\equiv \frac{\vec{V}(x_>,x')\,\overleftarrow{V}(x_<,x')/\,\vec{V}(x_o,x')\,\overleftarrow{V}(x_o,x')}{\overleftrightarrow{Y}(x_o)} \\ &= \frac{\overleftarrow{V}(x_>,x_o)\,\vec{V}(x_<,x_o)}{\overleftrightarrow{Y}(x_o)} \end{aligned} \tag{2.37}$$

2.5 Derivation of the eigen (modal) functions

From Eqs.(2.17),(2.28) and (2.33) one obtains

$$\begin{aligned}\frac{\delta(x-x')}{w(x')} &= -\frac{1}{2\pi j}\oint_C g(x,x',\lambda)\,d\lambda = \sum_m \psi_m(x)\psi_m(x') \\ &= -\frac{1}{2\pi j}\oint_C \frac{\overleftarrow{V}(x_<,x_o,\lambda)\,\overrightarrow{V}(x_>,x_o,\lambda)\,d\lambda}{j\omega\mu_o\overleftrightarrow{Y}(x_o,\lambda)}\end{aligned} \tag{2.38}$$

where the dependence of the functions on λ is shown explicitly. Since $\overleftrightarrow{Y}(x_o,\lambda)$ contains simple zeroes at $\lambda = \lambda_m$ then by the *Residue Theorem*,

$$\sum_m \psi_m(x)\psi_m(x') = \sum_m \frac{\overleftarrow{V}(x_<,x_o,\lambda_m)\,\overrightarrow{V}(x_>,x_o,\lambda_m)}{-j\omega\mu_o \frac{\partial}{\partial\lambda}\overleftrightarrow{Y}(x_o,\lambda_m)} \tag{2.39}$$

where $\frac{\partial}{\partial\lambda}\overleftrightarrow{Y}(x_o,\lambda_m) \equiv \frac{\partial}{\partial\lambda}\overleftrightarrow{Y}(x_o,\lambda)\Big|_{\lambda=\lambda_m}$ then at the resonant condition,

$$\overleftarrow{V}(x,x') = \overrightarrow{V}(x,x') \tag{2.40}$$

This can be easily verified from Eqs.(2.33) and (2.34) and so from Eq.(2.39) we may then write

$$\sum_m \psi_m(x)\psi_m(x') = \sum_m \frac{\overleftarrow{V}(x,x_o,\lambda_m)\,\overleftarrow{V}(x',x_o,\lambda_m)}{-j\omega\mu_o \frac{\partial}{\partial\lambda}\overleftrightarrow{Y}(x_o,\lambda_m)} \tag{2.41}$$

and the normalised modal functions $\psi_m(x)$ are therefore given by

$$\psi_m(x) = \frac{\overleftarrow{V}(x,x_o,\lambda_m)}{\left(-j\omega\mu_o \frac{\partial}{\partial\lambda}\overleftrightarrow{Y}(x_o,\lambda_m)\right)^{\frac{1}{2}}} \tag{2.42}$$

As mentioned earlier a virtue of this procedure is that the mode functions are automatically normalised, with the normalising constant given as,

$$\frac{1}{\left(-j\omega\mu_o \frac{\partial}{\partial\lambda}\overleftrightarrow{Y}(x_o,\lambda_m)\right)^{\frac{1}{2}}} \tag{2.43}$$

For the TM mode problem, a corresponding representation can be deduced upon the use of the duality relations [Eq.(2.30)] to give

$$\Psi_m(x) = \frac{\overleftarrow{I}(x,x_o,\lambda_m)}{\left(-j\omega\epsilon_o \frac{\partial}{\partial\lambda}\overleftrightarrow{Z}(x_o,\lambda_m)\right)^{\frac{1}{2}}} \tag{2.44}$$

with the resonance condition as

$$\overleftrightarrow{Z}(x) = \overleftarrow{Z}(x) + \overrightarrow{Z}(x) = 0 \tag{2.45}$$

2.6 The modal functions of a slab waveguide

Consider now the specific problem of deriving the modal functions for the open slab guide of Fig 2.3. Since the structure is symmetrical about x = 0 , it is necessary to consider only one half of it(ie. $0 < x < \infty$). For symmetrical (even) TE modes, a magnetic wall is placed at the symmetry plane x = 0, y = 0 and the problem is reduced to that shown in Fig 2.5(a). If odd TE modes are considered, then the magnetic wall (**H** = 0) is replaced by an electric wall (**E** = 0). The separate regions in Fig 2.5(a) are piecewise constant and lossless dielectrics which is discontinuous at x = d with

$$\epsilon = \begin{cases} \epsilon_1 & 0 < x < d \\ \epsilon_2 & d < x < \infty \end{cases}$$

and a constant free space permeability μ_o is assumed so that $\mu'(x) = 1$ for $-\infty < x < \infty$.

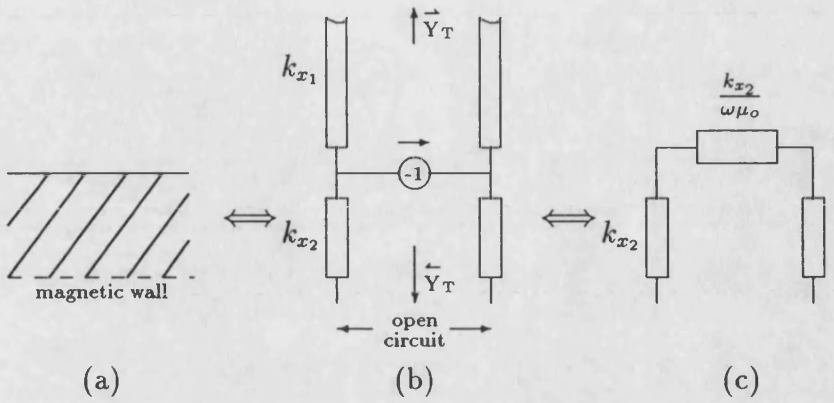

Fig 2.5 Equivalent network representation of one-half of the open slab waveguide.

The network configuration descriptive of the TE even mode problem is shown in Fig 2.5(b). In the earlier section, the location of the unit current source has been left completely arbitrary. For this problem it is convenient to choose $x' = d$ as it will lead to simple expressions for $\overleftrightarrow{Y}(x')$, $\overleftarrow{V}(x,x')$ and $\overrightarrow{V}(x,x')$. From Fig 2.5(b), it was found that

$$\overleftarrow{Y_T} = 0 \quad \text{and} \quad \overrightarrow{Y_T} = \frac{k_{x_1}}{\omega\mu_o} \tag{2.46}$$

with $k^2_{x_{1,2}} = \omega^2\mu_o\epsilon_{1,2} + \lambda$. We may recall from Eq.(2.33) the definition of the voltages looking to the left and right of x' are

$$\begin{aligned} \overrightarrow{V}(x,x') &= \cos k_x(x-x') - j\overrightarrow{Y'}(x')\sin k_x(x-x') \\ \overleftarrow{V}(x,x') &= \cos k_x(x-x') + j\overleftarrow{Y'}(x')\sin k_x(x-x') \end{aligned} \tag{2.47}$$

Using Eqs.(2.26) and (2.47) one obtains for the corresponding currents

$$\begin{aligned} j\omega\mu_o\overrightarrow{I}(x,x') &= k_x \sin k_x(x-x') + jk_x\overrightarrow{Y'}(x')\cos k_x(x-x') \\ -j\omega\mu_o\overleftarrow{I}(x,x') &= k_x \sin k_x(x-x') - jk_x\overleftarrow{Y'}(x')\cos k_x(x-x') \end{aligned} \tag{2.48}$$

Eqs.(2.47) and (2.48) may then be employed to deduce the relation between the admittances looking to the left and right at x' and the terminal admittances $\overleftarrow{Y_T}$

and $\vec{Y}_T$ at x_1 and x_2 respectively,

$$\vec{Y}(x') = \frac{\vec{I}(x', x_2)}{\vec{V}(x', x_2)} \tag{2.49}$$

$$= \frac{k_x \sin k_x(x' - x_2) + j\omega\mu_o \vec{Y}_T \cos k_x(x' - x_2)}{j\omega\mu_o \left(\cos k_x(x' - x_2) - \frac{j\omega\mu_o}{k_x} \vec{Y}_T \sin k_x(x' - x_2) \right)}$$

and,

$$\overleftarrow{Y}(x') = \frac{k_x \sin k_x(x' - x_1) - j\omega\mu_o \overleftarrow{Y}_T \cos k_x(x' - x_1)}{j\omega\mu_o \left(\cos k_x(x' - x_1) + \frac{j\omega\mu_o}{k_x} \overleftarrow{Y}_T \sin k_x(x' - x_1) \right)}$$

The results from Eqs.(2.46) and (2.49) then give,

$$\vec{Y}(x') = \vec{Y}_T = \frac{k_{x_1}}{\omega\mu_o} \quad , \quad \overleftarrow{Y}(x') = -\frac{k_{x_2}}{j\omega\mu_o} \tan k_{x_2} d \tag{2.50}$$

The resonance condition is then given as

$$\overleftarrow{Y}(x') + \vec{Y}(x') = \frac{k_{x_1}}{\omega\mu_o} - \frac{k_{x_2}}{j\omega\mu_o} \tan k_{x_2} d = 0 \tag{2.51}$$

or $$jk_{x_1} = k_{x_2} \tan k_{x_2} d$$

Eqs.(2.47) and (2.51) then gives

$$\overleftarrow{V}(x) = \cos k_{x_2}(x - d) - \tan k_{x_2} d \sin k_{x_2}(x - d)$$

$$= \frac{\cos k_{x_2} x}{\cos k_{x_2} d} \qquad : 0 < x < d \tag{2.52}$$

$$\vec{V}(x) = \cos k_{x_1}(x - d) - j \sin k_{x_1}(x - d)$$

$$= e^{-jk_1(x-d)} \qquad : d < x < \infty \tag{2.53}$$

Since the problem is of a symmetric slab waveguide, it is desirable to define the amplitude of the voltages $\overleftarrow{V}(x)$ and $\vec{V}(x)$ with respect to the middle of the guide. This is easily accomplished by referring to Eq.(2.37) where we set $x_o = 0$, to yield

$$\overleftarrow{V}(x_o, x') = \vec{V}(x_o, x') = \frac{1}{\cos k_{x_2} d} \tag{2.54}$$

so that Eqs.(2.52) and (2.53) now gives

$$\begin{aligned} \overleftarrow{V}(x,x_o) &= \cos k_{x_2}x \qquad : 0 < x < d \\ \overrightarrow{V}(x,x_o) &= \cos k_{x_2}d e^{-jk_{x_1}(x-d)} \qquad : d < x < \infty \end{aligned} \tag{2.55}$$

Notice that $\overleftarrow{V}(x)$ has a standing waveform and $\overrightarrow{V}(x)$ a travelling waveform. This must be the case since $\overrightarrow{V}(x)$ represents the part of the field in the semi-infinite region and $\overleftarrow{V}(x)$ the field "trapped" in the dielectric slab. For $\overrightarrow{V}(x)$ to remain finite at infinity, a restriction

$$Im\ k_{x_1} < 0 \tag{2.56}$$

must be imposed. Furthermore, $\overleftarrow{V}(x)$ and $\overleftrightarrow{Y}(x)$ are even functions of k_{x_2} (ie. containing only ${k_{x_2}}^2$ terms) but not of k_{x_1}; and since

$$\begin{aligned} k_{x_{1,2}} &= \sqrt{\omega^2\mu_o^2\epsilon_{1,2} + \lambda} \\ &= \sqrt{{k_{o_{1,2}}}^2 + \lambda} \end{aligned} \tag{2.57}$$

this implies that $\lambda = -{k_{o_2}}^2$ is a regular point in the complex λ plane but $\lambda = -{k_{o_1}}^2$ is a branch point of order 1.

To understand the effects of the restriction on $Im\ k_{x_1}$ and the branch point at $\lambda = -{k_{o_1}}^2$ we shall consider the contour integral on $g(x,x_o,\lambda)$ [Eq.(2.38)] which is restated here for convenience.

$$\begin{aligned} \sum_m \psi_m(x)\psi_m(x') &= -\frac{1}{2\pi j}\oint_C g(x,x_o,\lambda)\,d\lambda \\ &= -\frac{1}{2\pi j}\oint_C \frac{\overleftarrow{V}(x_<,x_o,\lambda_m)\ \overrightarrow{V}(x_>,x_o,\lambda_m)\,d\lambda}{j\omega\mu_o\ \overleftrightarrow{Y}(x_o,\lambda_m)} \end{aligned} \tag{2.58}$$

If the above integral is transformed to the complex $\hat{\lambda}$ plane where we define

$$\hat{\lambda} = {k_{x_1}}^2 = |\hat{\lambda}|\,e^{j\gamma} \tag{2.59}$$

such that

$$k_{x_1} = \left|\hat{\lambda}\right|^{\frac{1}{2}} e^{j\frac{\gamma}{2}}$$

then the requirement that $Imk_{x_1} < 0$ must mean that γ be restricted to the range

$$0 > \gamma > -2\pi \tag{2.60}$$

This condition is imposed if a branch cut is chosen along the positive real axis as shown in Fig 2.6.

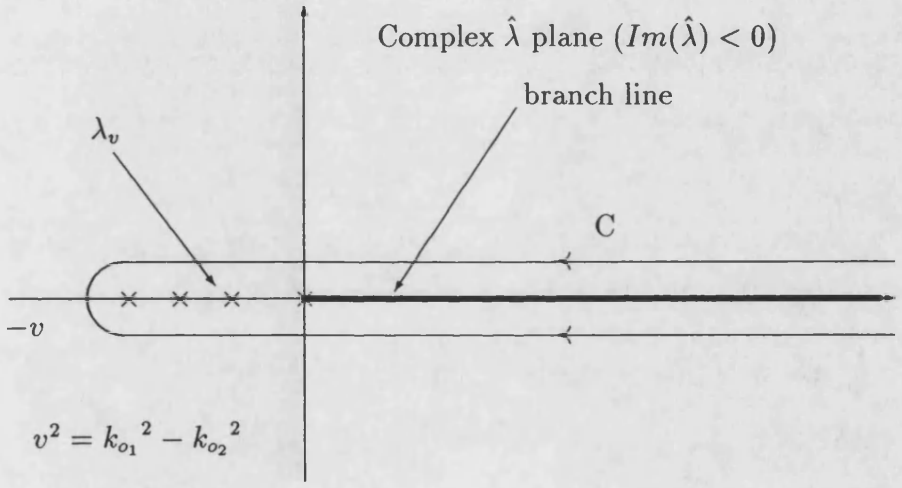

Fig 2.6 Path of integration and the singularities of the Green's function in the complex $\hat{\lambda}$ plane.

The relevant pole singularities of the Green's function are at the zeros of $\overleftrightarrow{Y}(x')$, given by the transcendental equation (2.51). Upon performing an integration as in Eq.(2.58) about the contour C in Fig 2.6 enclosing all the singularities of $g(x, x', \hat{\lambda})$ in the complex $\hat{\lambda}$ plane, one obtains after residue evaluation at the poles $\hat{\lambda}_v$, the series in Eq.(2.58). The remaining contour integral about the branch cut

can be written as

$$I = -\frac{1}{2\pi j}\int_{\infty e^{-2j\pi}}^{0} g(x,x',\lambda)\,d\hat{\lambda} - \frac{1}{2\pi j}\int_{0}^{\infty e^{-j0}} g(x,x',\lambda)\,d\hat{\lambda} \tag{2.61a}$$

$$= -\frac{1}{2\pi j}\int_{0}^{\infty e^{-j0}} [g(x,x',\hat{\lambda} - {k_{o_1}}^2) - g(x,x',\hat{\lambda}e^{-j2\pi} - {k_{o_1}}^2)]\,d\hat{\lambda} \tag{2.61b}$$

$$= -\frac{2}{\pi} Im \int_{0}^{\infty} k_{x_1} g(x,x',k_{x1}^2 - k_{o1}^2)]\,dk_{x_1} \tag{2.61c}$$

The transition from Eq.(2.61a) to (2.61b) is based on the reflection property of the Green's function, that is :-

$$g(x,x',\hat{\lambda}e^{-j2\pi}) = g(x,x',\hat{\lambda}^*) = g^*(x,x',\hat{\lambda}) \tag{2.62}$$

Upon substituting the appropriate form of $g(x,x',\lambda)$ [Refer to Eq.(2.58)], one obtains directly the delta representation

$$\epsilon'(x)\,\delta(x-x') = -\frac{1}{2\pi j}\oint_C g(x,x',\lambda)\,d\lambda$$

$$= \sum_{\nu} \frac{\overleftarrow{V}(x,x_o)\,\overleftarrow{V}(x',x_o)}{-j\omega\mu_o \frac{\partial}{\partial\lambda}\overleftrightarrow{Y}(x_o)}_{\nu} - \frac{2}{\pi} Im \int_{0}^{\infty} k_{x_1} g(x,x',k_{x1}^2 - k_{o1}^2)]\,dk_{x_1}$$

$$= \sum_{\nu} \psi_\nu(x)\psi_\nu(x') + \int_{0}^{\infty} \phi(x,k_{x_1})\phi(x',k_{x_1})\,dk_{x_1} \tag{2.63}$$

where

$$\psi_\nu(x) = \frac{\overleftarrow{V}(x)}{\left(-j\omega\mu_o \frac{\partial}{\partial\lambda}_{\nu} \overleftrightarrow{Y}(x_o)\right)^{\frac{1}{2}}} \tag{2.64}$$

and

$$\phi(x,k_{x_1}) = \sqrt{\frac{2}{\pi}} Im \left\{ \frac{\overleftarrow{V}(x,k_{x_1})}{\left(\frac{-j\omega\mu_o}{k_{x_1}\overleftrightarrow{Y}(x_o)}\right)^{\frac{1}{2}}} \right\}$$

are the required normalised eigenfunctions of the "surface" and "radiation" modes respectively. The application of Eqs.(2.49) and (2.55) on Eq.(2.64) then gives

Surface waves modes

$$\begin{aligned} \psi_\nu(x) &= A\cos\kappa x \qquad : 0 < x < d \\ &= A\cos\kappa d\, e^{-\gamma(x-d)} \qquad : d < x < \infty \\ \beta^2 &= n_1^2k_o^2 - \kappa^2 = n_2^2k_o^2 + \gamma^2 \quad , \quad A = \left(\frac{2}{d+\frac{1}{\gamma}}\right)^{\frac{1}{2}} \end{aligned} \tag{2.65}$$

Continuum modes

$$\begin{aligned} \phi(x) &= \sqrt{\frac{2}{\pi}}\frac{1}{C}\cos\sigma x \qquad : 0 < x < d \\ &= \sqrt{\frac{2}{\pi}}\cos[\rho(x-d) + \alpha] \qquad : d < x < \infty \end{aligned} \tag{2.66}$$

$$\begin{aligned} \beta^2 &= n_1^2k_o^2 - \sigma^2 = n_2^2k_o^2 - \rho^2 \\ C &= \left[1 + \left(\frac{v}{\rho}\right)^2 \sin^2\sigma d\right]^{\frac{1}{2}} \\ \alpha &= \tan^{-1}\left(\frac{\sigma}{\rho}\tan\sigma d\right) \end{aligned}$$

The derivation of the above modes are given in Appendices A and B.

2.7 Experimental results

It is relatively simple to verify experimentally some of the main features of a surface mode of an open dielectric slab guide. The two parameters of a surface mode which can be measured are β (the propagating constant) and α (the decay

constant transverse to the slab).[Refer to Appendix A] The propagation constant being given by

$$\beta = \frac{2\pi}{\lambda_g} \tag{2.67}$$

where λ_g is the guide wavelength of the slab guide.

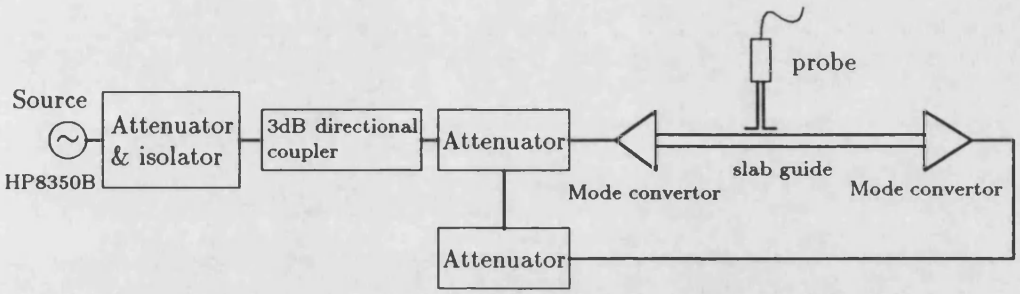

Fig 2.7 Experimental setup for the measurement of guide wavelength

The experimental setup for measuring the guide wavelength of a dielectric slab in the 10 GHz region is shown schematically in Fig 2.7. The dielectric slab used is a 1 cm thick perspex sheet and measured 60 cm wide by 1000 cm long. The mode converter/launcher shown in the schematic are specially built horns with an inset perspex lens designed to give a parallel wavefront at 10 GHz. The simple design principles for the lens is given in Appendix C. Besides giving a parallel wavefront (which is essential for our assumption of an infinite slab) the lens also serve to reduce the reflection from the side of the finite width slab guide. The converters/launchers are further tuned by an adjustable inductive post at the input flange to give an input VSWR of less than 1.2 across the whole X-band.

The adjustable attenuators are present at the input of each converter/launcher for fine tuning to achieve a large VSWR on the slab guide. The standing wave pattern in the slab is detected by a small dipole probe on a semi-rigid cable

connected to a stub tuner and diode detector.

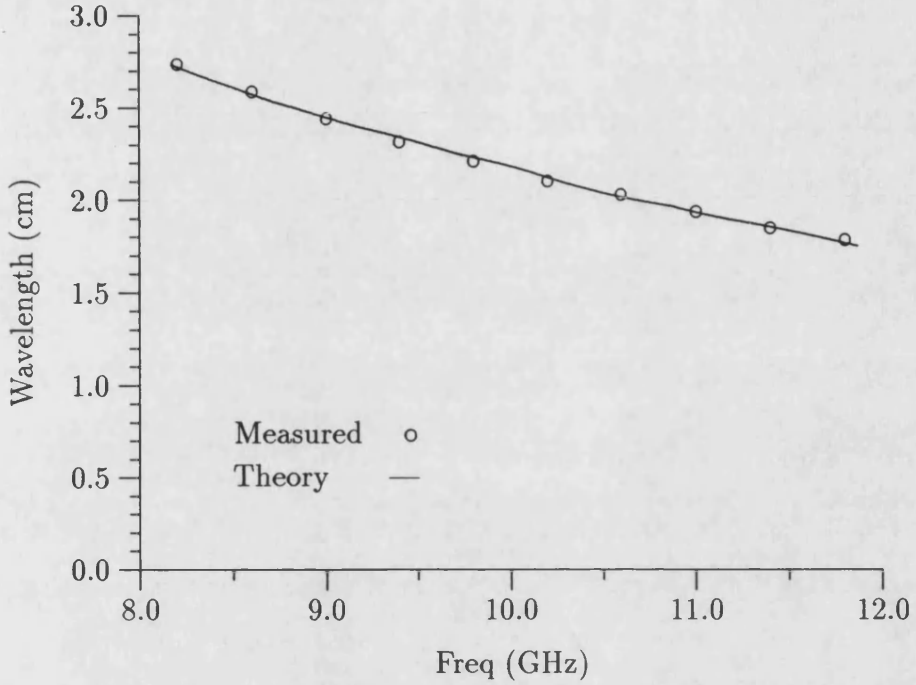

Fig 2.8 A comparision of measured and calculated guide wavelength for a 1 cm thick perspex slab at X-band.

The surface mode launched into the slab is predominantly of the fundamental even TE mode and the dipole probe is aligned so as to pick up the E_y field component of this mode. The measured wavelength shows good agreement with the theoretically predicted values as can be seen in Fig 2.8. The surface wave field attenuation constant α was measured by replacing one of the launchers by a matched load. In this experiment, the matched load is two pieces of tapered absorbing material stuck onto both sides of the dielectric slab (Fig 2.9). The comparison between the measured and calculated values are shown in Fig 2.10.

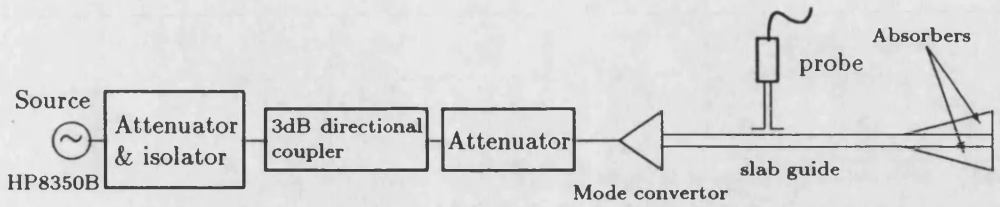

Fig 2.9 Experimental setup for the measurement of field attenuation away from a slab guide.

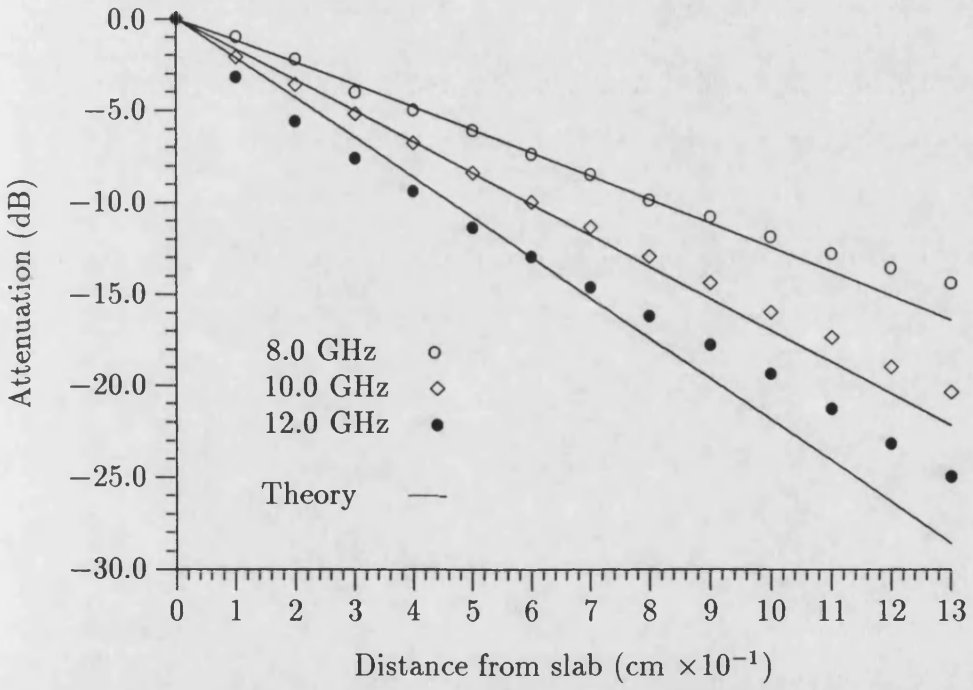

Fig 2.10 A comparision of measured and calculated surface wave field attenuation away from the slab guide.

References

[1] P.M.Morse,H.Feshbach,"Methods of Theorical Physics - Part I", McGraw Hill, 1953, pp 719.

[2] V.Schevchenko,"Continuous transitions in open waveguides",Golem Press,1971

[3] N.Marcuvitz,"On field representations in terms of Leaky modes or eigenmodes",Trans IRE Antennas and Propagation, pp 192, July 1956

[4] T.Tamir,A.A.Oliner,"Guided Complex waves - Part I",Proc IEE, vol 110, Feb 1963, pp 310-325

[5] T.Tamir,A.A.Oliner,"Guided Complex waves - Part II",Proc IEE, vol 110, Feb 1963, pp 325-333

[6] D.Marcuse,"Mode conversion by Surface Imperfections of a Dielectric Slab waveguide",Bell Syst. Tech. J. vol 48, pp 3187-3215 Dec 1969

[7] P.K.Tien,"Light waves on thin films and Integrated Optics",Applied Optics, vol 10, pp 2335-2413 Nov 1971

[8] R.E.Collin,"Field Theory of Guided Waves",New York: McGraw Hill, 1960 pp 470-477

[9] L.M.Brekhovskikh,"Waves in Layered Media", New York: Academic Press, 1960.

[10] L.B.Felsen,N.Markuvitz,"Radiation and Scattering of waves", Englewoods Cliffs, N.J: Prentice Hall, 1973

[11] R.Ogawa et. al,"A theoretical Analysis of Etched Grating Couplers for Integrated Optics",IEEE Journal Quantum Electronics, vol QE9, pp 29-42 Jan 1973

[12] E.C.Titchmarsh,"Eigenfunction Expansions Associated with Second-order Differential Equations - Part I", Oxford: University Press, 1946

[13] E.C.Titchmarsh,"Eigenfunction Expansions Associated with Second-order Differential Equations - Part II", Oxford: University Press, 1958

[14] D.Marcuse,"Theory of Dielectric Optical Waveguides",New York: Academic Press, 1974

[15] G.H.Owyang,"Foundations of Optical Waveguides",London: Edward Arnold Ltd, 1981

Chapter 3

The single step discontinuity

3.1 Introduction

Step discontinuities in planar dielectric waveguides occur frequently in integrated circuits ranging from sub-millimeter to optical frequencies. With recent renewed interest in low lost and low cost dielectric components suitable for integrated circuits applications, such as resonators, grating antennas, optical couplers and so on ; it is essential that reliable and accurate theoretical predictions of the performance of these circuit elements are available. The need for accurate theoretical models is made more acute by the fact that once the integrated components are made, they cannot be easily tuned. However, before any of the above mentioned waveguide structures can be analysed, an accurate theoretical understanding of the scattering properties of a single step discontinuity is required.

The main difficulty in the study of open waveguide discontinuities is caused by the presence of a continuous spectrum of modes which can only be represented by an integral term. Although it can be shown that this integral term is bounded,

its rigorous analytical evaluation is almost certainly impossible. Direct numerical integration of the integral is fraught with convergence problems since the continuous spectrum describes not only the radiated field from the guide but the infinitely fine field structure (which may be weakly singular) at the vicinity of the discontinuity.

Existing methods for solving the problem of the abrupt step [2-7] have relied on various means of 'discretizing' the continuum [ref Chap1]. In this approach, there are two main school of thoughts. One is to discretize the continuum in the spectral domain and the other in the spatial domain. Both methods employ a complete series of expanding functions (which is invariably orthogonal and infinite) to represent the continuum in discrete form. Since the actual number of expanding functions used in the computation is necessarily finite, the chosen functions must give a good fit in the Fourier sense, over a relatively few number of terms. In this respect, there is very little to choose between the two methods since they both encounter difficulties in representing the fine field structures which are present in the proximity of a discontinuity. This difficulty arises from the choice of the expanding functions, which are usually well behaved polynomial series such as Legendre or Laguerre which are not designed to cope with the singular nature of the continuous field. To overcome this problem, a new set of expanding functions is proposed which are not orthogonal but complete, and will account for each surface wave mode, the radiation modes and the edge singularity fields explicitly. A technique capable of using such a non-orthogonal set of expanding functions have been given by Rozzi[6] and is adopted here. The new scheme will however, offer better convergence particularly for the TM field incidence case where the field is known to be weakly singular at the dielectric corner of an abrupt step [8-10].

3.2 Statement of the field problem

The simplest and most natural approach to solving the problem of the electromagnetic field scattering at an abrupt discontinuity is to employ the process of field matching at the discontinuity itself. To do this, it is first necessary to describe the field on either side of a discontinuity. It is well known that the complete field propagating in an open slab waveguide can be resolved into a finite set of surface wave modes and a continuum of radiation modes. The eigenvalue problem of finding these characteristic modes was discussed in detail for the case of a uniform symmetrical slab waveguide in the previous chapter. This representation by the characteristic modes transforms the two-dimensional field problem into a one-dimensional problem of conventional transmission line form. It is evident that modal analysis plays the same role in spatial problems that steady-state analysis does in temporal problems.

With this transformation, one can obtain a circuit representation of the field problem by introducing voltages and currents as measures of the modal amplitudes for the electric and magnetic fields respectively. The introduction of voltages and currents is really a matter of convenience since the mathematics remains the same, but it does allow one to think of the problem in a network sense. The step discontinuity for instance will now be represented by a generalised 2n-port scattering network where both a finite number of discrete ports and a continuum of ports are present on either side of the network as shown in Fig. 3.1. Each port corresponds to a particular mode of the field on either side of the discontinuity. There is no problem in the use of a continuum of ports since the continuum modes and the discrete modes form an orthogonal and complete set and each mode in the continuum can be addressed individually in the Dirac sense.

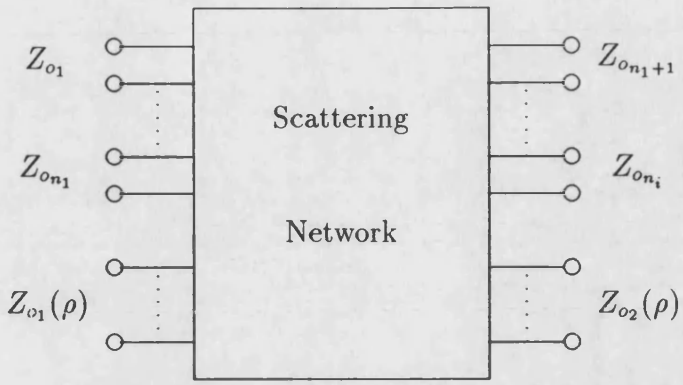

Fig 3.1 Generalized 2n-port scattering network.

Finally, to make the formulation amenable to numerical computation, the Ritz-Galerkin procedure is applied where the modal fields are expanded spatially by a complete set of functions. Different sets of expanding functions will be used and their result on the convergence of the solutions is compared.

3.3 Scattering matrix formulation (TE case)

3.3.1 Field representation

For TE mode excitation, only three field components exist, and they are related as follows :-

$$\begin{aligned} H_x(x,z) &= \frac{1}{j\omega\mu_o}\frac{\partial}{\partial z}E_y(x,z) \qquad (3.1)\\ &= \frac{\beta}{\omega\mu_o}E_y(x,z)\\ &= \frac{1}{z_o}E_y(x,z)\\ H_z(x,z) &= -\frac{1}{j\omega\mu_o}\frac{\partial}{\partial x}E_y(x,z) \qquad (3.2) \end{aligned}$$

where $E_y(x,z)$ may be expressed in its modal form as

$$E_y(x,z) = \left\{ \sum_k a_k \psi_k(x) + \int_0^\infty b(\rho)\phi(x,\rho)d\rho \right\} e^{j(\omega t - \beta z)} \tag{3.3}$$

with a_k and $b(\rho)$ the arbitrary amplitude constants of the surface and continuum modes respectively.

Surface wave modes

The surface mode function $\psi_k(x)$ has been derived in the previous chapter for a symmetrical slab waveguide and is stated here again for ease of reference: [ref Sect. 2.6, Eq(2.65)]

$$\begin{aligned} \psi(x) &= A\cos \kappa x && : x \leq d \\ &= A\cos \kappa d e^{-\gamma(x-d)} && : x \geq d \end{aligned} \tag{3.4}$$

where A is the normalised constant such that

$$\int_0^\infty \psi^2(x)\, dx = 1 \tag{3.5}$$

$$A = \left(\frac{2}{d + \frac{1}{\gamma}} \right)^{\frac{1}{2}} \tag{3.6}$$

Furthermore, the transverse (x-direction) propagation constants γ and κ satisfy the eigenvalue equation [ref Eq(2.51)]

$$\kappa \tan \kappa d = \gamma \tag{3.7}$$

as well as the conservation of wavenumbers [ref Eq(2.23)]

$$\kappa^2 + \gamma^2 = (n_1^2 - n_2^2)\, k_o^2 = v^2 \tag{3.8}$$

with

$$\beta^2 = n_1^2 k_o^2 - \kappa^2 = n_2^2 k_o^2 + \gamma^2 \tag{3.9}$$

Continuum modes

Similarly, the continuum mode function was given as [ref Eq(2.66)]

$$\begin{aligned} \phi(x,\rho) &= \left(\frac{2}{\pi}\right)^{\frac{1}{2}} \frac{1}{C} \cos \sigma x \qquad : x \leq d \\ &= \left(\frac{2}{\pi}\right)^{\frac{1}{2}} \cos\left[\rho(x-d) + \alpha\right] \qquad : x \geq d \end{aligned} \tag{3.10}$$

where

$$\begin{aligned} C &= \left[1 + \left(\frac{v}{\rho}\right)^2 \sin^2 \sigma d\,\right]^{\frac{1}{2}} \\ \alpha &= \tan^{-1}\left(\frac{\sigma}{\rho} \tan \sigma d\right) \end{aligned}$$

with the transverse wavenumbers σ and ρ satisfying the relations

$$\begin{aligned} \sigma^2 &= v^2 + \rho^2 \\ \beta^2 &= n_1^2 k_o^2 - \sigma^2 = n_2^2 k_o^2 - \rho^2 \end{aligned} \tag{3.11}$$

Clearly for $0 < \rho < n_2 k_o$, β is real and positive and the continuum modes in this range propagate to give the radiation modes. For $\rho > n_2 k_o$, β is negative imaginary and the modes are effervescent and they represent the reactive part of the continuum.

3.3.2 Incident surface wave field

The problem is steady-state and source free, with two different semi-infinite slab waveguides forming a step discontinuity at z=0 [ref Fig. 3.2]. The incident field considered here will be composed of surface waves only. The case of incident

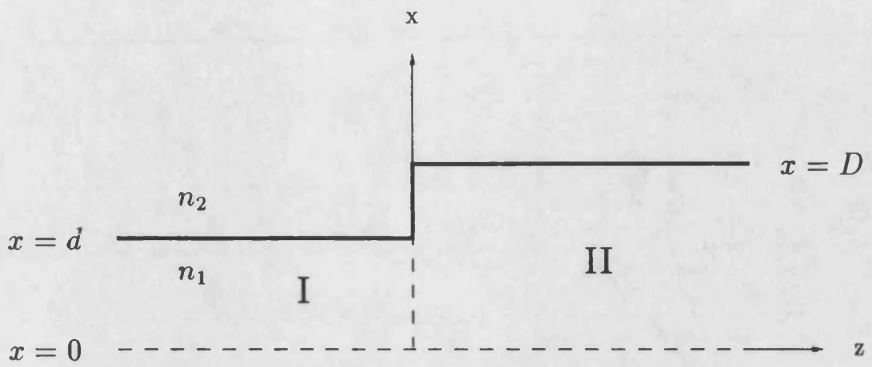

Fig 3.2 Single step discontinuity.

radiation field is dealt with separately in a later section where the problem of coupling of incident radiation field to the guided-wave fields of a slab-waveguide is discussed.

For now, let us assume that there are n_l surface modes which are capable of propagating in guide I and n_r surface modes which can propagate in guide II with

$$n_i = n_l + n_r$$

The continuity of the electric field $E_y(x,z)$ and the magnetic field $H_x(x,z)$ at z=0 is then expressed as

$$\begin{aligned} E_y(x,0) &= \sum_{k=1}^{n_l}(V_k^i + V_k^r)\psi_k(x) + \int_0^\infty V^I(\rho)\phi^I(x,\rho)\,d\rho \\ &= \sum_{k=n_l+1}^{n_i}(V_k^i + V_k^r)\psi_k(x) + \int_0^\infty V^{II}(\rho)\phi^{II}(x,\rho)\,d\rho \end{aligned} \tag{3.12a}$$

$$\begin{aligned} H_x(x,0) &= \sum_{k=1}^{n_l} -\frac{1}{z_{ok}}(V_k^i - V_k^r)\psi_k(x) + \int_0^\infty \frac{V^I(\rho)\phi^I(x,\rho)}{Z_o^I(\rho)}d\rho \\ &= \sum_{k=n_l+1}^{n_i} -\frac{1}{z_{ok}}(-V_k^i + V_k^r)\psi_k(x) - \int_0^\infty \frac{V^{II}(\rho)\phi^{II}(x,\rho)}{Z_o^{II}(\rho)}d\rho \end{aligned} \tag{3.12b}$$

Since a scattering formulation is sought, the incident (V_k^i) and the reflected (V_k^r) surface wave amplitudes are stated explicitly with $V^I(\rho)$ and $V^{II}(\rho)$ representing

the amplitudes of the (scattered) continuum fields in guide I and guide II respectively. It is interesting to note that the matching of the magnetic fields $H_x(x,z)$ at z=0 is equivalent to the matching of the gradient of the electric fields $E_y(x,z)$ at z=0. By using the orthogonality of the modal functions in Eq(3.12b), one may express the unknown modal amplitudes in terms of the unknown magnetic field $H_x(x,0)$ as

$$V_k^r = V_k^i + s_k z_{ok} \int_0^\infty \psi_k(x) H_x(x,0)\, dx \tag{3.13a}$$

$$\begin{Bmatrix} V^I(\rho) \\ V^{II}(\rho) \end{Bmatrix} = \int_0^\infty \begin{Bmatrix} \phi^I(x,\rho) \\ \phi^{II}(x,\rho) \end{Bmatrix} z_o(\rho)\, H_x(x,0)\, dx \tag{3.13b}$$

where

$$s_k = \begin{cases} 1 & for\ k \le n_I \\ -1 & for\ k > n_I \end{cases}$$

Upon substituting the above expressions into Eq(3.12a) and re-arranging, one obtains

$$\sum_{k=1}^{n_i} s_k V_k^i \psi_k(x) = \int_0^\infty \Psi(x,x')\, H_x(x')\, dx' \tag{3.14}$$

where

$$\Psi(x,x') = \frac{1}{2}\left\{ \sum_{k=1}^{n_i} z_{ok}\psi_k(x)\psi_k(x') + \int_0^\infty \left[z_o^I(\rho)\phi^I(x,\rho)\phi^I(x',\rho) + z_o^{II}\phi^{II}(x,\rho)\phi^{II}(x',\rho) \right] d\rho \right\}$$

The summation on the right-hand side of Eq(3.14) represents the total incident electric field impinging on either side of the discontinuity. The term $\Psi(x,x')$ is a Green's function which may be viewed as the 'impedance' of the step discontinuity. This 'impedance' function is made up of known modal functions and modal impedances and completely characterise the step discontinuity. From it and the known incident fields, the unknown modal amplitudes can be solved through the use of Eqs (3.13) and (3.14).

The linear relationship between the scattered (reflected and transmitted) and the incident modal amplitudes in Eq(3.13) suggest that we may obtain a scattering matrix formulation of the form

$$[V^r] \;=\; [S]\,[V^i] \tag{3.15}$$

To this end, let us first consider the case of a single surface wave incident on the discontinuity. Since the amplitude of the incident surface mode is arbitrary, it is possible to set

$$V_l^i \;=\; 1 \quad \textit{and} \quad V_{k\neq l}^i \;=\; 0 \tag{3.16}$$

and Eq(3.15) reduces to

$$V_k^r \;=\; S_{kl} \tag{3.17}$$

Let the scattered magnetic field be $h_l(x)$; then according to Eq(3.14) we have

$$s_l V_l^i \psi_l(x) \;=\; \int_0^\infty \Psi(x,x')\,h_l(x')\,dx' \tag{3.18}$$

In the above equation, $h_l(x)$ is the unknown function to be determined. Its solution however is not straight forward because $h_l(x)$ is described in an integral. One possible way of resolving this problem is to discretize the equation by means of the Ritz-Galerkin procedure. For this, an orthonormal basis is introduced for the interval $0 \leq x \leq \infty$ and represent $\psi_l(x)$ as

$$\psi_l(x) \;=\; \sum_{n=0}^{\infty} Q_{nl} f_n(x) \tag{3.19a}$$

$$Q_{nl} \;=\; \int_0^\infty f_n(x)\psi_l(x)\,dx$$

Similarly for $\phi^I(x,\rho)$, $\phi^{II}(x,\rho)$ and $h_l(x)$, we have

$$\phi^I(x,\rho) \;=\; \sum_{n=0}^{\infty} P_n(\rho,d)\; f_n(x) \tag{3.19b}$$

$$\phi^{II}(x,\rho) \;=\; \sum_{n=0}^{\infty} P_n(\rho,D)\; f_n(x) \tag{3.19c}$$

$$h_l(x) \;=\; \sum_{n=0}^{\infty} \lambda_{nl} f_n(x) \tag{3.19d}$$

Using the above series representation in Eq(3.18) and then multiplying both sides by $f_n(x)$ and integrating with respect to x then gives

$$s_l V_l^i \int_0^\infty \sum_{n=0}^{\infty} Q_{nl} f_n(x) f_n(x)\, dx \;=\; \int_0^\infty dx \int_0^\infty dx' \Psi(x,x') \sum_{n=0}^{\infty} \lambda_{nl} f_n(x') f_n(x) \quad (3.20)$$

or

$$s_l V_l^i Q_{nl} \;=\; Z_{mn} \lambda_{nl} \quad (3.21)$$

with

$$\begin{aligned} Z_{mn} &= \int_0^\infty \int_0^\infty dx' \Psi(x,x') f_n(x) f_n(x') \\ &= \frac{1}{2} \left\{ \sum_{k=1}^{n_i} z_{ok} Q_{nk} Q_{mk} \right. \\ &+ \left. \int_0^\infty z_o(\rho) \left[P_n(\rho,d)\, P_m(\rho,d) \;+\; P_n(\rho,D)\, P_m(\rho,D) \right] d\rho \right\} \end{aligned}$$

This is written more compactly in matrix form as

$$s_l [Q_l] \;=\; [Z]\, [\lambda_l] \quad (3.22)$$

which gives

$$[\lambda_l] \;=\; s_l [Z]^{-1} [Q_l] \quad (3.23)$$

By similarly applying the series representation in Eq(3.13a) and using the relation in Eq(3.17), we obtain

$$\begin{aligned} S_{kl} = V_k^r &= \delta_{kl} - s_l s_k z_{ok} \sum_{n=0}^{\infty} Q_{nk} \lambda_{nl} \quad (3.24) \\ &= \delta_{kl} - s_l s_k z_{ok} [Q_k]^t\, [\lambda_l] \\ &= \delta_{kl} - s_l s_k z_{ok} [Q_k]^t [Z]^{-1} [Q_l] \end{aligned}$$

which is the desired scattering matrix formulation. Eq(3.24) specifies the scattering coefficient of the incident l^{th} surface mode to the k^{th} surface mode. In the Ritz-Galerkin approach, the infinite column matrices $[Q_k]$, and $[Q_l]$ and square

matrix $[Z]$ are replaced by their finite truncations ($0 \leq n \leq N$) and Eq(3.24) becomes a finite matrix equation. In principle the solution can thus be approached as accurately as possible by increasing N. However since matrix sizes increases with N the numerical calculations will become increasingly ill conditioned for large N and it is imperative that the solution should converge before that sets in. As a consequence of the lossy nature (the presence of radiation) of the problem, the Green's impedance matrix $[Z]$ is complex and the exact solution will represent neither a maximum or minimum. As a result, the solution will not converge in a monotonic fashion with increasing order N; but by careful choice of the series of expanding functions $f_n(x)$, the oscillation in the solutions will decrease rapidly with increasing order and convergence is quickly achieved.

Moreover, the step discontinuity is a reciprocal junction, and its scattering matrix should be symmetrical. This will only be so if all the scattering network ports are terminated by the same characteristic impedance. This is easily achieved by normalising the above scattering matrix.

3.3.3 Normalised scattering matrix

A normalised scattering matrix requires each port to be terminated with a unit impedance. Hence to pass from the un-normalised scattering formulation of Eq(3.24) to the normalised form, ideal transformers are introduced to be connected at each port as shown in Fig. 3.3 such that

$$\begin{aligned} & \bar{z} = 1 = n^2 z_{ok} \\ \Rightarrow \quad & n = \frac{1}{\sqrt{z_{ok}}} \end{aligned} \tag{3.25}$$

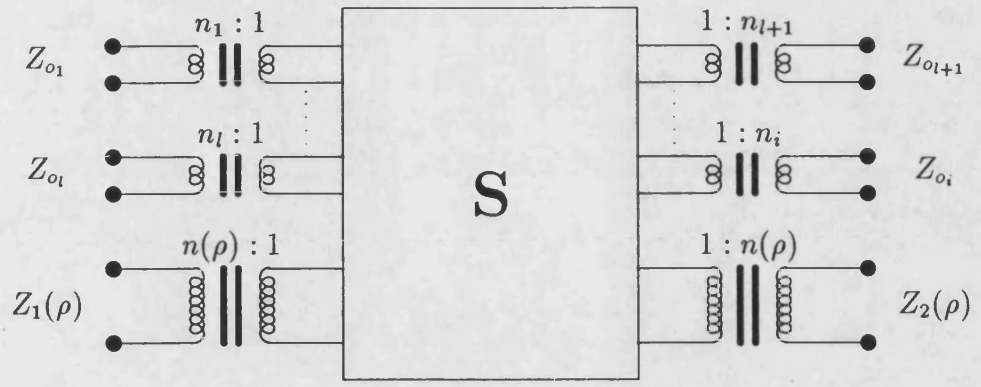

Fig 3.3 Normalised scattering network with embedded ideal transformers.

where z_{ok} is the characteristic impedance of the k^{th} surface mode. This means that the new incident ($\bar{V}^i$) and reflected ($\bar{V}^r$) wave amplitudes are related to the old values by the linear transformation

$$\begin{aligned} [V^i] &= diag\ [\sqrt{z_o}]\ [\bar{V}^i] \\ [V^r] &= diag\ [\sqrt{z_o}]\ [\bar{V}^r] \end{aligned} \tag{3.26}$$

which implies (Ref. Eq(3.15))

$$[\bar{V}^r] = [Z_o^{-\frac{1}{2}}][S][Z_o^{\frac{1}{2}}][\bar{V}^i] \tag{3.27}$$

The normalised scattering matrix is then written as

$$[\bar{S}] = [Z_o^{-\frac{1}{2}}][S][Z_o^{\frac{1}{2}}] \tag{3.28}$$

or in the form of Eq(3.24) as

$$\bar{S}_{kl} = \delta_{kl} - s_k s_l \sqrt{z_{ok} z_{ol}} [Q_k]^t [Z]^{-1} [Q_l] \tag{3.29}$$

which now displays the symmetry required by the reciprocity of the ports. Owing to the orthogonality of modes,the scattering formulation between continuous

modes can be easily derived,

$$S_{\rho\rho'} = \delta(\rho-\rho') + s_\rho s'_\rho \sqrt{z_o(\rho)\, z_o(\rho')}\, [V^r(\rho)]^t\, [Z]^{-1}\, [V^r(\rho)] \tag{3.30}$$

and between a continuum mode and a surface mode

$$S_{\rho k} = s_k s_\rho \sqrt{z_o(\rho)\, z_{ok}}\, [V^r_k]^t\, [Z]^{-1}\, [V^i(\rho)] \tag{3.31}$$

The extension to the case where the incident field consists of surface modes and radiation modes is obvious by the theory of superposition; with the scattering of a surface mode to a continuum mode formally given as

$$S_{k\rho} = s_k s_\rho \sqrt{z_o(\rho)\, z_{ok}}\, [V_k(\rho)]^t\, [Z]^{-1}\, [V^i_k] \tag{3.32}$$

3.3.4 Radiation loss at the step

If the incident field to the step is considered to be primarily guided (ie. consist only of surface modes), then the radiation loss at the step is the result of coupling of the surface modes to the radiative part of the continuum modes.

Hence the radiation loss can be computed directly from our knowledge of the scattering matrix. The simplest and most economical way is to find the difference in power between the incident surface modes and the scattered surface modes. Using the normalised scattering parameters, the percentage power loss to radiation is simply given as

$$(1 - \frac{1}{n}\sum_i^n \sum_j^m S_{ij} S^*_{ij}) \times 100 \tag{3.33}$$

where n is the total number of incident surface waves. Alternatively, the integral of the power density over the radiative part of the continuous spectrum will give the same result as the above expression, thus

$$\text{Percentage radiation loss} = \left(\sum_k^n \int_0^{n_2 k_o} S_{k\rho} S^*_{k\rho}\, d\rho \right) \times 100 \tag{3.34}$$

with $S_{k\rho}$ as given in Eq(3.32).

Obviously Eq(3.34) will require a lot more computational time, but it does provide a valuable means of comparison and a check on the results obtained from Eq(3.33).

3.4 Scattering matrix formulation. (TM case)

3.4.1 Field representation

The analysis of the TM modes closely follows that for the TE case and as such the description will be kept brief. The three field components for the TM mode excitation can be written as

$$\begin{aligned} E_x(x,z) &= \frac{\beta}{\omega\epsilon_o\varepsilon(x)}H_y(x,z) \\ &= \frac{Z_o}{\varepsilon(x)}H_y(x,z) \qquad (3.35) \\ E_z(x,z) &= \frac{1}{j\omega\varepsilon(x)}\frac{\partial H_y(x,z)}{\partial x} \qquad (3.36) \\ \varepsilon(x) &= \begin{cases} n^2{}_1 & : \ x < d \\ n^2{}_2 & : \ x > d \end{cases} \end{aligned}$$

The $E_x(x,z)$ component of the field is discontinuous at $x = d$. This is due to the discontinuous nature of $\varepsilon(x)$. Hence the modal form of $E_x(x,z)$ may best be expressed as

$$E_x(x,z) = \frac{1}{\varepsilon(x)}\left\{\sum_k a_k\psi(x) + \int_0^\infty b(\rho)\phi(x,\rho)\,d\rho\right\}e^{j(\omega t-\beta z)} \qquad (3.37)$$

with the $\varepsilon(x)$ term explicitly given.

Surface modes

The surface mode function $\psi_k(x)$ can be similarly derived to give

$$\begin{aligned} \psi(x) &= a \cos \kappa x &&: x \leq d \\ &= a \cos \kappa d \, e^{-\gamma(x-d)} &&: x \geq d \end{aligned} \tag{3.38}$$

where the normalisation constant a is now fixed by the requirement

$$\int_0^\infty \frac{1}{\varepsilon(x)} \psi^2(x) \, dx = 1 \tag{3.39}$$

which gives

$$a = n_1 \left[\frac{2}{d + \dfrac{(n_1 n_2)^2}{\gamma} \dfrac{\kappa^2 + \gamma^2}{n_2^4 \kappa^2 + n_1^4 \gamma^2}} \right]^{\frac{1}{2}} \tag{3.40}$$

The transverse propagation constants γ and κ now satisfy the eigenvalue equation

$$\kappa \tan \kappa d = \left(\frac{n_1}{n_2} \right)^2 \gamma \tag{3.41}$$

while the conservation of wavenumbers still requires

$$\begin{aligned} \kappa^2 + \gamma^2 &= (n_1^2 - n_2^2) \, k_o^2 = v^2 \\ \beta^2 &= n_1^2 k_o^2 - \kappa^2 = n_2^2 k_o^2 + \gamma^2 \end{aligned} \tag{3.42}$$

Continuous mode

For the continuum, we have

$$\begin{aligned} \phi(x, \rho) &= \sqrt{\frac{2}{\pi}} \frac{n_2}{C} \cos \sigma x &&: x \leq d \\ &= \sqrt{\frac{2}{\pi}} \, n_2 \cos [\rho(x - d) + \alpha] &&: x \geq d \end{aligned} \tag{3.43}$$

with

$$\begin{aligned} \sigma^2 &= \rho^2 + v^2 \\ C &= \left[\cos^2 \sigma d + \left(\frac{n_2}{n_1}\right)^4 \left(\frac{\sigma}{\rho}\right)^2 \sin^2 \sigma d \right]^{\frac{1}{2}} \\ \alpha &= \left[\tan^{-1} \frac{\sigma}{\rho} \left(\frac{n_2}{n_1}\right)^2 \tan \sigma d \right] \end{aligned} \tag{3.44}$$

and the normalising condition is

$$\int_0^\infty \frac{1}{\varepsilon(x)} \phi(x,\rho)\, \phi(x,\rho')\, dx = \delta(\rho - \rho') \tag{3.45}$$

3.4.2 Field representation at the step discontinuity

By a development analogous to that of Section 3.3.2 the integral equation for the unknown E_x field is obtained.

$$\sum_{k=1}^{n_i} V_k^i Y_{ok} \psi_k(x) = \int_0^\infty Y(x,x')\, E_x(x')\, dx' \tag{3.46}$$

where

$$\begin{aligned} Y(x,x') = \frac{1}{2} \Bigg\{ & \sum_{k=1}^{n_i} Y_{ok} \psi_k(x) \psi_k(x') + \\ & \int_0^\infty Y_o(\rho) \left[\phi^I(x,\rho)\, \phi^I(x',\rho) + \phi^{II}(x,\rho)\, \phi^{II}(x',\rho) \right] d\rho \Bigg\} \end{aligned}$$

Unfortunately for the TM polarisation the E_x field exhibit a discontinuous jump at the dielectric interface($x = d$). Because of this complication, a piecewise continuous expansion set is introduced as oppose to the set of basis functions used for the TE case [Eq(3.19)] which are continuous over the entire interval $0 \leq x \leq \infty$.

Consider now a function $f(x)$, continuous over each subinterval where it takes the form $f_1(x)$ and $f_2(x)$ respectively, but possibly discontinuous at $x = d$. Then the scalar product of f with $\psi(x)/\varepsilon(x)$ say, (in the functional sense) is just

$$\left\langle \frac{\psi(x)}{\varepsilon(x)}, f(x) \right\rangle = \int_0^\infty \frac{\psi(x)}{\varepsilon(x)} f(x)\, dx \tag{3.47}$$

$$= \frac{1}{n_1^2}\int_0^d \psi_1(x) f_1(x)\, dx + \frac{1}{n_2^2}\int_d^\infty \psi_2(x) f_2(x)\, dx$$

However, if in each interval, a series of expanding functions can be found, such that

$$\begin{aligned} &C_m(x) \quad : \ 0 \le x \le d \qquad m = 0, 1 \ldots M \\ &L_n(x-d) \ : \ x \ge d \qquad\quad n = 0, 1 \ldots N \end{aligned} \tag{3.48}$$

where $C_m's$ and $L_n's$ are possibly orthonormal over the interval of definition and are complete in the limit $M, N \longrightarrow \infty$. Then

$$\begin{aligned} \psi_1(x) &= \sum_{m=0}^{M} Q_{1m}\, C_m(x) \qquad : \ 0 \le x \le d \\ \psi_2(x) &= \sum_{n=0}^{N} Q_{2n}\, L_n(x-d) \qquad : \ x \ge d \\ f_1(x) &= \sum_{m=0}^{M} F_{1m}\, C_m(x) \qquad : \ 0 \le x \le d \\ f_2(x) &= \sum_{n=0}^{N} F_{2n}\, L_n(x-d) \qquad : \ x \ge d \end{aligned} \tag{3.49}$$

and Eq(3.47) becomes,

$$\left\langle \frac{\psi(x)}{\varepsilon(x)}, f(x) \right\rangle = \frac{1}{n_2^2}\sum_{m=0}^{M}\sum_{m'=0}^{\bar{M}} Q_{1m} F_{1m'} \int_0^d C_m(x) C_{m'}(x)\, dx + \tag{3.50}$$

$$\frac{1}{n_2^2}\sum_{n=0}^{N}\sum_{n'=0}^{\bar{N}} Q_{2n} F_{2n'} \int_d^\infty \mathcal{L}_n(x-d)\, \mathcal{L}_{n'}(x-d)\, dx$$

Then with the $C_m's$ and $L_n's$ orthonormalised over their range of definition, Eq(3.50) reduces to

$$\left\langle \frac{\psi(x)}{\varepsilon(x)}, f(x) \right\rangle = \frac{1}{n_1^2} \sum_{m=0}^{M} Q_{1m} F_{1m} + \frac{1}{n_2^2} \sum_{n=0}^{N} Q_{2n} F_{2n} \tag{3.51}$$

Note that its not necessary for the $C_m's$ to be orthogonal to the $L_n's$. Thus the scalar product of Eq(3.47) reduces to the scalar product of two vectors

$$\left\langle \frac{\psi}{\varepsilon}, f \right\rangle = \left(\frac{1}{n_1^2} Q_1^t , \frac{1}{n_2^2} Q_2^t \right) \begin{pmatrix} F_1 \\ F_2 \end{pmatrix} = \mathbf{Q}^t \mathbf{F} \tag{3.52}$$

When the above transformation is applied to Eq(3.46), it then becomes the matrix equation,

$$\sum_{k=1}^{n_i} A_k Y_{ok} \mathbf{Q_k} \tag{3.53}$$
$$= \frac{1}{2} \left\{ \sum_{k=1}^{n_i} Y_{ok} \mathbf{Q}_k \mathbf{Q}_k^t \mathbf{F} + \int_0^\infty \left[Y^I(\rho) \mathbf{P}\, \mathbf{P}^t \mathbf{F} + Y^{II}(\rho) \mathbf{P}' \mathbf{P}'^t \mathbf{F} \right] d\rho \right\}$$

with

$$\int_0^\infty E_x(x) f(x)\, dx \Rightarrow \begin{pmatrix} \frac{1}{n_1^2} F_1 \\ \frac{1}{n_2^2} F_2 \end{pmatrix} = \mathbf{F}$$

$$\int_0^\infty \psi_k(x) f(x)\, dx \Rightarrow \begin{pmatrix} \frac{1}{n_1^2} Q_{1k} \\ \frac{1}{n_2^2} Q_{2k} \end{pmatrix} = \mathbf{Q}_k$$

$$\int_0^\infty \phi(x) f(x)\, dx \Rightarrow \begin{pmatrix} \frac{1}{n_1^2} P_1 \\ \frac{1}{n_2^2} P_2 \end{pmatrix} = \mathbf{P}$$

Again Eq(3.53) can be re-written more precisely as

$$\sum_{k=1}^{n_i} A_k Y_{ok} \mathbf{Q}_k = [Y][F] \tag{3.54}$$

where

$$[Y] = \frac{1}{2} \left\{ \sum_{k=1}^{n_i} Y_{ok} \mathbf{Q}_k \mathbf{Q}_k^t + \int_0^\infty \left[Y^I(\rho) \mathbf{P}\mathbf{P}^t + Y^{II}(\rho) \mathbf{P}'\mathbf{P}'^t \right] d\rho \right\}$$

Then for $A_l = 1$ and $A_{k\neq l} = 0$, (ie. consider a single incident surface wave) the unknown $E_x(x)$ component of the field (expressed as a M+N+2 dimensional vector $[F]$) is given as,

$$[F] = Y_{ol}\,[Y]^{-1}\,[Q_l] \tag{3.55}$$

Following the same procedure as for the TE case then gives the familiar scattering matrix formulation,

$$\begin{aligned} S_{kl} &= -\delta_k + Y_{ol}\,[Q_l]^t\,[F] \\ &= -\delta_k + Y_{ol}\,[Q_l]^t\,[Y]^{-1}\,[Q_l] \end{aligned} \tag{3.56}$$

with the normalised form as

$$\bar{S}_{kl} = -\delta_k + \sqrt{Y_{ok}\,Y_{ol}}\,[Q_l]^t\,[Y]^{-1}\,[Q_l] \tag{3.57}$$

3.5 Choice of basis functions

The accuracy and efficiency with which the procedure described above can find the solutions will depend entirely on a good choice of the basis functions. The objective here therefore is to find a set that will provide convergence with the use of just the first few terms of a potentially infinite set.Three different choices of basis functions will be presented, each with increasing sophistication, and each providing further insights to the problem of field representation at the step discontinuity.

3.5.1 A cosine series hybrid set

It has been noted that most of the energy of the guided field in the slab guides will be carried by the surface waves. Therefore it seems reasonable to have the basis functions model this particular spectrum of the field well. The modal functions as given by Eq(3.4) and Eq(3.38) shows the surface waves to have a cosine shape in the guide and an exponential decay outside. This suggest an appropriate choice of the expanding functions may be :-

$$C_m(x) = \sqrt{\frac{2\eta_m}{d}} \cos \frac{m\pi x}{d} \qquad \eta_m = \begin{cases} \frac{1}{2} & m = 0 \\ 1 & m > 0 \end{cases} \tag{3.58}$$

for the region $0 < x < d$ (inside the slab) and

$$\mathcal{L}_n(x-d) = \frac{1}{\sqrt{x_o}} L_n\left(\frac{x-d}{x_o}\right) e^{-\frac{x-d}{2x_o}} \tag{3.59}$$

for the region $x > d$ (outside the slab). $L_n((x-d)/x_o)$ is the general Laguerre polynomials with an arbitrary scale variable x_o. The above functions demonstrate orthogonal properties in their interval of definition such that

$$\begin{aligned} \int_0^d C_m(x)\, C_n(x)\, dx &= \delta_{mn} \\ \int_d^\infty \mathcal{L}_m(x-d)\mathcal{L}_n(x-d)\, dx &= \delta_{mn} \end{aligned} \tag{3.60}$$

There are two useful criteria for minimising the error in the representation of the field. The first one is the straightforward minimum square law approximation of the modal function for a finite truncation. The second criterion requires the continuity of the expanded fields at the dielectric interface ($x = d$). More precisely, the first criterion requires

$$\begin{aligned} \int_0^d \psi^2(x)\, dx &= \sum_{m=0}^{M} Q_m^2 \\ \int_d^\infty \psi^2(x)\, dx &= \sum_{n=0}^{M} \bar{Q}_n^2 \\ \Longrightarrow \quad \sum_{m=0}^{M} Q_m^2 + \sum_{n=0}^{M} \bar{Q}_n^2 &= 1 \end{aligned} \tag{3.61}$$

where Q_m and $\bar{Q}_n$ are the coefficients of the expansion functions $C_m(x)$ and $\mathcal{L}_n(x)$ respectively. Their values are given in Appendix D.

The second requirement of continuity at $x = d$ is simply

$$\sum_{m=0}^{M} Q_m C_m(d) = \sum_{n=0}^{M} \bar{Q}_n \mathcal{L}_n(d) \tag{3.62}$$

$$\Longrightarrow \quad \sum_{m=0}^{M} Q_m (-1)^m \sqrt{\frac{2\eta_m}{d}} = \sum_{n=0}^{M} \bar{Q}_n(x_o) \frac{1}{\sqrt{x_o}}$$

The above condition is met by optimising the arbitrary variable x_o.

3.5.2 A surface modes hybrid set

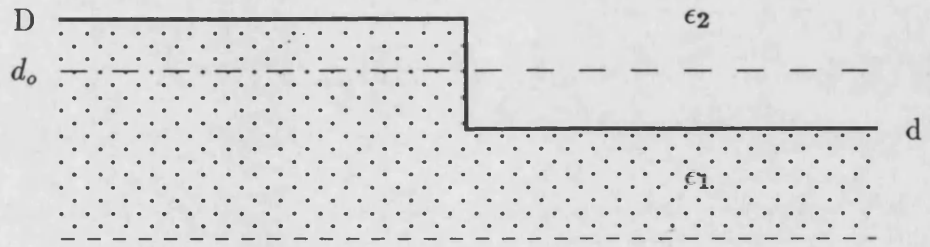

Fig 3.4 Intermediate guide as a transition between two waveguides.

Although the cosine series will fit the modal functions well after a few terms, it is our intention here to obtain an equally good fit with only one or two terms. To achieve this a "trial field" is required which is already the same shape as the surface modes on either side of the step. This "trial field" will necessarily be another surface mode function. However the surface modal functions on either side of the step will not be suitable as by their very nature they are orthogonal to their respective continuum modes. We shall use instead the modal functions of an intermediate guide with its guide thickness d_o chosen as $d_o = \sqrt{dD}$. This

is little different to making the intermediate guide an EDC (Effective Dielectric constant) approximation of the two actual waveguides which constitutes the step discontinuity, where we require

$$\epsilon_{eff} = \sqrt{\epsilon_1 \epsilon_2}$$

To be mathematically rigourous, the modal "trial field" can be completed by the addition of a set of orthonormal exponentially weighted Laguerre polynomials with the $\bar{N}^{th}$ order set given as

$$\{G_n : 1 \leq n \leq \bar{N}\} = \{\psi_1 \ldots \psi_i , \mathcal{L}_o \ldots \mathcal{L}_{\bar{N}-i-1}\} \tag{3.63}$$

As opposed to the set of basis functions in the previous section, each of the function ψ and $\mathcal{L}$ are defined over the entire interval $0 \leq x < \infty$. The question of orthogonality of ψ with $\mathcal{L}$ is not an issue as the Ritz-Galerkin approach do not require it [18]. The unknown field $\bar{\psi}$ may thus be written as

$$\bar{\psi}(x) = \sum_n Q_{1n}\psi_n(x) + \sum_m Q_{2m}\mathcal{L}_m(x) \tag{3.64a}$$

$$\begin{aligned} Q_{1n} &= \int_0^\infty \bar{\psi}(x)\,\psi_n(x)\,dx \\ Q_{2m} &= \int_0^\infty \bar{\psi}\,\mathcal{L}_m(x)\,dx \end{aligned} \tag{3.64b}$$

The optimising criteria for the Laguerre series in this case is that they should be made as orthogonal to the intermediate modes as possible. This is done again via the scaling factor x_o [ref. Eq(3.59)]. That is we need to minimise the function

$$\sum_{m=0}^{N-i-1} \int_0^\infty \sum_{k=0}^{i} \psi_k(x)\,\mathcal{L}_m(x)\,dx \tag{3.65}$$

The values of the coefficients Q_{1n} and Q_{2m} are given in Appendix E. It is expected that there will be very little difference between the spectra of the guides on

either side of the step and that of the intermediate guide particularly when the step size is small and the Laguerre set will not normally be needed for a good approximation to be achieved.

3.5.3 A single "trial field" with edge effects.

Although the electromagnetic fields around the edges (90° and 270° corners) at the step are localised and reactive in nature and do not contribute to the propagated fields, they nevertheless have an effect on the mode coupling of the fields. It seems reasonable therefore if this behaviour is included in the formulation of the problem, then a much better approximation of the field at the step will be achieved. From the work of [8],[10] it is understood that a component of the electric field transverse to a dielectric edge may become singular while the components of the electric field parallel to it does not. Hence for TM polarisation its E_x field component will become singular at the edges at $x = d, D$ of the step, while for TE polarisation, the E_y component will remain regular. A series expansion of such a singular field using a regular set of basis functions will suffer from what is known as Gibbs phenomenon in Fourier analysis [3]. The solutions will converge slowly and exhibits oscillations when truncated after a finite number of terms. This explain why previous methods [1-7] of solving for TM scattering always gives poorer convergence when compared to the same problem with TE polarisation.

For a dielectric wedge of aperture θ between dielectrics ϵ_1 and ϵ_2, the singularity exhibit a dependence like r^α where r is the distance from the wedge and α ($-1 <$

$\alpha < 0$) is given by the transcendental equation [10]

$$\sin[(\alpha+1)\pi] \pm \frac{\epsilon_1 - \epsilon_2}{\epsilon_1 + \epsilon_2} \sin[(\alpha+1)(\theta-\pi)] = 0 \tag{3.66}$$

For $\theta = \frac{\pi}{2}$ (corner at $x = D$) and $\theta = \frac{3\pi}{2}$ (corner at $x = d$) the order of the singularity remains the same and is given by

$$\alpha = \frac{2}{\pi} \cos^{-1}\left(\frac{1}{2}\frac{\epsilon_1 - \epsilon_2}{\epsilon_1 + \epsilon_2}\right) - 1 \tag{3.67}$$

To include the effect of this singularity in the solution, a new trial field is developed, based on the surface mode function of the intermediate guide of the previous section, but with the singularity added in. This results in a trial function of the form :-

$$\begin{aligned} E_y &= A\bar{\psi}(x) \qquad (3.68)\\ &= \frac{A}{\epsilon_2} e^{-\gamma_o(x-d_o)} (x-D)^\alpha \qquad : x > D \\ &= \frac{A}{\epsilon_2} e^{-\gamma_o(x-d_o)} (D-x)^\alpha \qquad : d_o \le x \le D \\ &= \frac{A}{\epsilon_1}\frac{\cos(\kappa_o x)}{\cos(\kappa_o d)} (x-d)^\alpha \left(\frac{D-d_o}{d_o-d}\right)^\alpha \qquad : d \le x \le d_o \\ &= \frac{A}{\epsilon_1}\frac{\cos(\kappa_o x)}{\cos(\kappa_o d)} (d-x)^\alpha \left(\frac{D-d_o}{d_o-d}\right)^\alpha \qquad : 0 \le x \le d \end{aligned}$$

The constant A is the normalising constant given by

$$A = \left(\int_0^\infty \bar{\psi}^2(x)\, dx\right)^{-\frac{1}{2}} \tag{3.69}$$

The trial function is applied in exactly the same manner as the surface mode functions of the previous section.

3.6 Computation of the far-field pattern of a single step.

The far-field or the radiative part of the E_y component of the electric field is given by Eq(3.3) as

$$E_y^r = \int_0^\infty b(\rho)\phi(x,\rho)\, e^{-j\beta z}\, d\rho \tag{3.70}$$

and by using the modal form of $\phi(x,\rho)$ as given in Eq(3.10) we get,

$$E_y^r = \frac{1}{\sqrt{2\pi}} \int_{-\infty}^{\infty} b(\rho)\, e^{-j[\rho(x-d)\, +\, \alpha\, +\, \beta z]}\, d\rho \tag{3.71}$$

The integral equation above is best evaluated using the saddle-point method of approximate integration. To facilitate the application of this method, it is convenient to apply the following transformation.

$$\begin{aligned} (x-d) &= r\, \sin(\theta) \quad , \quad z = r\, \cos(\theta) \\ \rho &= n_2 k_o \sin(w) \quad , \quad \beta = n_2 k_o \cos(w) \end{aligned} \tag{3.72}$$

This will greatly simplify the details of the saddle-point integration, and when applied to Eq(3.71) gives

$$E_y^r = \frac{1}{\sqrt{2\pi}} \int_{\frac{-\pi}{2}-j\infty}^{\frac{\pi}{2}+j\infty} f(w)\, e^{-jrn_2k_o\cos(w-\theta)}\, dw \tag{3.73}$$

with,

$$f(w) = n_2 k_o \cos w \times b(n_2 k_o \sin w) e^{-j\alpha(w)}$$

The transformation of Eq(3.72) represents a mapping of the complex ρ-plane into strips of the complex w-plane as shown by the shaded region of Fig 3.5.

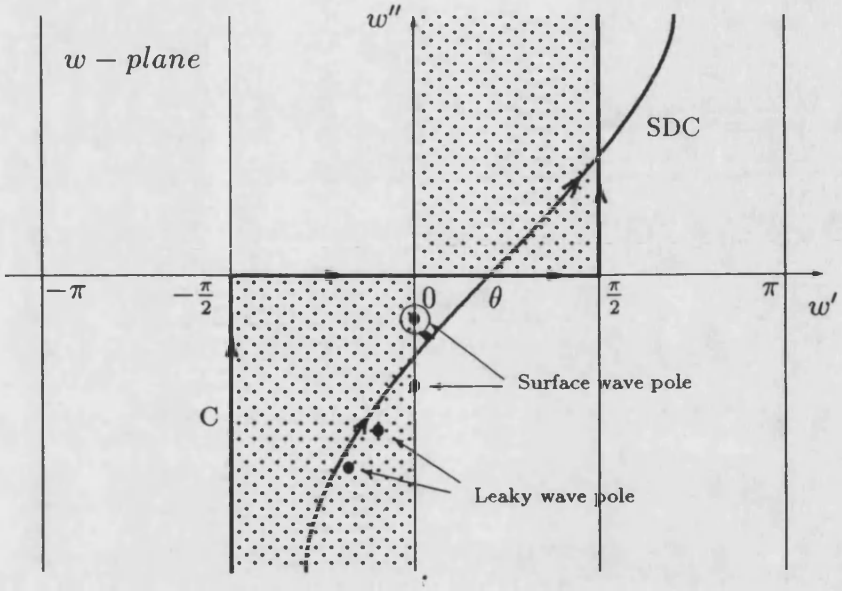

Fig 3.5 Deformation of contour **C** into the steepest-descent contour **SDC**

The original integration path along the real-axis of the ρ-plane is now mapped onto the path **C** in the w-plane. The shaded region is the area in which $Im\beta < 0$ for decaying fields in the z-direction. Along the contour **C**, ρ is real but as the path of integration **C** is deformed to the steepest descent path **SDC**, ρ will take complex values. The change from the path **C** to the path **SDC** should not change the value of the integral [Eq(3.71)] as long as no poles in the w-plane has been swept across. If poles has been crossed then their residues should be included. In the integrand of Eq(3.73), let

$$g(w) = -jn_2k_o\cos(w-\theta) \tag{3.74}$$

then,

$$\frac{dg}{dw} = jn_2k_o\sin(w-\theta) \tag{3.75}$$

which is equal to 0 at $w = \theta$. Since the complex function g(w) cannot have a maximum or a minimum, the stationary point at $w = \theta$ is a saddle point [Ref

13, page 378-379].

Thus if the integration path **SDC** is made to go through the saddle point and r is made arbitrarily large, then the value of the integrand of Eq(3.73) would be negligible away from the saddle point. This will only be true of course if the real part of g(w) is negative. That is we require

$$Re[-jn_2k_o\cos(w-\theta)] \;<\; 0$$

Since n_2 and k_o are real and if we let $w \;=\; w' + jw''$ then for $w'' \;>\; 0,$ we require

$$w' \;<\; \pi \;+\; \theta$$

and for $w'' \;<\; 0,$ we require

$$w' \;<\; \theta$$

Both the above conditions are satisfied along the **SDC** path as is evident in Fig 3.5. Furthermore if the **SDC** path is chosen to be along the path of constant phase such that

$$Im[\, g(w) \;-\; g(\theta)] \;=\; 0 \tag{3.76}$$

then only the real part of $g(w)$ will vary, and it can be shown that this constant phase path is also the steepest descent path from the saddle point. From Eq(3.74) and Eq(3.76),the governing condition for the **SDC** path can be obtained, which is

$$\cos(w' \;-\; \theta)\;\cosh\; w'' \;-\; 1 \;=\; 0 \tag{3.77}$$

By expanding g(w) as a Taylor series around the saddle point θ and using it in the integral equation Eq(3.73), a second order approximation of the integral for arbitrarily large r can be obtained as

$$E_y^r \;\simeq\; f(\theta)\left(\frac{1}{rn_2k_o}\right)^{\frac{1}{2}} e^{-j(rn_2k_o \;-\; \frac{\pi}{4})} \tag{3.78}$$

We may recall from Eq(3.73) that $f(\theta)$ is a function which contains b(w) which is the modal amplitude of the continuous spectrum; the solution of which may be inferred from Eq(3.32) as

$$b(\rho) = \sum_k s_l Z_o(\rho) [V(\rho)]^t [Z]^{-1} [V_k^i] \tag{3.79}$$

Moreover, the radiated power from the step may be written as

$$\begin{aligned} P_{rad} &= -\frac{1}{2} Re(E_y H_\phi^*) \\ &= \frac{1}{2} \frac{n_2 k_o}{\omega \mu_o} E_y E_y^* \end{aligned} \tag{3.80}$$

and by using Eq(3.78), we get

$$P_{rad} = \frac{|f(\theta)|^2}{2\omega\mu_o r} \tag{3.81}$$

There are two kind of poles that will be crossed as θ is varied from 0 to $\pi/2$. The first kind are the surface wave poles which occur along the negative imaginary axis in the w-plane. Then there are the leaky wave poles which exist in the region $-\pi/2 < w' < 0$ and $w'' < 0$ as shown in Fig 3.5. Their contribution to the integral however become less important as the distance from the step r is increased. For large r, as is the case with the saddle point integration, the residues of the surface and leaky wave poles is negligibly small.

3.7 Experimental measurements and results

For the measurement of the radiation pattern of a single step in a slab guide, we adapted a microwave test bench which was used to characterize the radiation pattern of waveguide horns. The movable arm which holds the horn detector is 1 meter in length and it moves over an angular scale graduated in units of 1 degree. Although this is a fairly crude setup, it is thought to be sufficient as a simple verification of predicted field pattern.

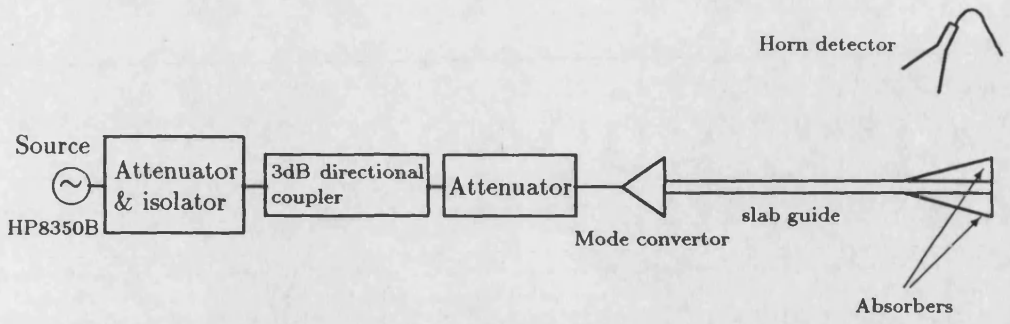

Fig 3.6 Experimental setup for the measurement of field radiation from a step discontinuity.

The incident power at the step discontinuity is determined by measuring the power delivered to one end of a plain slab by a mode launcher attached to the other end. Loss due to the plain slab is assumed to be negligible. Furthermore, as a control for the radiation measurements the "radiation pattern" of a plain slab is first determined. It is noticed that the mode launcher leaked power at various angles away from the slab, but was reduced by tuning and placement of absorbers near the launcher. The radiated power is nevertheless taken to be the difference between the measurements of the plain slab and that of the slab with the step present.

The calculated far field shown in Fig 3.7 shows a rapid increase in radiated power as frequency is increased. There is also a small but discernible shift of the radiation peaks towards $\theta = 0$ as frequency is increased. The results were calculated using a 5^{th} order cosine basis function.

The results compare reasonable well with the measurements (Figs 3.8 to Fig 3.11) considering the small amount of radiated power at the lower frequencies. The radiated power varies from 0.26% at 8 GHz to 5.7% at 12 GHz of total incident power.

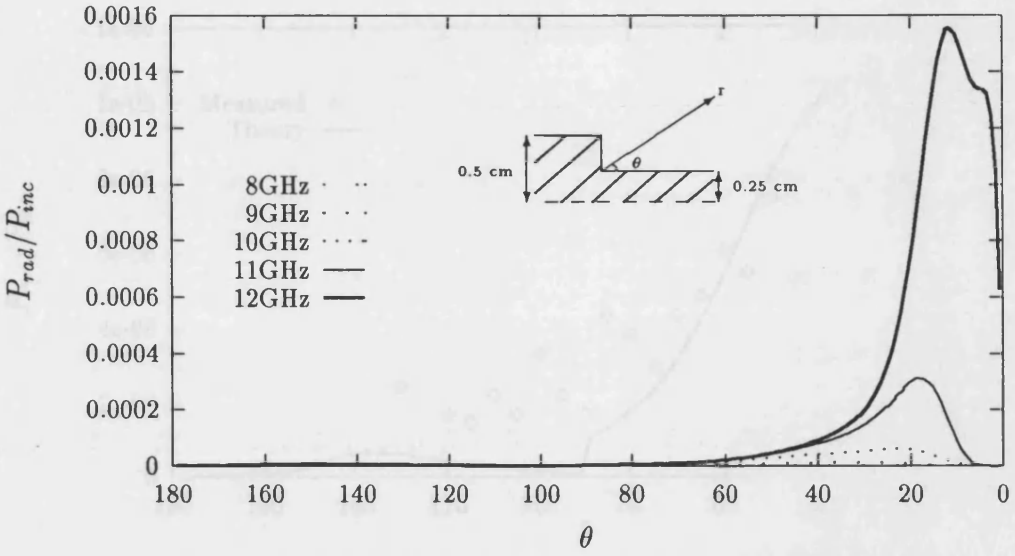

Fig 3.7 Calculated far field pattern of a single step.(TE polarization)

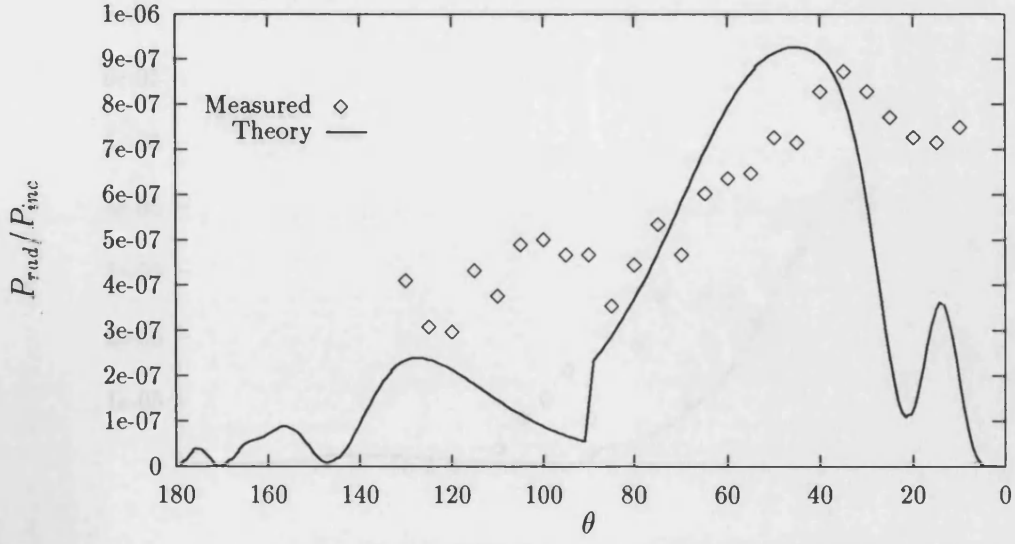

Fig 3.8 Far field pattern of a single step at 8GHz

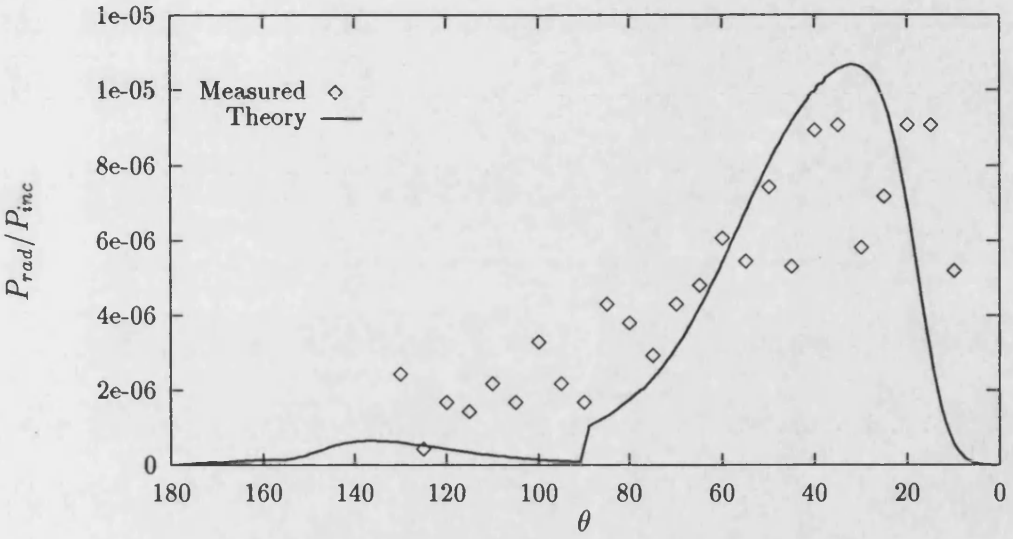

Fig 3.9 Far field pattern of a single step at 9GHz

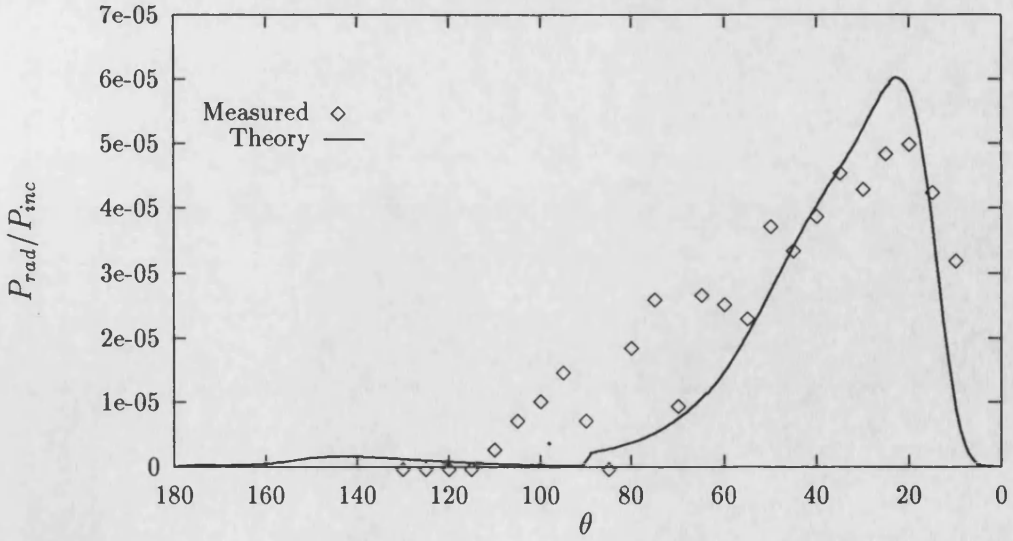

Fig 3.10 Far field pattern of a single step at 10GHz

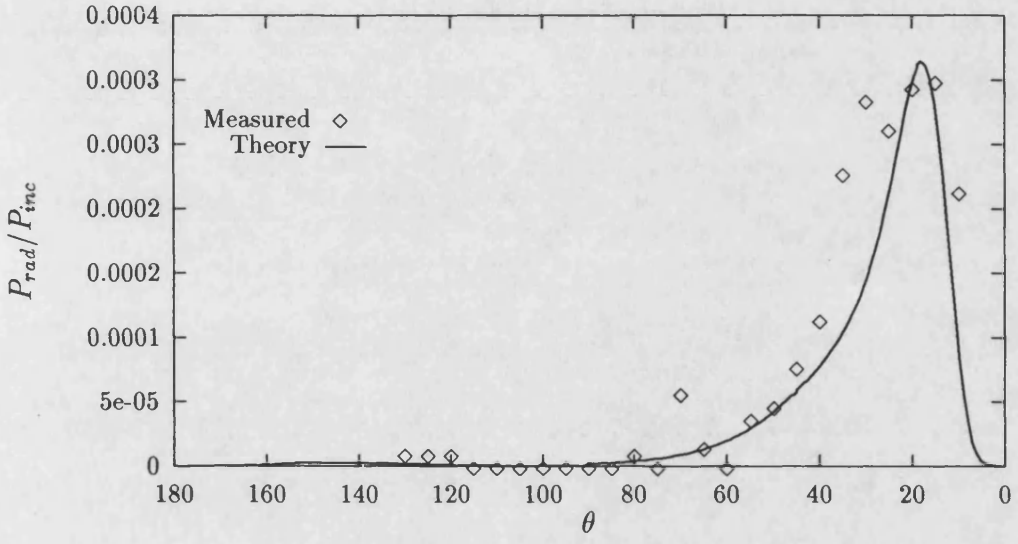

Fig 3.11 Far field pattern of a single step at 11GHz

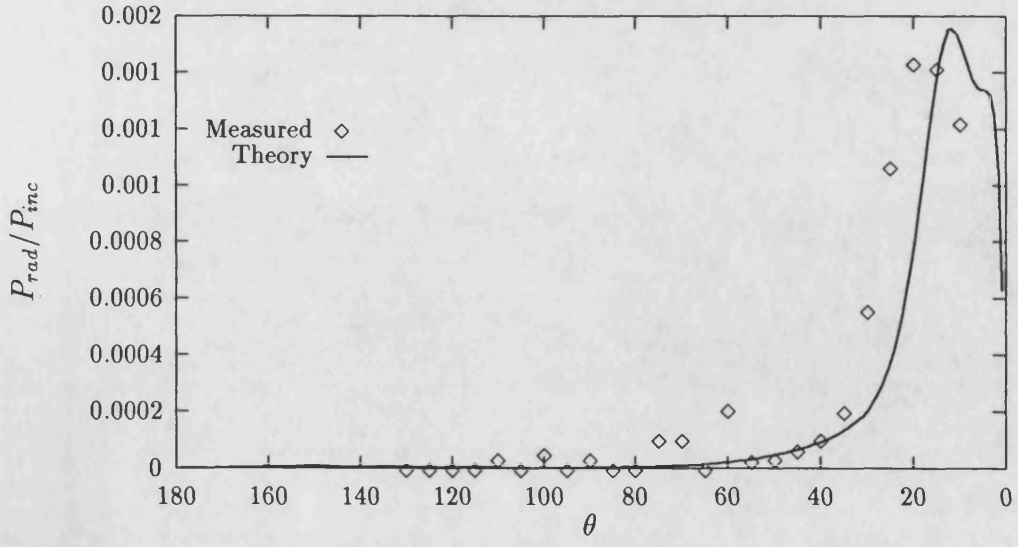

Fig 3.12 Far field pattern of a single step at 12GHz

The convergence of the solutions using the different set basis functions are compared in Table 3.1 for TE polarisation and Table 3.2 for TM polarisation. The figures show rapid convergence for the cosine-Laguerre and intermediate surface mode set for TE polarisation, achieving 4 significant digit accuracy in only the second term and 5 significant digit accuracy by the fifth term on the magnitude of S_{11}. Convergence for TM polarisation is only slightly worst off but still giving 4 significant digit accuracy by the fifth term.

The singular trial function gives a good approximation for TM polarisation. It shows that the singular trial function does provide a good account of the edge singularity of the TM polarised field. In contrast the straight forward normalised Laguerre basis gives relatively poor convergence.

TABLE 3.1
Comparison of S_{11} for step $d/D = 0.5$ at 10GHz
for a perspex slab with permitivity $\epsilon_1 = 2.57$
(TE polarisation)

	Laguerre polynomials		Cosine-Laguerre set		Intermediate surface mode	
m	$\lvert S_{11}\rvert$	$\angle\ \pi$ rad	$\lvert S_{11}\rvert$	$\angle\ \pi$ rad	$\lvert S_{11}\rvert$	$\angle\ \pi$ rad
1	6.6442e-2	9.8332e-1	6.9392e-2	9.9758e-1	6.8197e-2	1.0132
2	6.7027e-2	9.8407e-1	6.8015e-2	1.0101	6.8015e-2	1.0124
3	6.7793e-2	9.8656e-1	6.8015e-2	1.0124	6.8015e-2	1.0125
4	6.8419e-2	9.8873e-1	6.8014e-2	1.0125	6.8014e-2	1.0126
5	6.8759e-2	9.8967e-1	6.8014e-2	1.0127	6.8014e-2	1.0125

TABLE 3.2
Comparison of S_{11} for step $d/D = 0.5$ at 10GHz
for a perspex slab with permitivity $\epsilon_1 = 2.57$
(TM polarisation)

	Laguerre polynomials		Cosine-Laguerre set		Intermediate surface mode		Singular Surface mode	
m	$\lvert S_{11}\rvert$	$\angle\ \pi$ rad	$\lvert S_{11}\rvert$	$\angle\ \pi$ rad	$\lvert S_{11}\rvert$	$\angle\ \pi$ rad	$\lvert S_{11}\rvert$	$\angle\ \pi$ rad
1	1.9242e-2	0.0332	1.8225e-2	0.0308	1.8116e-2	0.0312	1.779e-2	0.033
2	1.7027e-2	0.0247	1.7916e-2	0.0294	1.8001e-2	0.0303	–	–
3	1.7493e-2	0.0565	1.7733e-2	0.0142	1.7715e-2	0.0164	–	–
4	1.7119e-2	0.0921	1.7694e-2	0.0125	1.7684e-2	0.0122	–	–
5	1.7335e-2	0.0765	1.7683e-2	0.0107	1.7688e-2	0.0103	–	–
10	1.7735e-2	0.0533	1.7683e-2	0.0092	1.7684e-2	0.0101	–	–

A comparison of the shape of various trial functions with the fundamental surface mode on either side of the step is shown in Fig 3.13 The variation of the scattering parameter with step height is shown in Fig 3.14 for a TE polarised field. For small values of step height, the reflection coefficients for incident wave from either side of the step is seen to be the same. However as d_1 diminishes to zero the reflection coefficient for the surface mode incident from the right namely $|S_{22}|$ is seen to approach a limit which is the value of the reflection coefficient of a semi-infinite slab guide. The value of $|S_{11}|$ tends towards zero as it should since the surface mode is barely guided for the thin slab guide. It is interesting to note that even when d_1 reaches extremely small values the value of $|S_{12}|$ is still fairly substantial at about 0.3.

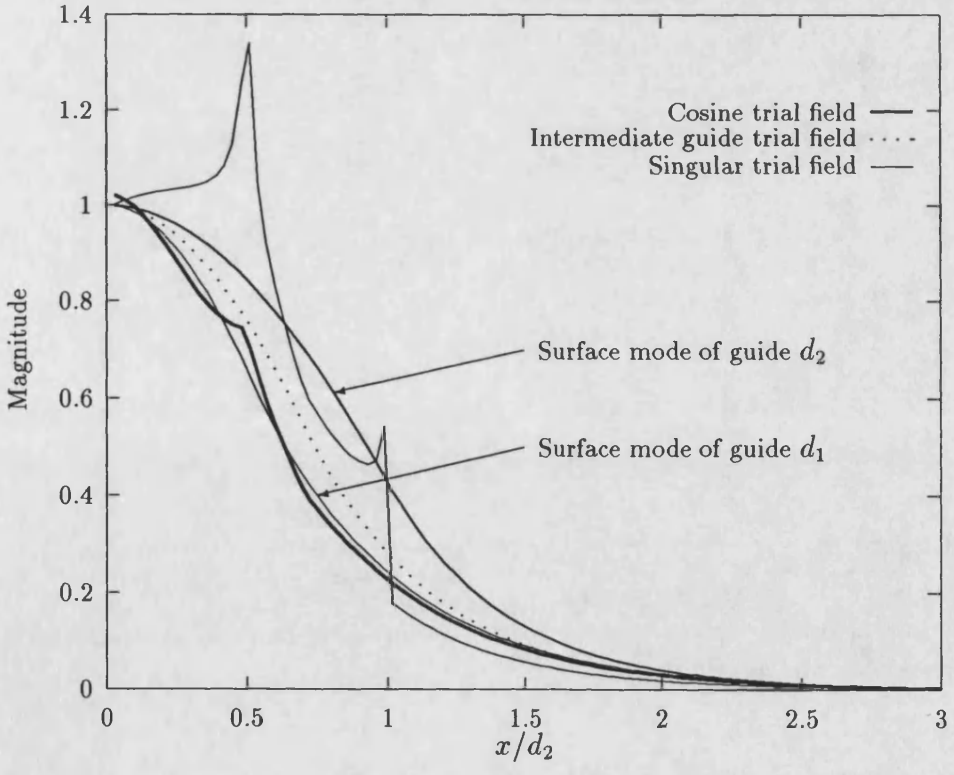

Fig 3.13 Comparison of modal function with various trial fields when $d_1 = 0.5\,d_2$

A comparison of results of the present variational method using a 5^{th} order cosine-

Laguerre basis with the published work of Brooke & Kharadly[5] is shown in Fig 3.15 for TE polarisation and Fig 3.16 for TM polarisation. The figures show the variation of the scattering parameters against normalised frequency. Agreement is generally good for both polarisations. There is only a slight difference evident for both polarisation when the normalised frequency is small. A guess would be for the lower frequency value the surface modes are not well guided and the field tails of these modes will extend a considerable distance away from the slab guide. This might effect the solutions obtained by Brooke & Kharadly if they had not placed their metal walls far enough away.

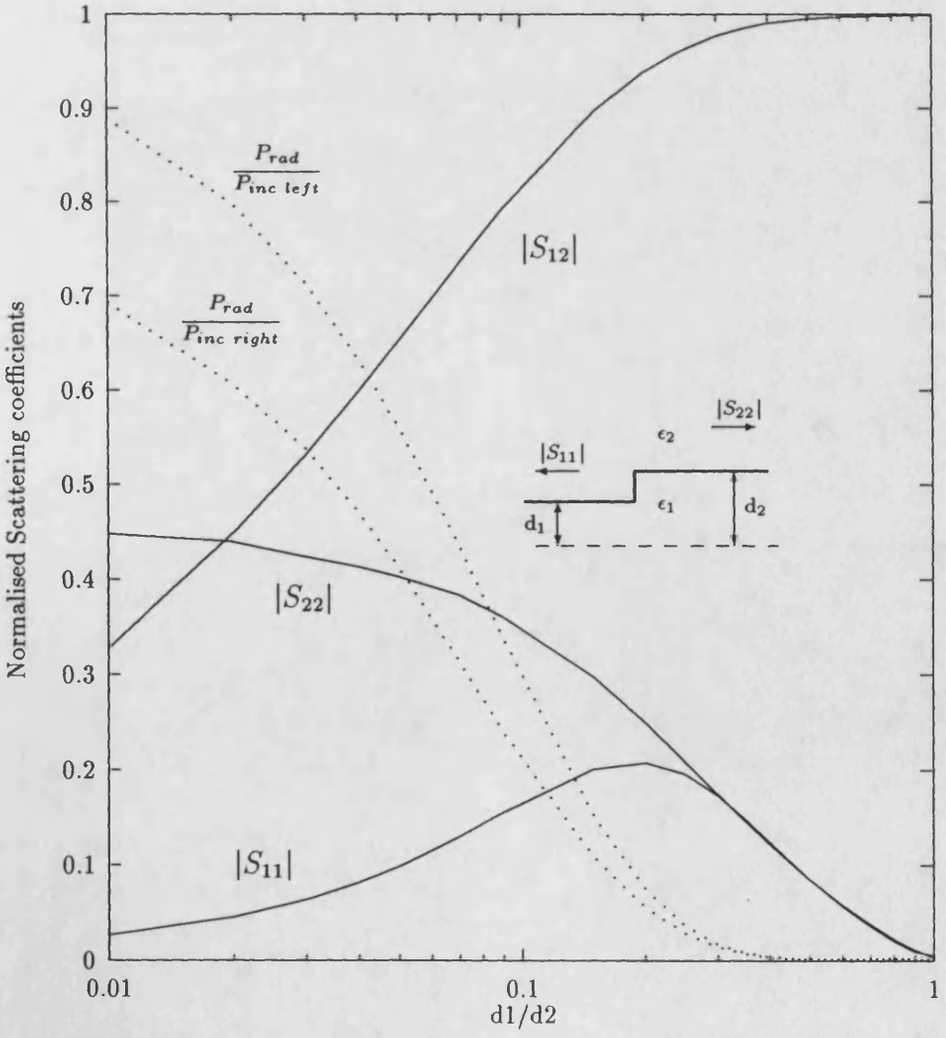

Fig 3.14 Calculated scattering parameters for varying step height d_1/d_2 with $k_o d_2 = 1.0$, and $\epsilon_1 = 5$

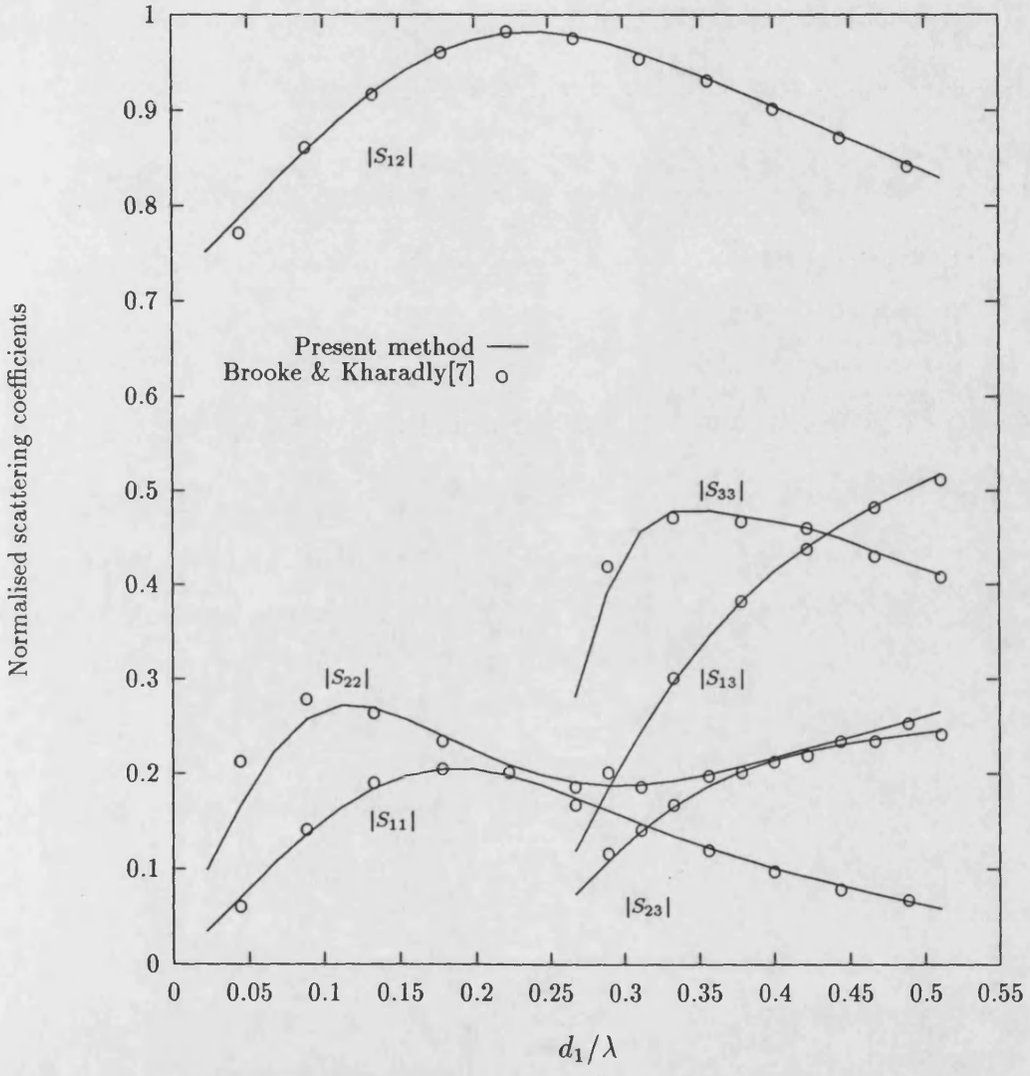

Fig 3.15 TE scattering parameters against normalised frequency.

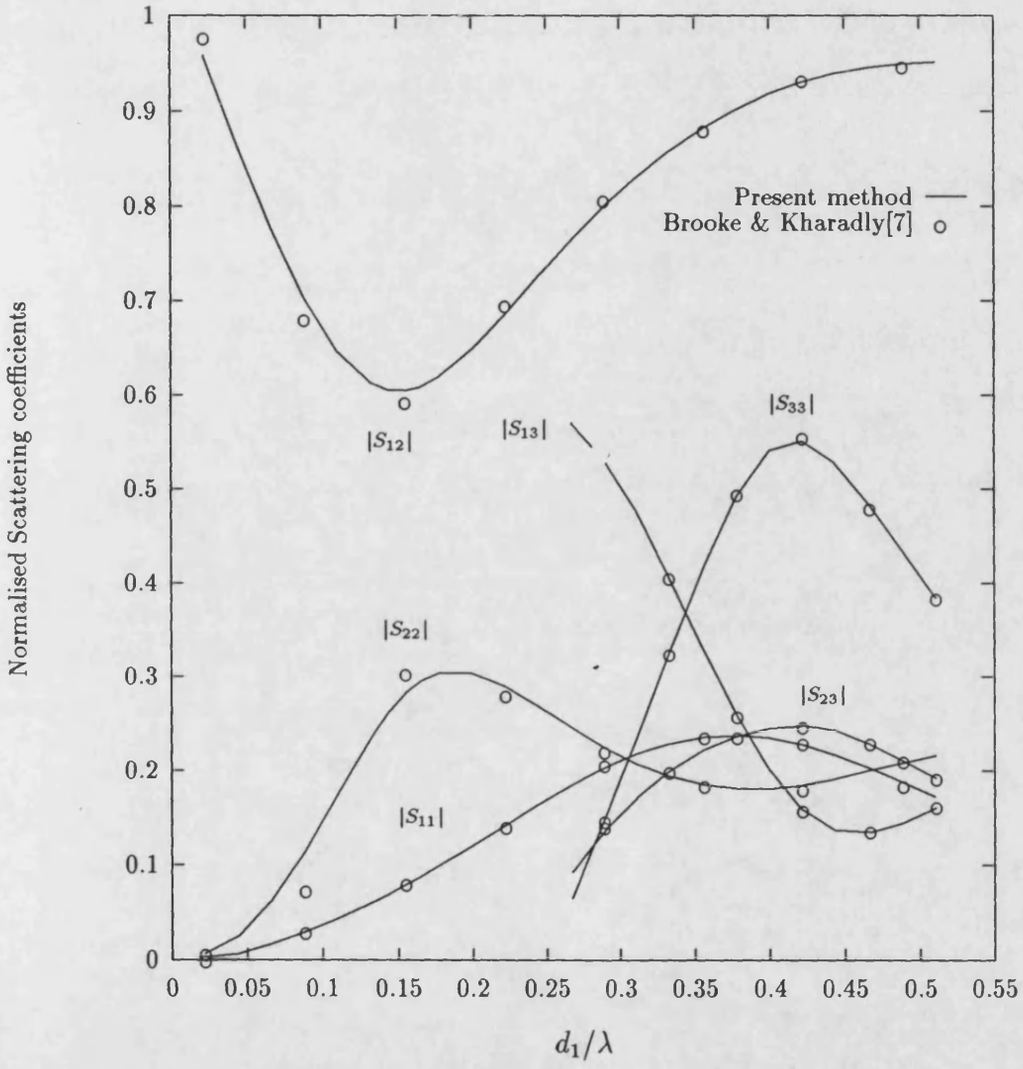

Fig 3.16 TM scattering parameters against normalised frequency.

References

[1] P.J.B.Clarricoats,A.B.Sharpe,"Modal matching applied to a discontinuity in planar surface waveguide",Electron Letter,vol 8, pp 28-29, Jan 1972

[2] D.Marcuse,"Radiation losses of tapered dielectric slab waveguides",Bell System J. vol 49, no. 2, pp 273-290 Feb 1970.

[3] H.Shigesawa,M.Tsuji,K.Takiyama,"Mode propagation through a step discontinuity in dielectric planar waveguide." IEEE MTT-S Digest, pp 121-123,1984

[4] S.Miyanagu,T.Asakura,M.Imai,"Scattering characteristics of a beam mode in dielectric-slab optical guide. Part 2", Optical and Quantum Electronics, pp 23-33, 1980

[5] G.H.Brooke,M.M.Z.Kharadly,"Scattering by abrupt discontinuities on Planar dielectric waveguides." IEEE Trans. MTT, vol MTT-30, No 5, pp 760-769, May 1982

[6] T.E.Rozzi,"Rigorous analysis of the step discontinuity in planar dielectric waveguide", IEEE Trans. MTT, vol MTT-26 pp 738-746, Oct 1978

[7] G.H.Brooke,W.K.McRitchie,"Effect of dielectric edge conditions on mode matching solutions.",Electron Letter vol 11, pp 422-423, Aug 1975

[8] J.Meixner,"The behaviour of electromagnetic fields at edges",IEEE Trans. Antennas Propagation, vol AP-20, pp 442-446, July 1972

[9] C.Vasallo,"On a direct use of the edge condition in modal analysis",IEEE Trans. Microwave Theory Tech., vol MTT-24, pp 208-212, Apr 1976

[10] J.B.Anderson,V.V.Solodukhov,"Field behaviour near a dielectric edge", IEEE Trans. Antenna Propagation, vol AP-26, pp 598-602, July 1978

[11] K.Morishita,S.Inagaki,N.Kumagai,"Analysis of discontinuities in dielectric waveguides by means of the least squares boundary-residual method", IEEE Trans. Microwave Theory Tech., vol MTT-27, pp 310-315, Apr 1979

[12] S.T.Peng,S.J.Xu,F.K.Schewering,"Scattering of surface waves by non-uniform waveguides", IEEE MTT-S Digest, pp 627-629, 1985

[13] L.B.Felsen,N.Markuvitz,"Radiation and Scattering of waves", Englewoods Cliffs, N.J, Prentice Hall, 1973

[14] K.Uchida,K.Aoki,"Scattering of surface waves on transverse discontinuities in symmetrical three-layer dielectric waveguides." IEEE Trans., Microwave Theory Tech., vol MTT-32, No. 1 Jan 1984, pp 11-19

[15] H.Shigesawa,M.Tsuji,K.Takiyama,"Mode propagation through a step discontinuity in dielectric planar waveguide."IEEE MTT-S Digest 1984, pp 121-123

[16] Y.L.Chow,S.C.Wu,"A moment method with mixed basis functions for scattering by waveguide junctions." IEEE Trans. Microwave Theory Tech.,Vol MTT-21, No 5, May 1973, pp 333-340

Chapter 4

The double step discontinuity

4.1 Introduction

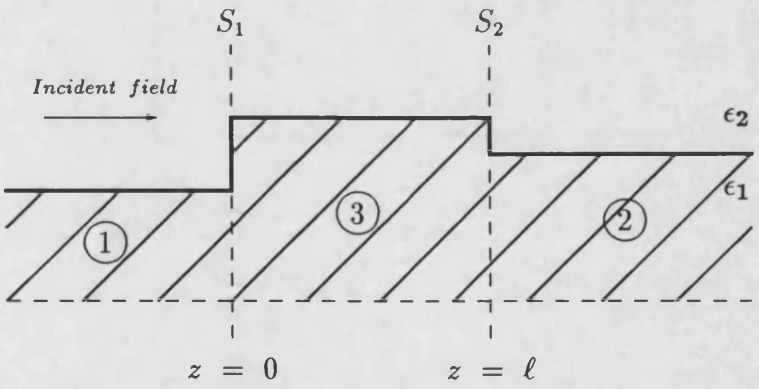

Fig 4.1 Double step discontinuity.

The extension from the case of a single step discontinuity to a double step poses a non-trivial problem. A surface wave incident from the left in Fig 4.1 will be scattered by the step S_1, creating all surface and continuous modes allowable on either side of S_1. A finite range of the continuous modes will be propagating, travelling away from either side of the step. The rest is reactive and non-propagating, representing localised energy storage in the neighbourhood of

the step. The propagating surface and continuous modes that reaches the second step S_2 will be further scattered into all allowable modes on either side of S_2. If the distance between S_1 and S_2 is short compared with the wavelength of the incident field there will be considerable interaction between the scattered waves of the two steps.

For the simple case when the field is well guided and step sizes are small, we may disregard the interaction due to the continuum modes. The problem then reduces to that of two simple steps in cascade. This analysis then results in a model consisting of two discrete multiports connected by transmission lines with each transmission line corresponding to a single surface mode. This is analogous to the representation of interacting discontinuities on closed waveguides [7-8].

Unfortunately for some open structures of interests, such as grating couplers and leaky wave antennas it is precisely the strong interaction of the step discontinuities with the continuum modes that is required for these devices to be effective. Hence the simple model mentioned above cannot be used to describe them.

The double step discontinuities in slab waveguides have already been investigated by a few authors [1-6]. In the case of Shigesawa et.al [1] they have chosen to ignore the interactions of the continuum modes entirely. The reason given was that for the image guide band-stop filter they were analysing, the field will be strongly guided and at the stopband frequencies any contribution from the continuum will be minimal. Although the assumptions seems valid for that specific situation, their analysis is clearly not one of general applicability.

Several variational techniques have also been proposed [2][3][6]. Rozzi's [2] ap-

proach employed normalised Laguerre polynomials to discretize the integral equations, while Uzunoglu [3] solves the coupled integral equations by direct numerical integration in conjunction with repeated iterations to achieve convergence. The approach adopted by the latter seems rather strange as it seems to couple an analytically complex variational method with a brute force numerical integration and iteration process. Although it solves the problem, the process must be exceptionally time consuming. In the case of [6] they have made the assumption that the discontinuities are far apart and non-propagation modes do not cause appreciable interaction in their analysis of double steps in a coaxial line.

While in Hosono's [5] case they have discretized the entire mode spectrum by replacing the problem of an open waveguide with that of a periodical multilayer optical waveguide. This was claimed as a generalisation of a similar method of mode discretization employed by Brooke and Kharadly [4] where a variable bound approach was first proposed. Essentially the method of Hosono's reduces the problem of the interacting double steps to that of two simple steps in cascade. However in this formulation they will have an infinite number of waveguide modes in each region and an approximate solution will be obtained by using a finite number of such modes. Typically the method require a large number of modes before convergence is achieved. In their convergence test it took 20 modes to obtain a solution with relative error of 4.5% and greater than 70 modes to achieve relative error of 0.05%.

It will be shown here, that using the variational approach and the new basis functions presented in the previous chapter a worst case convergence with relative error better than 1.0% can be achieved with only a few terms of the expansion set. Hence the numerical evaluation of the solutions are both efficient and short.

A comparison of our results with Hosono's and another method based on finite element analysis by Koshiba [4] will be given.

4.2 Interacting double steps

Consider the simple case of a single moded semi-infinite slab. It can be modelled by an equivalent semi-infinite transmission line whose characteristic impedance z_o is that of the single moded field travelling in the slab waveguide. By network theory, the Thevenin's equivalent circuit for the transmission line is then as shown in Fig 4.2. This equivalent circuit may be used to represent regions ① and ② of Fig 4.1 for each mode travelling in these regions.

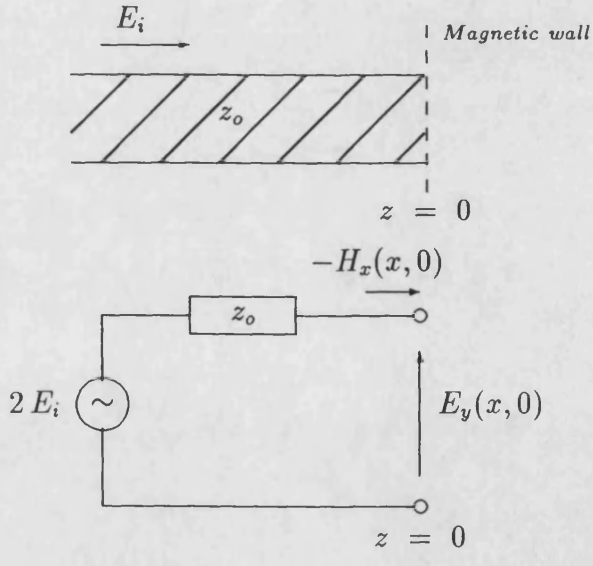

Fig 4.2 Thevenin's equivalent circuit of a semi-infinite slab guide.

The total electric and magnetic fields in region ① can be written in modal form as

$$E_y(x,0) = \sum_{k=1}^{n}(a_k + b_k)\,\varphi_k(x) + \int_0^{\infty} b(\rho)\,\varphi(x,\rho)\,d\rho \qquad (4.1)$$

$$H_x(x,0) \;=\; \sum_{k=1}^{n} \frac{1}{z_{ok}}(a_k - b_k)\,\varphi_k(x) \;-\; \int_0^{\infty} \frac{b(\rho)}{z_o(\rho)}\,\varphi(x,\rho)\;d\rho$$

where a_k is the amplitude of the incident modal fields and $b_k\,, b(\rho)$ are the amplitudes of the reflected modal fields for the surface and continuous modes respectively. $z_{o_1}, \ldots\, z_{o_n}$ are the characteristic impedances of the surface modes and $z(\rho)$ the corresponding impedance of a component of the continuum. By using orthogonality of modes $\varphi_k(x)$ and $\varphi(x,\rho)$ in Eq(4.1) we obtain

$$\begin{aligned} b_k \;&=\; a_k \;-\; z_{ok}\int_0^{\infty} \varphi_k(x')H_x(x')\;dx' \\ b(\rho) \;&=\; z_o(\rho)\int_0^{\infty} \varphi(x',\rho)H_x(x')\;dx' \end{aligned} \tag{4.2}$$

and on substituting for b_k and $b(\rho)$ the scattered field representation at $z \;=\; 0$ can then be given as :-

$$\begin{aligned} E_y(x,0) \;&=\; \sum_{k=1}^{n_1} 2a_k\varphi_k(x) \;+\; \int_0^{\infty} \mathcal{Z}_1(x,x')\,H(x',0) \\ &=\; 2E_1 \;-\; \hat{Z}_1 \cdot [-H(x',0)] \\ \text{with} \quad \hat{Z}_1 \;&=\; \sum_{k=1}^{n_1} z_{ok}\varphi_k(x)\varphi_k(x') \;+\; \int_0^{\infty} z_o(\rho)\varphi(x',\rho)\,\varphi(x,\rho)\;d\rho \end{aligned} \tag{4.3}$$

where $\hat{Z}_1$ is the Green's impedance function (which may also be viewed as the driving-point impedance) of a semi-infinite slab with E_1 the incident field. The dot in the above equation is understood as an integration over x'. By a similar argument, for a field E_2 incident from the right in region ②, we get

$$E_y(x,\ell) \;=\; -2E_2 \;+\; \hat{Z}_2 \cdot [-H(x',\ell)] \tag{4.4}$$

where the positive sign convention is from left to right.

Region ③, which is sectioned off by magnetic walls on both sides, may be similarly modelled by finite lengths of transmission lines (open circuited at both ends) with

each pair of transmission lines corresponding to a mode in the region. Developing this analogy further, each pair of transmission lines may in turn be represented by an equivalent T-network as shown in Fig 4.3.

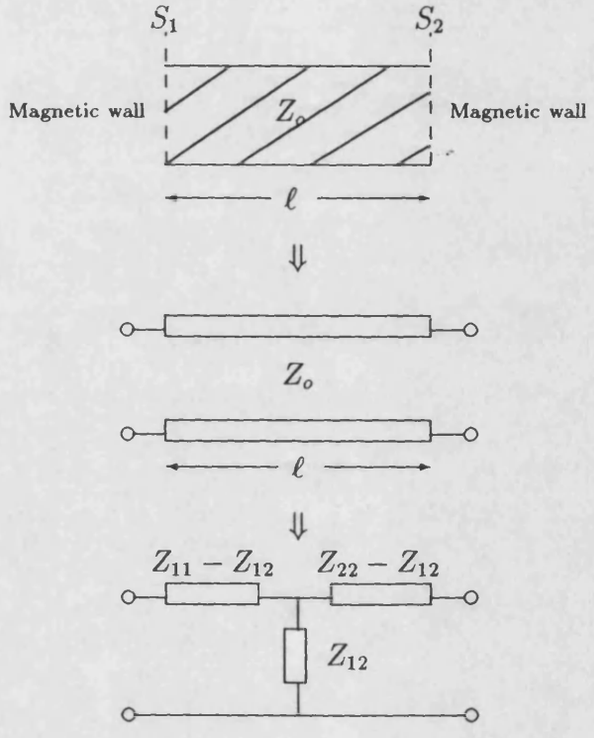

Fig 4.3 Equivalent network representation of a finite length of slab waveguide.

The equivalent values for z_{11}, z_{12} and z_{22} is easily obtained as

$$z_{11} = z_{22} = z_o \coth \gamma\ell \tag{4.5}$$

$$z_{12} = z_o \operatorname{cosech} \gamma\ell$$

where ℓ is the length of region ③ and γ, z_o are respectively the propagation constant and the characteristic impedance of a mode in the region. By applying this analogy to every field mode in region ③ we may infer from Fig 4.3 the relationship of the fields at $z = 0$ and $z = \ell$ of the open circuited section of a

slab as

$$\begin{bmatrix} E_y(x,0) \\ E_y(x,\ell) \end{bmatrix} = \begin{bmatrix} \hat{Z}_{11} & -\hat{Z}_{12} \\ \hat{Z}_{12} & -\hat{Z}_{11} \end{bmatrix} \cdot \begin{bmatrix} -H_x(x',0) \\ -H_x(x',\ell) \end{bmatrix} \tag{4.6}$$

where

$$\begin{aligned} \hat{Z}_{11} &= \sum_{k=1}^{n_3} z_{ok} \coth(\gamma_k \ell)\, \psi_k(x)\, \psi_k(x') \\ &+ \int_0^\infty z_o(\rho) \coth(\gamma(\rho)\ell)\, \varphi(x,\rho)\, \varphi(x',\rho)\, d\rho \end{aligned} \tag{4.7}$$

$$\begin{aligned} \hat{Z}_{12} &= \sum_{k=1}^{n_3} z_{ok} \mathrm{cosech}(\gamma_k \ell)\, \psi_k(x)\, \psi_k(x') \\ &+ \int_0^\infty z_o(\rho) \mathrm{cosech}(\gamma(\rho)\ell)\, \varphi(x,\rho)\, \varphi(x',\rho)\, d\rho \end{aligned}$$

The integral over ρ in $\hat{Z}_{11}$ and $\hat{Z}_{12}$ is evaluated analytically by the *method of residues.* The details of which is given in Appendix F. Eq (4.6) presents a "two-port" Green's impedance operator for the open circuited section of region ③. Consider now that this open circuited section is "loaded" by the semi-infinite slab guides of region ① and ② and that there are propagating fields E_1 incident from the left and E_2 from the right of

$$\begin{aligned} E_1(x,0) &= \sum_{k=1}^{n_1} a_k \psi_k(x) \\ E_2(x,\ell) &= \sum_{k=1}^{n_2} a_k \psi_k(x) \end{aligned} \tag{4.8}$$

The "loading" of the open circuited section of the guide in circuit terms is really equivalent to the imposition of field continuity at S_1 and S_2. The abstract network representation of this is shown in Fig 4.4 Hence from Eq(4.2),(4.3) and (4.4) the Green's impedance operator of the double step is obtained :-

$$\begin{bmatrix} E_1(x,0) \\ E_2(x,\ell) \end{bmatrix} = \frac{1}{2} \begin{bmatrix} \hat{Z}_1 + \hat{Z}_{11} & -\hat{Z}_{12} \\ -\hat{Z}_{12} & \hat{Z}_2 + \hat{Z}_1 1 \end{bmatrix} \cdot \begin{bmatrix} -H(x,0) \\ -H(x,\ell) \end{bmatrix} \tag{4.9}$$

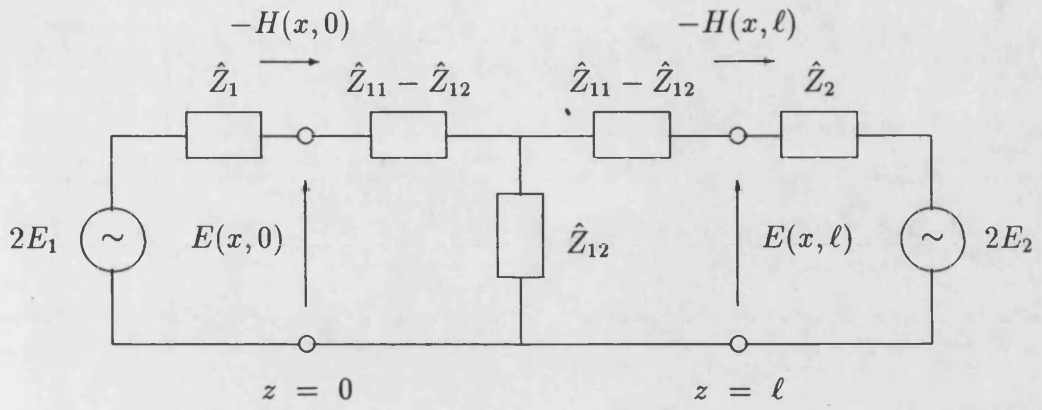

Fig 4.4 Equivalent network model of a interacting double step discontinuity.

The coupling of the modes between the interacting steps is essentially represented by the $\hat{Z}_{12}$ term in the above equation. In this form it is noted that the modes in the intervening length of guide are no longer accessible.

4.2.1 A discrete representation of the field.

The integral equations of Eq(4.9) can be reduced to a finite matrix equation by the usual projection of the modal functions onto a suitable set of basis functions. The mechanics of which have been described in the previous chapter and will not be repeated here.

There is however one point that is worthy of mention. That is two different sets of expansion functions may be used, one for each step S_1 and S_2. This is possible because the modal field terms in region ① and ② never mix in the scattering formulation of Eq(4.9). This is a considerable advantage especially if ① is very different from region ②, requiring a very different "fit" for the two set of basis

functions. Moreover we may write the vectorized form of Eq(4.9) as

$$\begin{bmatrix} \bar{\mathbf{E}}_1 \\ \bar{\mathbf{E}}_2 \end{bmatrix} = \frac{1}{2} \begin{bmatrix} \bar{\mathbf{Z}}_1 + \bar{\mathbf{Z}}_{11} & -\bar{\mathbf{Z}}_{12} \\ -\bar{\mathbf{Z}}_{12}^t & \bar{\mathbf{Z}}_2 + \bar{\mathbf{Z}}_{11} \end{bmatrix} \begin{bmatrix} -\bar{\mathbf{H}}_1 \\ -\bar{\mathbf{H}}_2 \end{bmatrix} \tag{4.10}$$

$$= \mathbf{Z}_s \begin{bmatrix} -\bar{\mathbf{H}}_1 \\ -\bar{\mathbf{H}}_2 \end{bmatrix}$$

Using Eq(4.2) and (4.10), the derivation of the normalised scattering matrix elements S_{kl} is formally the same as for the single step, and we get

$$S_{kl} = \delta_{kl} - s_k s_l \sqrt{z_{ok} z_{ol}}\ \mathbf{U}_k^t\, \mathbf{Z}_s^{-1}\, \mathbf{U}_l \tag{4.11}$$

$$\delta_{kl} = \begin{cases} 1 & : k = l \\ 0 & : k \neq l \end{cases}$$

$$1 \leq k, l \leq n_1 + n_2$$

$$s_k,\ s_l = \begin{cases} 1 & : k \leq n_1 \quad : \text{region } ① \\ -1 & : k > n_1 \quad : \text{region } ② \end{cases}$$

$$\mathbf{U}_k = \begin{cases} \mathbf{P}_k & : k \leq n_1 \quad : \text{region } ① \\ \mathbf{R}_k & : k > n_1 \quad : \text{region } ② \end{cases}$$

$\mathbf{P}_k$ and $\mathbf{R}_k$ are the column vectors of the modal expansion coefficients in region ① and ② respectively.

4.3 Numerical results

The results presented here are for a symmetric slab excited by even TE modes. As a demonstration of the rapid convergence of the variational solution using an intermediate mode basis function set, both the phase and magnitude of S_{11} and S_{12} of a double step were plotted against frequency for varying order of solution N. The results are shown in Fig 4.5a to Fig 4.5d. The slab guides on either side of the double step begins to support a second mode at 21 GHz. It is evident from the figures that the second mode has a strong effect on the 1^{st} order variational solution (N=1). This effect is particularly evident on the phase of S_{11} and starts

TABLE 4.1
Convergence test of surface mode basis functions at 21GHz

N	$\lvert S_{11}\rvert$	$\angle S_{11}$ (π rad)	$\lvert S_{12}\rvert$	$\angle S_{12}$ (π rad)	$1-\lvert S_{11}\rvert^2-\lvert S_{12}\rvert^2$
1	0.06621	2.1103	0.96742	1.0213	4.38376e-3
2	0.07047	1.3916	0.99513	1.0502	4.75026e-3
3	0.02295	1.2982	0.99878	1.0272	1.91181e-3
4	0.00330	1.4626	0.98172	1.0303	3.56991e-2
5	0.00338	1.5739	0.98340	1.0321	3.29130e-2
10	0.00335	1.5812	0.98331	1.0321	3.31099e-2

at around 16 GHz. This is because the "intermediate" guide from which the trial mode is derived from have a thickness given by $\sqrt{d_1 d_3}$ so its wider than the actual slab guides and becomes overmoded sooner.

However as soon as the second mode is included in the expansion set, the solution quickly converges. The numerical values of the scattering parameters at 21 GHz is given in Table 4.1. The error at N=5 is 0.594% relative to the 10^{th} order solution. The degenerate case when the double step completely disappears leaving an air gap between two semi-infinite slab have been analysed before [4],[2]. In this case the surface modes in the mid-region no longer exist and coupling of the modes are through degenerate continuum modes. The results given by the present method in Fig 4.6 compares well with those of Koshiba [4]. While the transmission coefficient S_{12} decreases slowly with increasing gap length, the reflection coefficient S_{22} is seen to approach that of a semi-infinite slab guide radiating into air half space.

The variation of S_{11} and S_{12} with increasing step height is given in Fig 4.7. The ratio of the radiated power to incident power is also shown. It is interesting to note that S_{11} , S_{12} and the radiated power all tends to a limit as the step height is increased. The reason is for very large step height, the middle region effectively

becomes a dielectric layer between two semi infinite slab and the incident wave no longer feels the effect caused by the corners of the step. The phase of S_{11} also an interesting 180° flip as the middle region changes from a groove to a ridge.

The effect of loss in the dielectric region has also been investigated. The results shown in Fig 4.8 for a sizeable step shows the reflection coefficient increasing rapidly for increasing loss, while the transmission coefficient decreases at a slower rate. Phase changes are negligible.

Another comparison with the results of [4] and [5] is given in Fig 4.8. The figure shows the results obtained by the present method display a stronger interaction of the steps, with the peaks of S_{11} being higher than those obtained by Hosono [5] and Koshiba [4]. However Koshiba stated in his paper that he may have taken an insufficient number of elements in the computation for $\ell/d_1 > 3.5$. In Hosono's case, he had used only 30 modes for his results which by his own calculations gives 3-10% error. In any case it seems quite improbable that he could have taken proper account of the continuous modes. On the other hand a 5^{th} order intermediate mode set with the present method is found to give a relative error of less than 0.8%. The stronger reflection peaks is likely to be due to the variational solution accounting for more of the interaction caused by the continuous modes. The peaks in the scattering values are the result of resonances in the middle region as its length is varied.

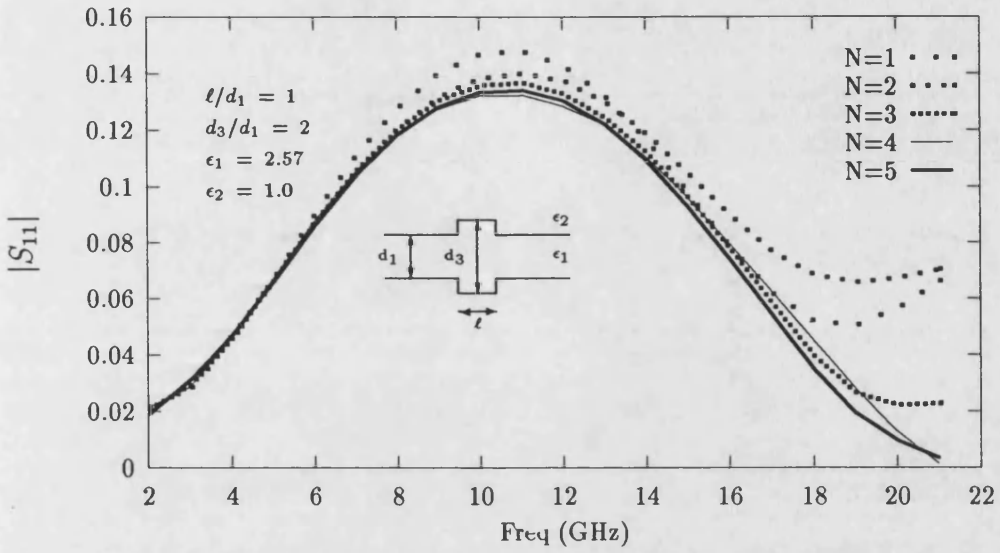

Fig 4.5a $|S_{11}|$ against frequency for different order of solution N.

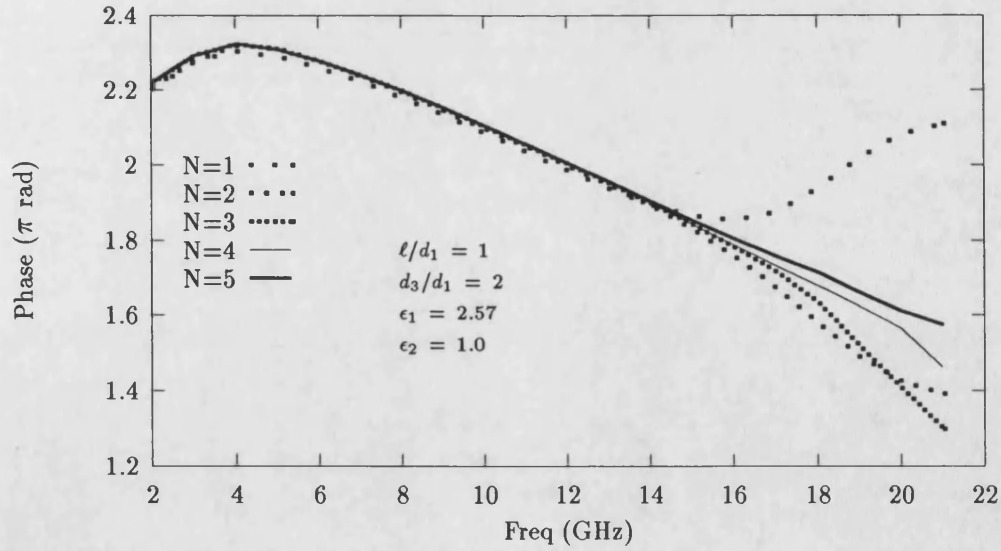

Fig 4.5b $\angle S_{11}$ against frequency for different order of solution N.

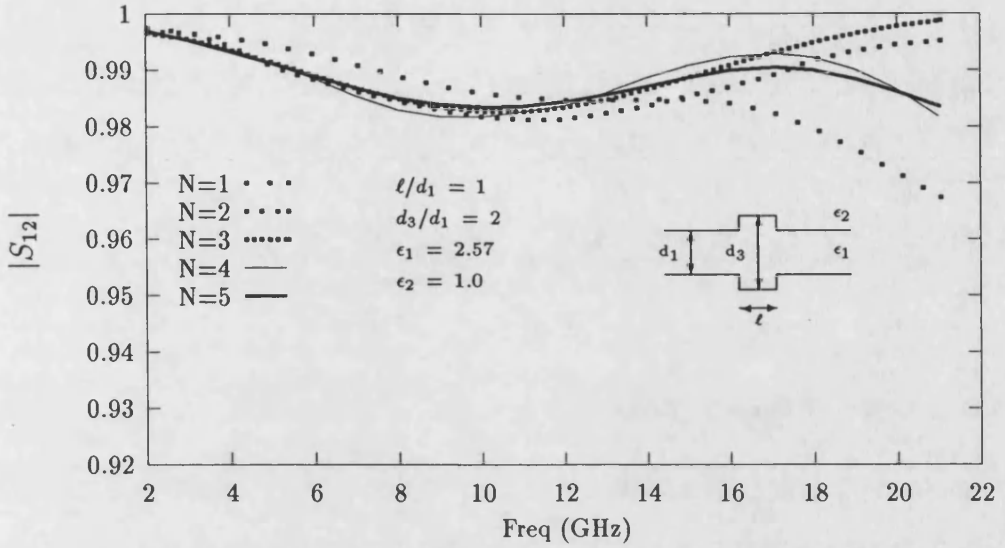

Fig 4.5c $|S_{12}|$ against frequency for different order of solution N.

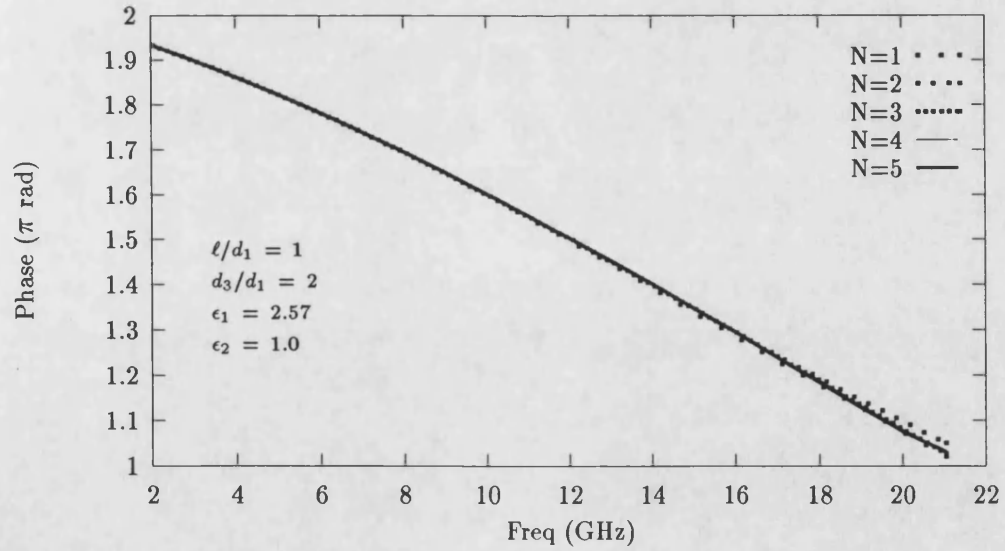

Fig 4.5d $\angle S_{12}$ against frequency for different order of solution N.

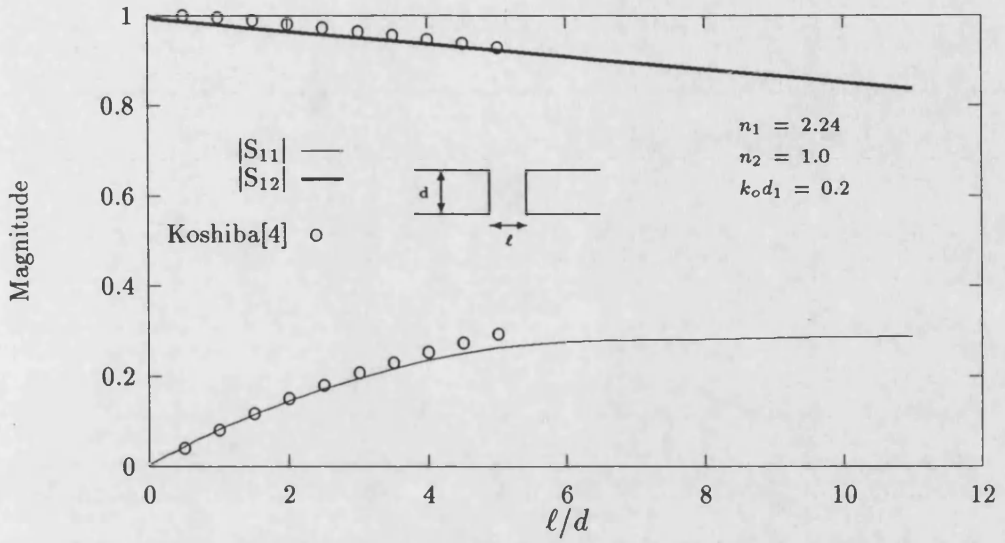

Fig 4.6a Scattering magnitude against gap length.

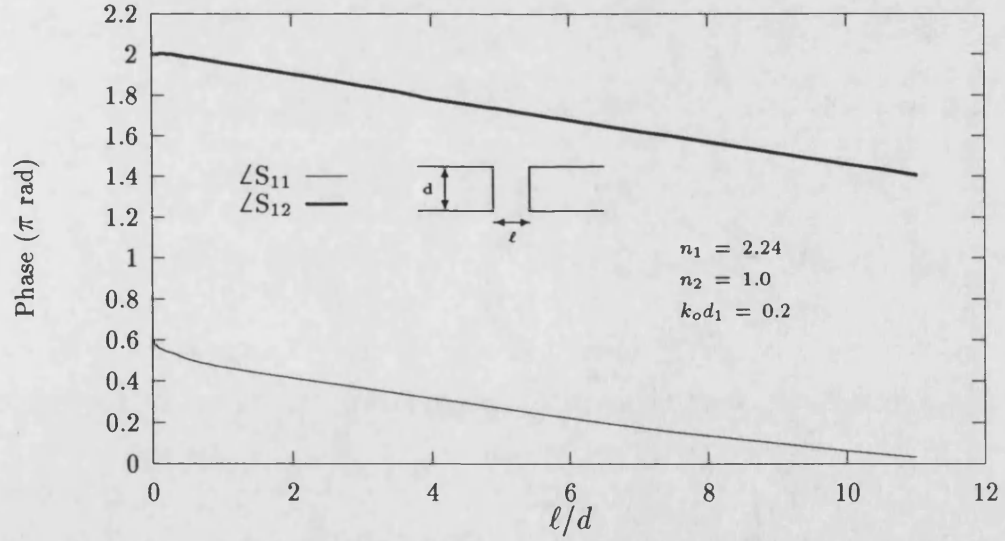

Fig 4.6b Scattering hase against gap length.

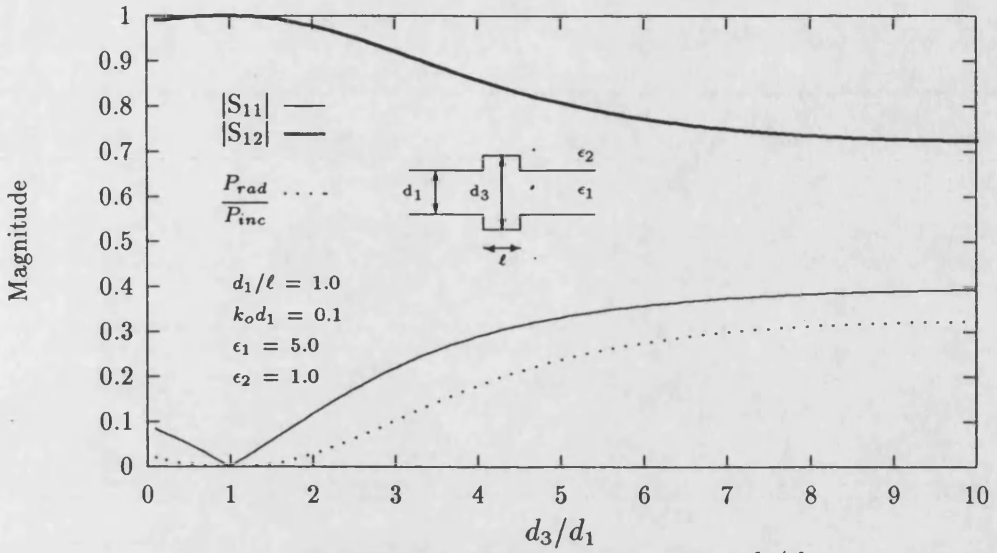

Fig 4.7a Scattering magnitude against d_3/d_1.

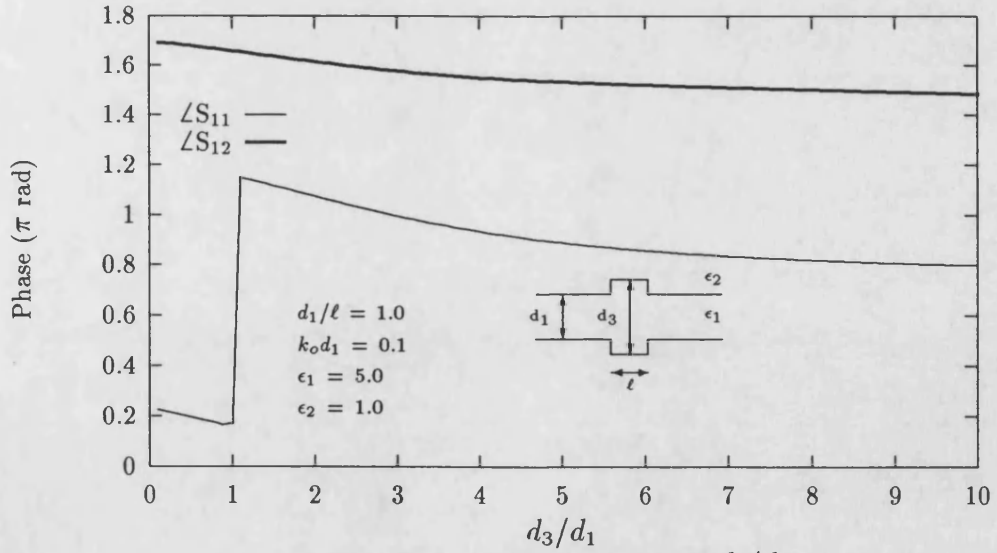

Fig 4.7b Scattering phase against d_3/d_1.

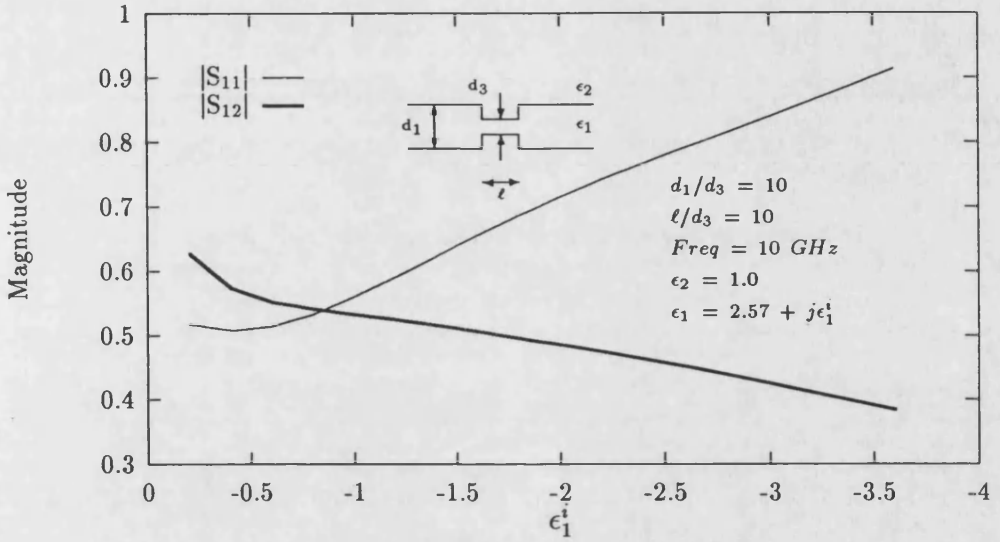

Fig 4.8a Scattering magnitude against loss.

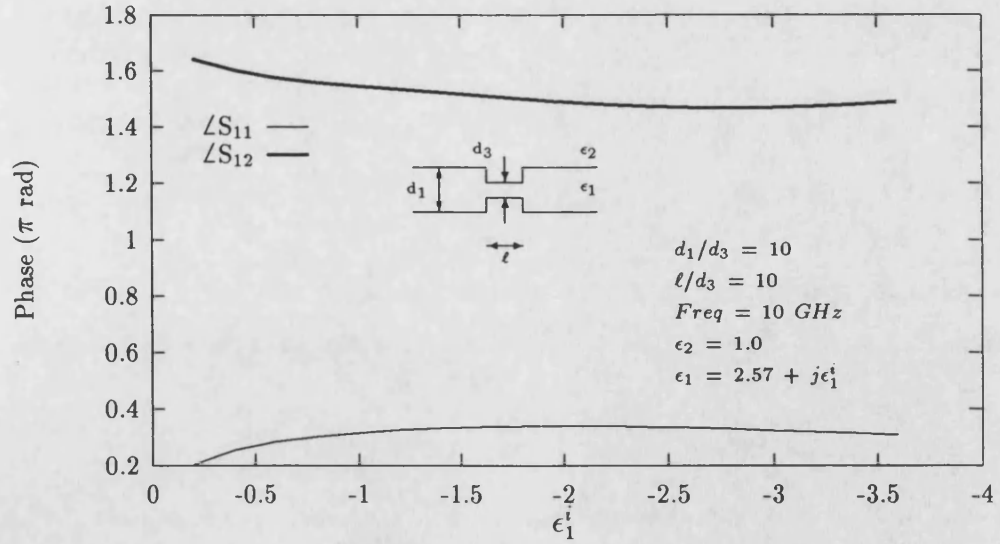

Fig 4.8b Scattering phase against loss.

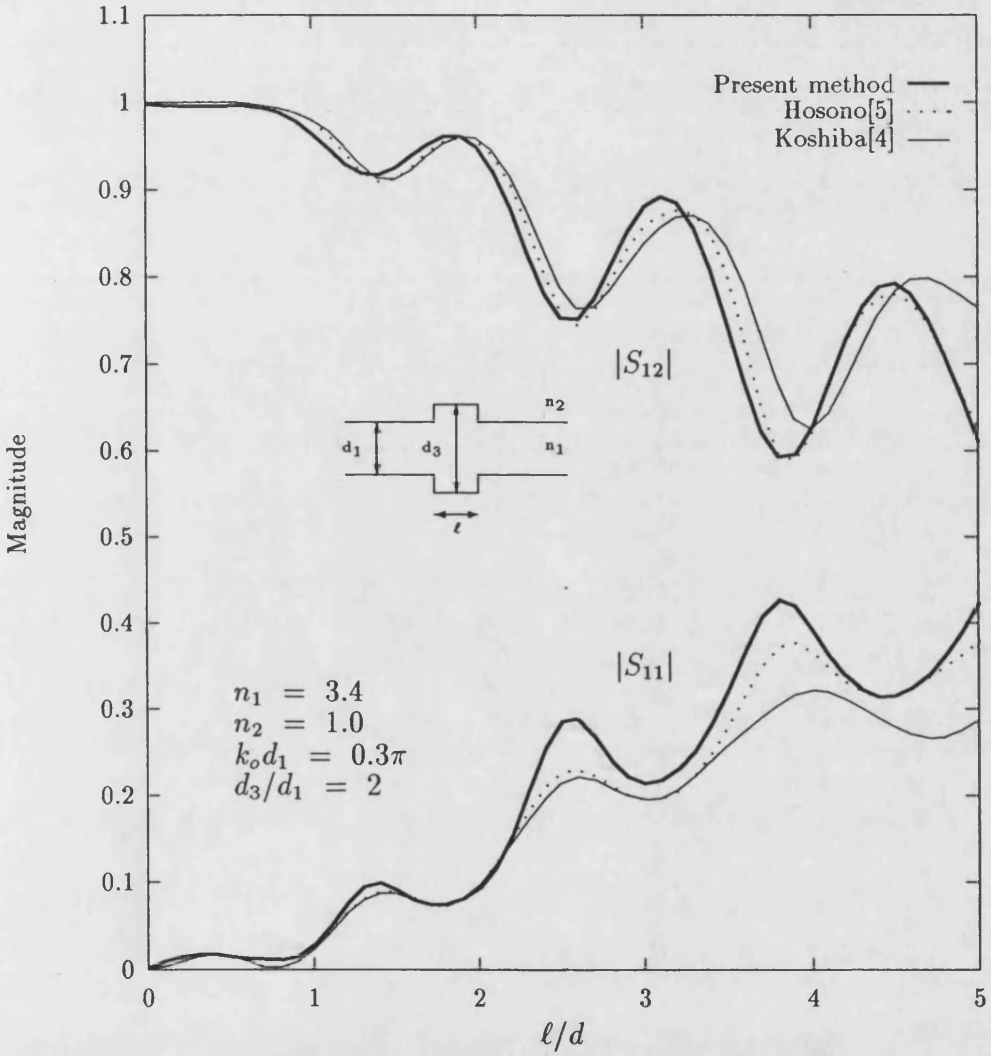

Fig 4.9 Scattering magnitudes against step length.

References

[1] H.Shigesawa,M.Tsuji,"A completely theoretical design method of dielectric image guide gratings in the Bragg Reflection region.", IEEE Trans, MTT, vol MTT-34, No 4, April 1986. pp 420-426

[2] T.Rozzi,G.H.In,t Veld,"Field and network analysis of interacting step discontinuities in planar dielectric waveguides." IEEE Trans, MTT, vol MTT-27, No 4, April 1979. pp 303-309.

[3] P.G.Cottis,N.K.Uzunoglu,"Analysis of longitudinal discontinuities in dielectric slab waveguides." J.Opt. Soc. Am. A/Vol.1 No 2, Feb 1984, pp 206-215

[4] M.Koshiba,T.Miki,K.Ooishi,M.Suzuki,"On Finite-Element Solutions of the Discontinuity Problems in a Bounded Dielectric Slab Waveguide", IECE Trans. vol. E 66 No 4 April 1983, pp 250-251

[5] T.Hosono,T.Hinata,A.Inoue,"Numerical analysis of the discontinuities in slab waveguides", Radio Science, Volume 17, No.1, pp 75-83, Jan-Feb 1982

[6] I.Screenvivasiah,D.C.Chang,"Variational expression for the scattering matrix of a double step discontinuity in a coaxial line and its application to a TEM cell." IEEE Trans., Vol MTT-29, No 1, Jan 1981, pp 40-47.

[7] H.Patzenlt,F.Arndt,"Double-plane steps in the rectangular waveguides and their applications for transformers, Irises, and Filters." IEEE Trans., Microwave Theory Tech., Vol MTT-30, No. 5, May 1982, pp 771-776

[8] D.Dasgupta,P.K.Saha,"Eigenvalue spectrum of rectangular waveguide with two symmetrically placed double ridges." IEEE Trans., vol MTT-29, No 1, Jan 1981, pp 47-51.

[9] H.Shigesawa,M.Tsuji,K.Takiyama,"Microwave network representation of discontinuity in open dielectric waveguides and its applications to periodic structures", Digest 1985, IEEE MTT-S INT. Microwave Symposium, June 1985

[10] M.Tsuji,S.Matsumoto,H.Shigesawa,K.Takiyama,"Guided-wave experiments with dielectric waveguides having finite periodic corrugations." IEEE Trans., MTT, Vol MTT-31, No 4, April 1983, pp 337-344

Chapter 5

Cascaded Step Discontinuities

5.1 Introduction

Cascaded structures in general and periodic structures in particular were the object of much study in the past. In the early 1970's, new development in the fabrication of thin film optical waveguides have found applications for periodic gratings in DFB and DBR lasers [6-10], and in grating couplers [2], bandstop filters [12-14] and modulators [15,16]. The advantages of these devices lies in their integratability with other devices on a planar circuit; and since their operation depends on the phase synchronised cumulative effects of each individual element they are also tolerant to random defects in the manufacturing process, and as in the case of DFB lasers, they can offer longitudinal mode selection and higher power handling capabilities.

As interest in millimeter wave systems has grown it was recognised that the same optical devices could be adapted for millimeter wavelength use. This has led to the design of bandstop filters on image guides [12,13] and leaky-wave antennas

[3,4]; the latter is very similar to the grating coupler. The same concept has also suggested the possible use of DBR oscillators employing several diodes to achieve a high power output [17].

Thus it is not surprising that most of the techniques used in the analysis of such devices followed the same techniques as were applied in integrated optics. These methods are either based on the approximate coupled modes approach or the more rigorous space harmonic expansion approach which involves solving a wave equation of the Hill's type. Both are however only effective for solving periodic structures of infinite extent. While this may not present any problems in the case of optical devices where very fine periodicities are used and the number of periods are of the order of 1000 or more such conditions do not apply to their microwave counterparts. The number of corrugations used for millimeter wavelength devices are limited by the inherent loss and the requirement for small size. A hundred corrugations at X-band will be over 50 cm long. Calculation of the exact radiation pattern of a leaky-wave antenna for instance, must therefore include a description of the discontinuities at either end since the terminations will cause effects such as radiation pattern distortion and increased side-lobe levels.

In this chapter a new method for solving field scattering by finite periodic structures is presented. The method is based on the extension of the technique used in solving the interacting double steps. Here the periodic structure is considered as a cascade of interacting step discontinuities. Several finite lengths of waveguide are cascaded together to form a unit cell. Since the field problem of a finite length of guide (ie. of the interacting step discontinuity) has already been solved in chapter 4 it will not be repeated here. Instead, we shall concentrate on the network approach to the field problem of cascaded structures.

Whereas in the previous chapter the field problem describing the finite length of waveguide was written in an impedance matrix form it is now more convenient to have it in a transmission matrix form. This is because the periodic structure is described by the equivalent cascade of multi-port networks, which will then be easily solved by the cascade multiplication of the transmission matrices. Once that has been done the impedance matrix will be recovered by a reverse transformation. The scattering parameters can then be obtained in a manner similar to that described for the interactive double steps.

It should be emphasised that in the present analysis we are not limited to the case of periodic structures with identical unit cells. Indeed, each unit cell may itself be composed of cascades of other cells to form structures of arbitrary complexities. For example, an approximation to the blazed grating [18,19] can be made by cascading together unit cells of increasing height.

Radiation coupling between the cascaded cells is also automatically included because the cell networks consists not only of the 2N ports for the N surface waves but also a continuum of ports for the continuous spectrum (ie. radiation). Together the ports represent the entire field in the area for $-\infty < x < \infty$ (see Fig 5.1)

The resultant composite *cell* can then be used to build the periodic structure. Similarly, cell elements with increasing periodicity can be cascaded together to give a chirped grating [21], which have the property of being able to focus its radiated power to a point outside the waveguide. Another interesting structure is the log-periodic grating. In this structure each element has its period and grating height increased in a log-periodic manner. Its behaviour is similar to

that of the blazed grating but its effects prevail over a much wider bandwidth.

It may be pointed out that although the present analysis is done in 2-dimensions, the results obtained may still be valid for 3-dimensions if the guiding structure is more than a wavelength wide in the 3rd dimension. This has been shown by [3] in which the effects of the width on the corrugated image guide was studied using the EDC (Effective Dielectric Constant) method. Moreover, the troublesome TE-TM coupling caused by oblique incidence of the guided wave on the periodic structure is absent in the frequency range of interest if symmetric excitation of the periodic structure is considered [14].

5.2 The Unit Cell

5.2.1 Impedance matrix

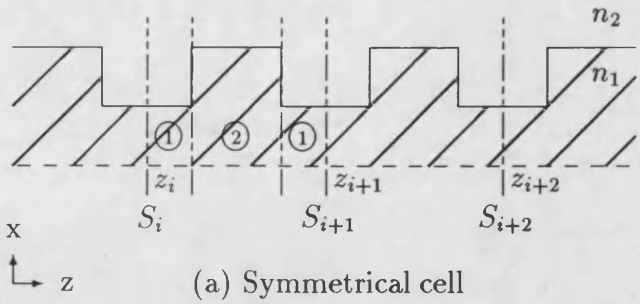

(a) Symmetrical cell

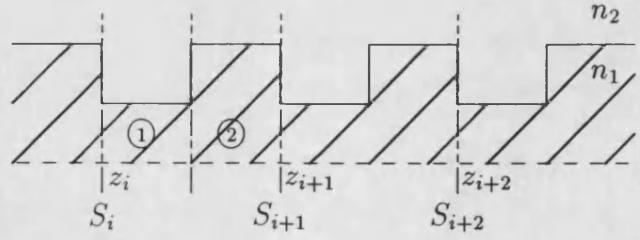

(b) Asymmetrical cell

Fig 5.1 Cascaded steps

Consider the finite length of guide between the planes S_i and S_{i+1} in Fig. 5.1. If magnetic walls are placed at S_i and S_{i+1}, then the uniform section of guide can be regarded as an open circuited stub and the electric and magnetic fields will be related by the expression (Ch.4, Eq.(4.10))

$$\begin{pmatrix} E(x,z_i) \\ E(x,z_{i+1}) \end{pmatrix} = \begin{pmatrix} \hat{\mathbf{Z}}_{11}^{(i)} & \hat{\mathbf{Z}}_{12}^{(i)} \\ \hat{\mathbf{Z}}_{12}^{(i)} & \hat{\mathbf{Z}}_{11}^{(i)} \end{pmatrix} \begin{pmatrix} -H(x,z_i) \\ -H(x,z_{i+1}) \end{pmatrix} \tag{5.1}$$

where $\hat{\mathbf{Z}}_{11}^{(i)}$ and $\hat{\mathbf{Z}}_{12}^{(i)}$ are the two port impedance operator of the i^{th} section. By employing an appropriate set of expanding functions the 2×2 operator form of Eq. (5.1) is transformed to a discrete matrix representation,

$$\begin{pmatrix} \mathbf{E}_1 \\ \mathbf{E}_2 \end{pmatrix} = \begin{pmatrix} \mathbf{Z}_{11} & \mathbf{Z}_{12} \\ \mathbf{Z}_{12}^t & \mathbf{Z}_{11} \end{pmatrix} \begin{pmatrix} \mathbf{H}_1 \\ \mathbf{H}_2 \end{pmatrix} \tag{5.2}$$

which can be translated to the equivalent network form of Fig. 5.2. Continuity of the transverse fields at z_i.

$$\begin{aligned} E(x,z_i^-) &= E(x,z_i^+) \\ H(x,z_i^-) &= H(x,z_i^+) \end{aligned} \tag{5.3}$$

then becomes the continuity of voltages and currents at the corresponding plane. To reflect this, Eq. (5.2) is re-written as,

$$\begin{pmatrix} \mathbf{V}_1 \\ \mathbf{V}_2 \end{pmatrix} = \begin{pmatrix} \mathbf{Z}_{11} & \mathbf{Z}_{12} \\ \mathbf{Z}_{12}^t & \mathbf{Z}_{11} \end{pmatrix} \begin{pmatrix} \mathbf{I}_1 \\ -\mathbf{I}_2 \end{pmatrix} \tag{5.4}$$

It should be pointed out that Eq. (5.1) relates the total field at the planes S_i and S_{i+1} and any interactions by the continuum within the finite section of guide is

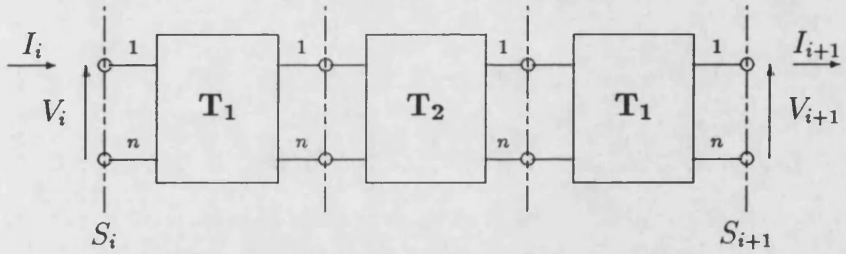

(a) Symmetrical cell

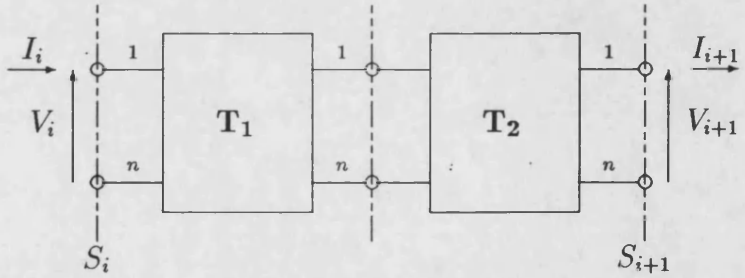

(b) Asymmetrical cell

Fig 5.2 Equivalent N-Port network.

built into the model. The problem of the cascaded structure, now becomes one of cascaded '2N-ports'. This is most conveniently solved by cascade multiplication of the transmission matrix of each individual block.

5.2.2 Transmission matrix

With reference to Fig 5.2, the transmission or ABCD matrix is written as,

$$\begin{pmatrix} \mathbf{V_1} \\ \mathbf{I_1} \end{pmatrix} = \begin{pmatrix} \mathbf{A} & \mathbf{B} \\ \mathbf{C} & \mathbf{D} \end{pmatrix} \begin{pmatrix} \mathbf{V_2} \\ \mathbf{I_2} \end{pmatrix} \tag{5.5}$$

Using Eq. (5.4),the above expression can easily be re-written in terms of the impedances to give,

$$\begin{pmatrix} \mathbf{V_1} \\ \mathbf{I_1} \end{pmatrix} = \begin{pmatrix} \mathbf{Z_{11}(Z_{12}^t)^{-1}} & \mathbf{Z_{11}(Z_{12}^t)^{-1}Z_{22} - Z_{12}} \\ \mathbf{(Z_{12}^t)^{-1}} & \mathbf{(Z_{12}^t)^{-1}Z_{22}} \end{pmatrix} \begin{pmatrix} \mathbf{V_2} \\ \mathbf{I_2} \end{pmatrix} \tag{5.6}$$

The impedance matrix formulation in terms of the ABCD parameters can be similarly derived, and is given as,

$$\begin{pmatrix} \mathbf{V_1} \\ \mathbf{V_2} \end{pmatrix} = \begin{pmatrix} \mathbf{AC^{-1}} & \mathbf{AC^{-1}D - B} \\ \mathbf{C^{-1}} & \mathbf{C^{-1}D} \end{pmatrix} \begin{pmatrix} \mathbf{I_1} \\ \mathbf{-I_2} \end{pmatrix} \tag{5.7}$$

Not surprisingly, this is very similar in form to Eq. (5.6). For a symmetrical two-port,

$$Z_{11} = Z_{11}^t = Z_{22} ,$$

$$Z_{12} = {Z_{12}}^t \tag{5.8}$$

From Eqs. (5.6) and (5.8),one can further deduce that,

$$\mathbf{D} = \mathbf{A}^t$$

$$\mathbf{I} = \mathbf{A}\mathbf{C}^{-1}\mathbf{D}\mathbf{C} - \mathbf{B}\mathbf{C} \tag{5.9}$$

Depending on the choice of the reference planes the unit cell may be symmetrical or asymmetrical (Fig. 5.1). It may be possible in the case of uniform periodic structures to choose the reference planes such that the unit cell is always symmetrical. In the general case of non-uniform periodic structures the cell will be asymmetrical. As will be shown later the latter case has to be solved quite differently. The equivalent networks for the two different choice of reference planes is shown in Fig. 5.2. By inferring from Fig 5.2, the symmetrical case can be written as,

$$\begin{pmatrix} \mathbf{V}_i \\ \mathbf{I}_i \end{pmatrix} = \mathbf{T}_1\mathbf{T}_2\mathbf{T}_1 \begin{pmatrix} \mathbf{V}_{i+3} \\ \mathbf{I}_{i+1} \end{pmatrix} = \mathbf{T} \begin{pmatrix} \mathbf{V}_{i+3} \\ \mathbf{I}_{i+1} \end{pmatrix} \tag{5.10}$$

where $\mathbf{T}_1$ and $\mathbf{T}_2$ are the transmission matrices of regions ① and ② in Fig. 5.1a, and Tis the transmission matrix of the unit cell.

5.3 Canonical form of the Transmission Matrix

For a cascade of n unit cells, then T in Eq. (5.10) is merely raised to the power n. However, the evaluation of $\mathbf{T}^n$ may pose numerical problems, particularly for large n, since $\mathbf{T}$ is a $2N \times 2N$ matrix for a N^{th} order solution. We overcome this problem by first making use of the following canonical decomposition,

$$\mathbf{T} = \mathbf{M}\,\mathbf{S}\,\mathbf{M}^{-1} \tag{5.11}$$

where **M** is the *modal* matrix whose columns are the eigenvectors of **T**, and **S** is the diagonal *spectral* matrix, whose diagonal elements are the eigenvalues of **T**. Then,

$$\mathbf{T}^n = \mathbf{M}\,\mathbf{S}^n\mathbf{M}^{-1} \tag{5.12}$$

Since $\mathbf{S}^n$ only involves raising the individual eigenvalue to the power n, the problem of error propagation in computing the series product of **T** is avoided.

5.3.1 Transmission matrix of the 1^{st} order

At this point it may be instructive to consider the simple case when **T** is just a 2×2 matrix. This corresponds to a Ritz-Galerkin solution of the first order. The extension to the general N^{th} order solution will be given later, but the basic principles remain the same. Then for a cascade of n identical two-ports, we have,

$$\begin{pmatrix} V_1 \\ I_1 \end{pmatrix} = \mathbf{T}^n \begin{pmatrix} V_n \\ I_n \end{pmatrix} \tag{5.13}$$

or in expanded form,

$$\begin{pmatrix} V_1 \\ I_1 \end{pmatrix} = \begin{pmatrix} A & B \\ C & D \end{pmatrix}^n \begin{pmatrix} V_n \\ I_n \end{pmatrix} \tag{5.14}$$

In order to express **T** in the form of Eq. (5.12), the eigenvalues and eigenvectors of **T** needs to be determined. The eigenvalues are simply given by the roots of the characteristic equation,

$$\det(\,\mathbf{T} - \lambda\mathbf{I}\,) = \lambda^2 - (A + D)\lambda + (AD - BC) = 0 \tag{5.15}$$

which reduces to,

$$\lambda^2 + (A + D)\lambda + 1 = 0 \tag{5.16}$$

since $AD - BC = \det \mathbf{T} = 1$. The solution of the above quadratic then gives,

$$\begin{aligned} \lambda_1 &= t + \sqrt{(t^2 - 1)} \\ \lambda_2 &= t - \sqrt{(t^2 - 1)} \\ t &= \frac{A + D}{2} \end{aligned} \tag{5.17}$$

where they have the properties

$$\lambda_1 \lambda_2 = \det \mathbf{T} = 1 \tag{5.18a}$$

$$\lambda_1 + \lambda_2 = \text{trace } \mathbf{T} = A + D \tag{5.18b}$$

The condition of Eq. (5.18a) means that the eigenvalues can be written in the form,

$$\lambda_1 = e^{\gamma \ell} \ , \ \lambda_2 = e^{-\gamma \ell} \tag{5.19}$$

where γ is known as the propagation constant of the quadrapole. Eq. (5.19) is merely a statement of the reciprocity of the transmission matrix. The corresponding eigenvectors are then obtained from the requirement,

$$\begin{pmatrix} A & B \\ C & D \end{pmatrix} \begin{pmatrix} x_1 \\ x_2 \end{pmatrix} = \lambda \begin{pmatrix} x_1 \\ x_2 \end{pmatrix} \tag{5.20}$$

It is clear from Eq. (5.20) that only the ratio x_1/x_2 of the eigenvectors can be determined. These are given as,

$$\begin{aligned} Z_v = \left(\frac{x_1}{x_2}\right)_{\lambda=\lambda_v} &= \frac{\lambda_v - D}{C} \ , \ v = 1, 2 \\ &= \frac{A - D}{2C} \pm \frac{\sinh \gamma \ell}{C} \end{aligned} \tag{5.21}$$

If the four terminal network is symmetrical (or reversible), then by Eq. (5.9),

$$Z_1 = -Z_2 = \frac{\sinh \gamma \ell}{C} = \left(\frac{B}{C}\right)^{\frac{1}{2}} = Z_o \tag{5.22}$$

It is inferred from Eqs. (5.5) and (5.6) that Z_1 and Z_2 have dimensions of impedance. Z_o is commonly known as the characteristic impedance of **T**. Since only the ratios of the eigenvectors are specified is possible to define **M** as

$$\mathbf{M} = \begin{pmatrix} Z_1 & Z_2 \\ 1 & 1 \end{pmatrix} \tag{5.23}$$

and its inverse

$$\mathbf{M}^{-1} = \frac{1}{(Z_1 - Z_2)} \begin{pmatrix} 1 & -Z_2 \\ -1 & Z_1 \end{pmatrix} \tag{5.24}$$

This gives

$$\begin{aligned} \mathbf{T}^n &= \frac{1}{(Z_1 - Z_2)} \begin{pmatrix} Z_1 & Z_2 \\ 1 & 1 \end{pmatrix} \begin{pmatrix} e^{n\gamma\ell} & 0 \\ 0 & e^{-n\gamma\ell} \end{pmatrix} \begin{pmatrix} 1 & -Z_2 \\ -1 & Z_1 \end{pmatrix} \\ &= \frac{1}{(Z_1 - Z_2)} \begin{pmatrix} Z_1 e^{n\gamma\ell} - Z_2 e^{-n\gamma\ell} & -2\, Z_1 Z_2 \sinh\, n\gamma\ell \\ 2 \sinh\, n\gamma\ell & Z_1 e^{-n\gamma\ell} - Z_2 e^{n\gamma\ell} \end{pmatrix} \end{aligned} \tag{5.25}$$

When the network is symmetrical, Eq. (5.25) reduces to the important special case,

$$\mathbf{T}^n = \begin{pmatrix} \cosh\, n\gamma & Z_o \sinh\, n\gamma \\ \dfrac{\sinh\, n\gamma}{Z_o} & \cosh\, n\gamma \end{pmatrix} \tag{5.26}$$

and from Eq. (5.14),

$$\begin{aligned} \begin{pmatrix} V_n \\ I_n \end{pmatrix} &= \mathbf{T}^{-n} \begin{pmatrix} V_1 \\ I_1 \end{pmatrix} \\ &= \begin{pmatrix} \cosh\, n\gamma\ell & -Z_o \sinh\, n\gamma\ell \\ \dfrac{-\sinh\, n\gamma\ell}{Z_o} & \cosh\, n\gamma\ell \end{pmatrix} \begin{pmatrix} V_1 \\ I_1 \end{pmatrix} \end{aligned} \tag{5.27}$$

5.3.2 Infinite periodic structure

If for the moment, an infinite structure is assumed; then the input impedance of the periodic structure will be its characteristic impedance Z_o, so that,

$$V_n = Z_o I_n \tag{5.28}$$

Using this in Eq. (5.27) gives,

$$\begin{aligned} V_n &= V_1[\cosh\ n\gamma\ell - \sinh\ n\gamma\ell] = e^{-n\gamma\ell}V_1 \\ I_n &= \frac{V_1}{Z_o}[\cosh\ n\gamma\ell - \sinh\ n\gamma\ell] = \frac{V_1}{Z_o}e^{-n\gamma\ell} \end{aligned} \tag{5.29}$$

A cascade of symmetrical networks thus behave like a finite length of transmission line with a characteristic impedance of Z_o and a propagation constant γ. If the networks are asymmetrical however, the impedances will be different for the two different directions of propagation and their values are as given in Eq. (5.21).

5.4 The general N^{th} order solution.

5.4.1 Symmetrical case.

As stipulated by the reciprocity condition of Eq. (5.18), the $2N \times 2N$ spectral matrix $\mathbf{S}$ must have the form,

$$\mathbf{S} = \begin{pmatrix} e^{\gamma_1\ell} & & & & & \\ & \ddots & & & & \\ & & e^{\gamma_N\ell} & & & \\ & & & e^{-\gamma_1\ell} & & \\ & & & & \ddots & \\ & & & & & e^{-\gamma_N\ell} \end{pmatrix} \tag{5.30}$$

The expansion of the modal fields by N *basis* terms has introduced N propagation constants for the periodic structure. However, these propagation constants do not correspond to the *basis* terms but to the alternate system of eigenvectors. The eigenvectors may be viewed as representing a different co-ordinate system. Thus Eq. (5.11) may be interpreted as a process of successive transformations whereby the field is first resolved into the eigendirections by the transformation M^{-1}. Then the multiplication by S effectively scales each resultant eigen-component by the corresponding eigenvalue. Hence their interpretation as the propagation constants of each corresponding eigen-component. Finally, the scaled values are re-transformed back by M to the original representation in terms of the *basis* functions. Furthermore, with the modal matrix understood in the sense of Eq. (5.13), it is convenient to express the N^{th} order case in partitioned form as,

$$\mathbf{M} = \begin{pmatrix} \mathbf{V}_{m_1} & \mathbf{V}_{m_2} \\ \mathbf{I}_{m_1} & \mathbf{I}_{m_2} \end{pmatrix} \tag{5.31}$$

where $\mathbf{V}_{m_1}, \mathbf{V}_{m_2}, \mathbf{I}_{m_1}$ and $\mathbf{I}_{m_2}$ are each $N \times N$ matrices, which in the symmetrical case, reduces to

$$\mathbf{M} = \begin{pmatrix} \mathbf{V}_{m_1} & \mathbf{V}_{m_1} \\ \mathbf{I}_{m_1} & -\mathbf{I}_{m_1} \end{pmatrix} \tag{5.32}$$

The minus sign of $\mathbf{I}_{m_1}$ is a reflection on the current convention that was adopted in Eqs. (5.5) and (5.7). The choice of the above notations is now self evident. The canonical form of $\mathbf{T}$ now becomes

$$\mathbf{T} = \begin{pmatrix} \mathbf{V}_{m_1} & \mathbf{V}_{m_1} \\ \mathbf{I}_{m_1} & -\mathbf{I}_{m_1} \end{pmatrix} \begin{pmatrix} \text{diag}\,[\, e^{\gamma \ell}\,] & 0 \\ 0 & \text{diag}\,[e^{-\gamma \ell}\,] \end{pmatrix} \begin{pmatrix} \mathbf{V}_{m_1} & \mathbf{V}_{m_1} \\ \mathbf{I}_{m_1} & -\mathbf{I}_{m_1} \end{pmatrix}^{-1} \tag{5.33}$$

Using the condition in Eq. (5.9), $\mathbf{T}$ may also be given as

$$\mathbf{T} = \begin{pmatrix} \mathbf{A} & \mathbf{B} \\ \mathbf{C} & \mathbf{A}^t \end{pmatrix} \tag{5.34}$$

Hence the inverse of T is

$$\mathbf{T}^{-1} = \begin{pmatrix} \mathbf{A} & -\mathbf{B} \\ -\mathbf{C} & \mathbf{A}^t \end{pmatrix} \tag{5.35}$$

The proof of this result is given in Appendix G. Eqs. (5.34) and (5.35) may now be used to obtain the two diagonal forms,

$$\begin{aligned} \frac{1}{2}[\mathbf{T} + \mathbf{T}^{-1}] &= \begin{pmatrix} \mathbf{A} & 0 \\ 0 & \mathbf{A}^t \end{pmatrix} \\ \frac{1}{2}[\mathbf{T} - \mathbf{T}^{-1}] &= \begin{pmatrix} 0 & \mathbf{B} \\ \mathbf{C} & 0 \end{pmatrix} \end{aligned} \tag{5.36}$$

By performing the same operations on Eq. (5.33) and then comparing with the results in Eq. (5.36), then gives the equivalence,

$$\begin{aligned} \mathbf{A} &= \mathbf{V}_{m_1} \text{diag}\,[\cosh\ \gamma\ell].\mathbf{V}_{m_1}^{-1} \\ \mathbf{B} &= \mathbf{V}_{m_1} \text{diag}\,[\sinh\ \gamma\ell]\ \mathbf{I}_{m_1}^{-1} \\ \mathbf{C} &= \mathbf{I}_{m_1} \text{diag}\,[\sinh\ \gamma\ell]\ \mathbf{V}_{m_1}^{-1} \\ \mathbf{D} &= \mathbf{A}^t = \mathbf{I}_{m_1} \text{diag}\,[\sinh\ \gamma\ell]\ \mathbf{I}_{m_1}^{-1} \end{aligned} \tag{5.37}$$

The details of the derivation are given in Appendix H. To obtain $\mathbf{T}^n$, γ is simply replaced by $n\gamma$ in the above equation. The form of $\mathbf{T}^n$ is in fact very similar to the 2×2 case of Eq. (5.26). However, there remains one problem in the evaluation of $\mathbf{T}^n$. Since γ is nearly always complex, and may be written as,

$$\gamma = \alpha + j\beta \tag{5.38}$$

we see that for $|\alpha|$ not $\ll 1$, the elements of $\mathbf{T}^n$ may become extremely large for large n since each element grows as $e^{n|\alpha|}$. This condition arises when the periodic structure is radiating strongly or when the structure is inherently very lossy. Moreover, for a high order solution (i.e large N), α for the higher order terms will tend to be large and negative. That is because the higher order terms are rapidly attenuated in their direction of propagation; but numerically they grow

as $e^{n|\alpha|}$ and will completely mask the values of the lower terms, which represent most of the field.

Fortunately it is not required to evaluate $\mathbf{T}^n$ numerically since the transmission matrix formulation is only a means to obtain the overall T-network representation of the periodic structure. The impedances are recovered from Eqs. (5.7) and (5.37), to give,

$$\mathbf{Z}_{11} = \mathbf{A}\mathbf{C}^{-1} = \mathbf{V}_{m_1}\,\mathrm{diag}\,[\coth\ \gamma\ell]\ \mathbf{I}_{m_1}^{-1} \tag{5.39}$$

$$\mathbf{Z}_{12} = \mathbf{C}^{-1} = \mathbf{V}_{m_1}\,\mathrm{diag}\,[\mathrm{cosech}\ \gamma\ell]\ \mathbf{I}_{m_1}^{-1}$$

Since the structure is symmetrical, only $\mathbf{Z}_{11}$ and $\mathbf{Z}_{12}$ are required in order to completely specify the characteristics of the T-junction. Now, for large $|\alpha|$, $\mathbf{Z}_{11}$ is seen to tend to a constant value and $\mathbf{Z}_{12}$ tends towards zero.

5.4.2 Asymmetrical case

The modal matrix for the asymmetrical unit cell, will have the form of Eq. (5.31). Since no simplification is possible in this case the inverse of the modal matrix will have to be evaluated numerically. Again it is useful to write the modal matrix and its inverse in partitioned form; this time using an arbitrary notation as follows

$$\mathbf{M} = \begin{pmatrix} \mathbf{m}_{11} & \mathbf{m}_{12} \\ \mathbf{m}_{21} & \mathbf{m}_{22} \end{pmatrix} \quad , \quad \mathbf{M}^{-1} = \begin{pmatrix} \tilde{\mathbf{m}}_{11} & \tilde{\mathbf{m}}_{12} \\ \tilde{\mathbf{m}}_{21} & \tilde{\mathbf{m}}_{22} \end{pmatrix} \tag{5.40}$$

Then the partitioned matrix multiplication of the canonical form of Eq. (5.33) gives,

$$\begin{aligned} \mathbf{A} &= \mathbf{m}_{11}\,\mathrm{diag}\,[\,e^{\gamma\ell}\,]\,\tilde{\mathbf{m}}_{11} + \mathbf{m}_{12}\,\mathrm{diag}\,[e^{-\gamma\ell}\,]\,\tilde{\mathbf{m}}_{21} \\ \mathbf{C} &= \mathbf{m}_{21}\,\mathrm{diag}\,[\,e^{\gamma\ell}\,]\,\tilde{\mathbf{m}}_{11} + \mathbf{m}_{22}\,\mathrm{diag}\,[e^{-\gamma\ell}\,]\,\tilde{\mathbf{m}}_{21} \\ \mathbf{D} &= \mathbf{m}_{21}\,\mathrm{diag}\,[\,e^{\gamma\ell}\,]\,\tilde{\mathbf{m}}_{12} + \mathbf{m}_{22}\,\mathrm{diag}\,[e^{-\gamma\ell}\,]\,\tilde{\mathbf{m}}_{22} \end{aligned} \tag{5.41}$$

Note that only three parameters of the transmission matrix are uniquely defined as the fourth parameter (in this case **B**), is determined from the requirement,

$$\det \mathbf{T} = 1 \tag{5.42}$$

The impedances are then given by

$$\begin{aligned}
\mathbf{Z}_{12} &= \mathbf{C}^{-1} \qquad (5.43)\\
&= [\tilde{\mathbf{m}}_{11}^{-1}\, \mathrm{diag}\,[e^{-\gamma\ell}]\mathbf{m}_{21}{}^{-1}] \times \\
&\quad (I + \mathbf{m}_{22}\, \mathrm{diag}\,[e^{-\gamma\ell}]\, \tilde{\mathbf{m}}_{21}\tilde{\mathbf{m}}_{11}^{-1}\, \mathrm{diag}\,[e^{-\gamma\ell}]\, \mathbf{m}_{21}^{-1}) \\
\mathbf{Z}_{11} &= \mathbf{A}\, \mathbf{C}^{-1} \\
&= (\mathbf{m}_{11}\mathbf{m}_{21}{}^{-1} + \\
&\quad \mathbf{m}_{12}\, \mathrm{diag}\,[e^{-\gamma\ell}]\, \tilde{\mathbf{m}}_{21}\tilde{\mathbf{m}}_{11}^{-1}\, \mathrm{diag}\,[e^{-\gamma\ell}]\, \mathbf{m}_{21}{}^{-1}) \times \\
&\quad [\mathbf{I} + \mathbf{m}_{22}\, \mathrm{diag}\,[e^{-\gamma\ell}]\, \tilde{\mathbf{m}}_{21}\tilde{\mathbf{m}}_{11}^{-1}\, \mathrm{diag}\,[e^{-\gamma\ell}]\, \tilde{\mathbf{m}}_{21}^{-1}]^{-1} \\
\mathbf{Z}_{22} &= \mathbf{C}^{-1}\mathbf{D} \\
&= [\mathbf{I} + \tilde{\mathbf{m}}_{11}^{-1}\, \mathrm{diag}\,[e^{-\gamma\ell}]\, \mathbf{m}_{21}{}^{-1}\mathbf{m}_{22}\, \mathrm{diag}\,[e^{-\gamma\ell}]\, \tilde{\mathbf{m}}_{21}]^{-1} \times \\
&\quad (\tilde{\mathbf{m}}_{11}^{-1}\tilde{\mathbf{m}}_{12} + \tilde{\mathbf{m}}_{11}^{-1}\, \mathrm{diag}\,[e^{-\gamma\ell}]\, \mathbf{m}_{21}{}^{-1}\, \mathbf{m}_{22}\, \mathrm{diag}\,[e^{-\gamma\ell}]\, \tilde{\mathbf{m}}_{22})
\end{aligned}$$

Again for the case of $\mathbf{T}^n$, then γ is just replaced by $n\gamma$. Note that all the impedances only contain terms with $e^{-\gamma\ell}$ which will tend to zero for large $|\alpha|$ and n.

5.4.3 Infinite periodic structure, N^{th} order

The relations in Eq. (5.37), then give,

$$\mathbf{T}^{-1} = \begin{pmatrix} \mathbf{V}_{m_1}\mathrm{diag}\,[\cosh\ n\gamma\ell]\,\mathbf{V}_{m_1}^{-1} & -\mathbf{V}_{m_1}\mathrm{diag}\,[\sinh\ n\gamma\ell]\,\mathbf{I}_{m_1}^{-1} \\ -\mathbf{I}_{m_1}\mathrm{diag}\,[\sinh\ n\gamma\ell]\,\mathbf{V}_{m_1}^{-1} & \mathbf{I}_{m_1}\mathrm{diag}\,[\cosh\ n\gamma\ell]\,\mathbf{I}_{m_1}^{-1} \end{pmatrix} \tag{5.44}$$

Using this in Eq. (5.27) gives,

$$\begin{aligned} \mathbf{V}_n &= \mathbf{V}_{m_1}\mathrm{diag}\,[\cosh\ n\gamma\ell]\,\mathbf{V}_{m_1}^{-1}\mathbf{V}_1 - \mathbf{V}_{m_1}\mathrm{diag}\,[\sinh\ n\gamma\ell]\,\mathbf{I}_{m_1}^{-1}\mathbf{I}_1 \\ \mathbf{I}_n &= \mathbf{I}_{m_1}\mathrm{diag}\,[\cosh\ n\gamma\ell]\,\mathbf{I}_{m_1}^{-1}\mathbf{I}_1 - \mathbf{I}_{m_1}\mathrm{diag}\,[\sinh\ n\gamma\ell]\,\mathbf{V}_{m_1}^{-1}\mathbf{V}_1 \end{aligned} \tag{5.45}$$

As for the 1^{st} order case of Eq. (5.28), the characteristic impedance matrix of the infinite periodic structure will be given by,

$$\mathbf{Z}_o = \mathbf{V}_{m_1}\mathbf{I}_{m_1}{}^{-1} \tag{5.46}$$

Applying this to Eq. (5.45), gives

$$\begin{aligned} \mathbf{V}_n &= \mathbf{V}_{m_1}[\ \mathrm{diag}\,[\cosh\ n\gamma\ell] - \mathrm{diag}\,[\sinh\ n\gamma\ell]\ ]\mathbf{V}_{m_1}^{-1}\mathbf{V}_1 \\ &= \mathbf{V}_{m_1}\mathrm{diag}\,[e^{-n\gamma\ell}\ ]\,\mathbf{V}_{m_1}^{-1}\mathbf{V}_1 \\ \mathbf{I}_n &= \mathbf{I}_{m_1}[\ \mathrm{diag}\,[\cosh\ n\gamma\ell] - \mathrm{diag}\,[\sinh\ n\gamma\ell]\ ]\mathbf{I}_{m_1}^{-1}\mathbf{I}_1 \\ &= \mathbf{I}_{m_1}\mathrm{diag}\,[e^{-n\gamma\ell}\ ]\,\mathbf{I}_{m_1}^{-1}\mathbf{I}_1 \end{aligned} \tag{5.47}$$

Except for the similarity transform by the partial eigenvectors, the above relations are the same as for the simpler 2×2 case of Eq. (5.29). As before, the multiplication by $\mathbf{V}_{m_1}^{-1}$ and $\mathbf{I}_{m_1}^{-1}$, can be viewed as a coordinate transformation. It is clear that the results from Eq. (5.47) are exactly the same as for a finite periodic structure of length ℓ, terminated by its own characteristic impedance Z_o. This feature will be exploited in later examples to investigate the field at various points along an 'infinite' structure.

5.5 The general transmission line

In this section a brief outline of the relation between the commonly used space harmonic and coupled mode methods of analysis and the cascaded network approach is discussed.

5.5.1 A homogeneous system of two coupled equations.

Consider the system of two equations,

$$\frac{dx_1}{dz} = ax_1 + bx_2$$

$$\frac{dx_2}{dz} = cx_1 + dx_2 \tag{5.48}$$

This may be written more compactly in matrix form as

$$\frac{d\mathbf{X}}{dz} = \mathbf{AX} \tag{5.49}$$

where,

$$\mathbf{A} = \begin{pmatrix} a & b \\ c & d \end{pmatrix} \quad and \quad \mathbf{X} = \begin{pmatrix} x_1 \\ x_2 \end{pmatrix}$$

The solution to Eq. (5.49) is then simply [27,pp 115]

$$\mathbf{X} = e^{\mathbf{A}z}\mathbf{X}_o \tag{5.50}$$

where $\mathbf{X}_o$ is the column vector of $\mathbf{X}$ at $z = 0$. The exponential matrix function can be expanded using the Cayley-Hamilton theorem [27,pp 104] to obtain

$$\mathbf{X} = \left\{ e^{pz}[\cosh(qz) - \frac{p}{q}\sinh(qz)]\, I + \frac{e^{pz}}{q}\sinh(qz)\,\mathbf{A} \right\} \mathbf{X}_o \tag{5.51}$$

with

$$p = \frac{a+d}{2} \quad \text{and} \quad q = (p^2 - \det\mathbf{A})^{\frac{1}{2}}$$

We may recall that the solution of Eq. (5.50) can also be written in the transmission matrix form of Eq. (5.27), thus

$$\mathbf{X} = \mathbf{T}^{-1}\mathbf{X}_o = e^{\mathbf{A}z}\mathbf{X}_o \tag{5.52}$$

This is, in fact, a special case of the general solution of Eq. (5.50), as we require

$$\det \mathbf{T}^{-1} = \det e^{\mathbf{A}z} = 1 \tag{5.53}$$

It can be shown (Appendix I) that to satisfy the above condition , we require

$$\text{trace } \mathbf{A} \;=\; 0 \tag{5.54}$$

which is satisfied if we choose $a = d = 0$. In fact, if we let

$$\mathbf{A} \;=\; \begin{pmatrix} 0 & -Z \\ -Y & 0 \end{pmatrix} \tag{5.55}$$

and substitute into Eq. (5.51), then

$$e^{\mathbf{A}z} \;=\; \begin{pmatrix} \cosh\,\gamma z & -Z_o \sinh\,\gamma z \\ \dfrac{-\sinh\,\gamma z}{Z_o} & \cosh\,\gamma z \end{pmatrix} \tag{5.56}$$

where $\gamma = \sqrt{ZY}$ and $Z_o = \left(\frac{Z}{Y}\right)^{\frac{1}{2}}$.

This is the familiar form of Eq. (5.27) which is not very surprising since the choice of Eq. (5.55) when substituted into Eq. (5.48) gives us the well known transmission line equations.

5.5.2 A non-homogeneous system

Consider now the case when the elements of **A** are not constants but arbitrary functions of z. If we are only interested in transmission line systems, then Eq. (5.54) will apply. Let **A** be chosen as

$$\mathbf{A} \;=\; \begin{pmatrix} 0 & c \\ \dfrac{1}{c}F(z) & 0 \end{pmatrix} \tag{5.57}$$

where c is a constant but F(z) is a periodic function in z. Then,

$$\frac{dx_1}{dz} \;=\; cx_2 \quad , \quad \frac{dx_2}{dz} \;=\; \frac{1}{c}F(z)\,x_1 \tag{5.58}$$

so that

$$\frac{d^2x_1}{dz^2} \;=\; F(z)\,x_1 \tag{5.59}$$

The above is a wave equation of the Hill's type, which has been the starting point for all perturbation analysis of periodic structures [5]. Mathieu's equation is obtained by taking F(z) as a sine or cosine function. Furthermore, it is evident from Eqs. (5.51) and (5.54) that $e^{\mathbf{A}z}$ always gives a symmetrical transmission matrix. Hence Hill's equation corresponds to a continuous line of reversible four-terminal networks and cannot be used for describing a general non-uniform periodic structure. For a general non-uniform transmission line,

$$\mathbf{A} = \begin{pmatrix} 0 & b(z) \\ c(z) & 0 \end{pmatrix} \tag{5.60}$$

Substituting this into Eq. (5.49) yields

$$\frac{d\mathbf{X}}{dz} = \mathbf{A}\mathbf{X} \begin{cases} \dfrac{dx_1}{dz} = b(z)\,x_2 \\ \dfrac{dx_2}{dz} = c(z)\,x_1 \end{cases} \tag{5.61}$$

and its second-order form,

$$\frac{dx_1}{dz} = \frac{d}{dz}\left(\frac{1}{c}(z)\frac{dx_2}{dz}\right) = b(z)\,x_2 \tag{5.62}$$

which poses a problem of the Sturm-Liouville type. This problem has been studied extensively and many methods have been developed to provide an approximate solution. We shall present an approximate solution based on the method of cascaded networks which has the specific advantage of solving non-uniform structures of finite length.

Solution to a special case

It has been shown [24] that a solution to Eq. (5.62), analogous to that of Eq. (5.50) may be obtained for some special forms of **A**, such that

$$\begin{aligned} \mathbf{X}(z) &= \exp\Big(\int_0^z \mathbf{A}(z)\,dz \Big)\mathbf{X}_o{}^{\dagger} \\ &= \exp\big(\mathbf{B}(z) \big)\mathbf{X}_o \quad , \quad \mathbf{B}(z) = \int_0^z \mathbf{A}(z)\,dz \end{aligned} \tag{5.63}$$

The requirement for Eq. (5.63) to be correct is that the matrices $\mathbf{A}(z)$ and $\mathbf{B}(z)$ must commute. That is,

$$\mathbf{A}(z)\mathbf{B}(z) = \mathbf{B}(z)\mathbf{A}(z) \tag{5.64}$$

This condition proves to be extremely restrictive, and the method cannot be applied directly to most problems of interest. One important class of problems to have an **A** that satisfy the above form are the coupled mode equations. This is one of the reasons why the coupled mode analysis has been so very extensively used. It may be noticed, however, that any diagonal form of **A** will also satisfy the above condition.

General approximate solution

A general but approximate solution to the problem of non-uniform transmission lines (such as non-homogeneous guides) may be obtained by considering the transmission line to be divided up into short sections and then representing each section by an equivalent two-port network such that a finite length of non-uniform

[†]The integral of the matrix $\mathbf{A}(z)$ is taken as the integral of each element of the matrix.

transmission line may be represented as

$$\begin{pmatrix} V_1 \\ I_1 \end{pmatrix} = \prod_{p=1}^{n} \mathbf{T}_p^{-1} \begin{pmatrix} V_o \\ I_o \end{pmatrix} \tag{5.65}$$

where the transmission matrix $\mathbf{T}$ is as given in Eq. (5.52). The values for the complex propagation constant γ and characteristic impedance Z_o are taken to be the mean values of each small section. However, the series product of Eq. (5.66), may be difficult to evaluate for large n. The problem may be overcome by considering $\mathbf{T}^{-1}$ in its canonical form,

$$\mathbf{T}^{-1} = \mathbf{M} S^{-1} \mathbf{M}^{-1} \tag{5.66}$$

$$\prod_{p=1}^{n} \mathbf{T}_p^{-1} = \mathbf{M}_1 S_1^{-1} \mathbf{M}_1^{-1} \mathbf{M}_2 S_2^{-1} \mathbf{M}_1^{-1} \ldots\ldots \mathbf{M}_n S_n^{-1} \mathbf{M}_n^{-1} \tag{5.67}$$

Then the logarithm of the series product is evaluated, let

$$\mathbf{T}_t = \prod_{p=1}^{n} \mathbf{T}_p^{-1} \tag{5.68}$$

Then

$$\begin{aligned} ln(\mathbf{T}_t) &= ln(\mathbf{T}_1^{-1}) + ln(\mathbf{T}_2^{-1}) + \ldots\ldots + ln(\mathbf{T}_n^{-1}) \\ &= \mathbf{M}_1 \mathrm{diag}\,[\gamma_1 \delta z]\, \mathbf{M}_1^{-1} + \mathbf{M}_2 \mathrm{diag}\,[\gamma_2 \delta z]\, \mathbf{M}_2^{-1} + \\ &\quad \ldots\ldots + \mathbf{M}_n \mathrm{diag}\,[\gamma_n \delta z]\, \mathbf{M}_n^{-1} \end{aligned} \tag{5.69}$$

Then define $\mathbf{M}_t$ and γ_t such that

$$R.H.S = \mathbf{M}_t \mathrm{diag}\,[\gamma_t \ell]\, \mathbf{M}_t^{-1} \tag{5.70}$$

Using the result of Eq. (5.70) the problem can now be solved by following the procedure described in the earlier sections.

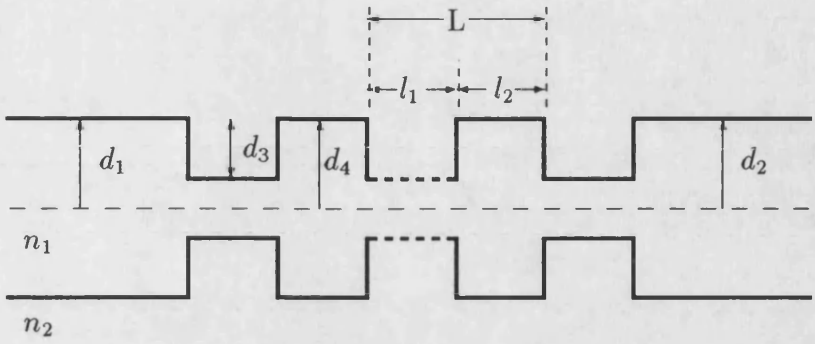

Fig 5.3 Grooved Periodic Grating

5.6 Numerical Results

The theory will now be illustrated by a few examples. The examples chosen will demonstrate the convergence of the method and provide further insights to the propagation of fields in finite periodic structures in open dielectric waveguides. Only TE polarised incident field is considered. These results have been presented at the 16th Microwave Conference in Dublin (1986) [26]. All the results are calculated on the assumption that the periodic structures are fed by and terminated with slab guides of the same thickness ($d_1 = d_2 = d_4 = 0.5$ cm) and of the same material ($n_1 = 1.603$) as the periodic structure itself with $n_2 = 1.0$. A grating spacing of $\ell_1 = \ell_2 = 0.628$ cm is used throughout. Unless otherwise stated, the periodic structure under consideration is of the form shown in Fig 5.3.

5.6.1 Effect of groove depth at the Bragg condition

Figs 5.4 to 5.7, shows the effect of increasing groove depth d_3 on the phase and magnitude of S_{11} and S_{12} for different order of solution N. The results are

calculated at the Bragg condition (i.e the periodic spacing of the grooves is re-adjusted for each calculation of a new groove depth), and the periodic structure is assumed lossless, so that this effect may be observed in isolation. It is not a problem to include loss in the model. The number of grating elements used is 20.

It is noted that for N=0, which corresponds to the 1st order solution, the agreement with the higher order solutions is surprisingly good, particularly at small groove depths d_3. It is only at groove depths of greater than 0.25cm that the 1^{st} order solution of $|S_{11}|$ is seen to differ considerably from the more accurate higher order solutions. This is due to the inability of the 1^{st} order solution to account for the increasing radiation loss at large groove depths. In our model the 1^{st} order solution will have only a single basis term as the trial field which was optimised to fit the fundamental mode alone. It is evident from this result that as radiation loss increases a higher order solution is necessary. It is also clear that for N=5 convergence is virtually achieved.

Furthermore, the phase of S_{12} in Fig 5.7 is seen to vary considerably for groove depths greater than 60% (or 0.3 cm). The reason for this may be the diminishingly small magnitude of the transmitted wave which makes it increasingly difficult to determine the phase accurately and there is a tendency for the higher order solution to 'hunt' for the phase due to the numerical accuracies that will creep in as larger and larger matrices are manipulated. Alternatively, Figs 5.8 and 5.9 show the effect of increasing groove depths on the stop bands of the same periodic grating. Here the magnitude of S_{11} and S_{12} are plotted against δV_ℓ, the normalised *difference* frequency, where,

$$\delta V_\ell = (V - V_o)\ell, \tag{5.71}$$

$$V_o = \frac{2\pi f_o(\epsilon_1 - \epsilon_2)}{c} \tag{5.72}$$

$$V = \frac{2\pi f(\epsilon_1 - \epsilon_2)}{c} \tag{5.73}$$

f_o = Bragg frequency,

ℓ = Period of grating

The fall in $|S_{11}|$ for groove depth greater than 0.3 cm is also evident from Fig 5.8. The figures also clearly show the characteristic broadening of the stop bands for increasing groove depths which effectively means a lowering of the Q of the structure. This happens because the number of grating elements that are actually 'active' at the Bragg condition decreases for increasing groove depths.

5.6.2 Effect of increasing number of corrugations

As expected, Fig 5.10 shows the decreasing number of corrugations needed for total reflection at the Bragg frequency with increasing groove depths.

Fig 5.11 however is slightly more interesting. It shows the phase of the transmitted field along the periodic structure at the Bragg condition. For the shallow groove depth of 0.1 cm a standing wave pattern exists for the entire length of the structure, ie, up to the 100th corrugation; whereas for the larger groove depths this standing wave pattern only exists up to a certain number of corrugations from the source end beyond which the phase is seen to change linearly with distance in effect behaving like a travelling wave. This phenomenon, which has not been reported before, clearly shows the active length of a reflection grating at the Bragg condition. The amount of radiation that occurs at the Bragg condition is usually very small, and is only noticeable at large groove depths. This is evident from Fig 5.12 which shows the reflection coefficients approaching unity as the number of corrugations are increased. Only for the large groove depth of 0.4 cm

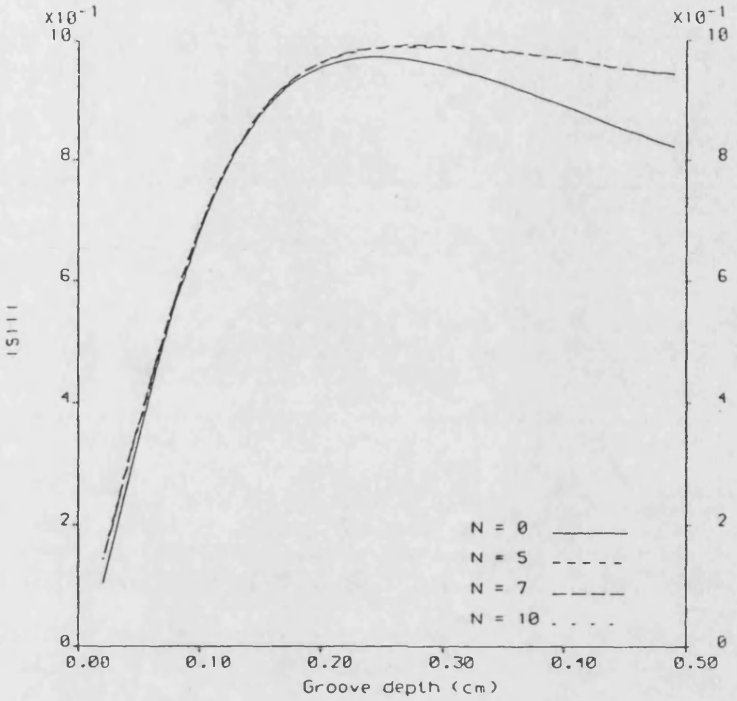

Fig 5.4 Variation of $|S_{11}|$ with groove depths at the Bragg frequency for various order of solution N.

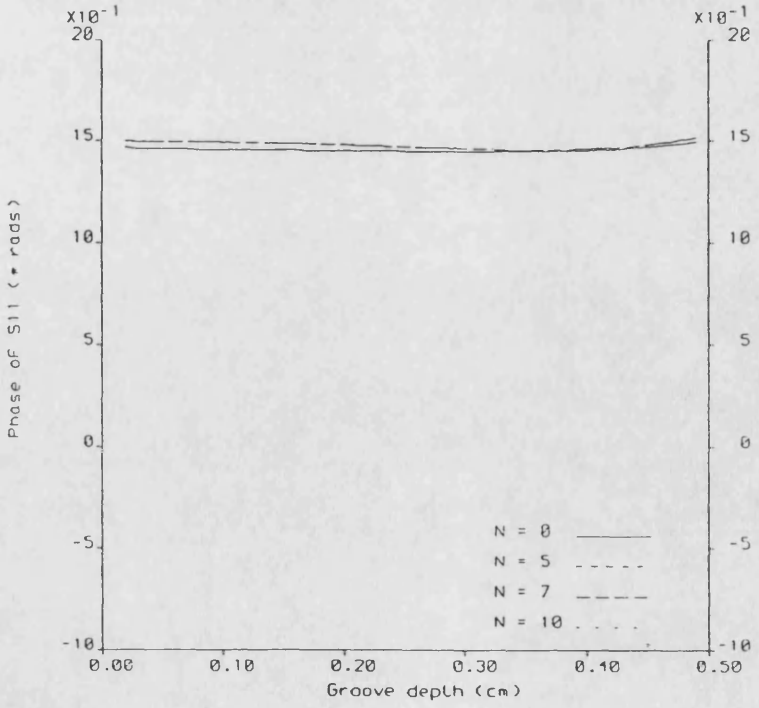

Fig 5.5 Corresponding variation of $\angle S_{11}$ against groove depth for different order of solution N.

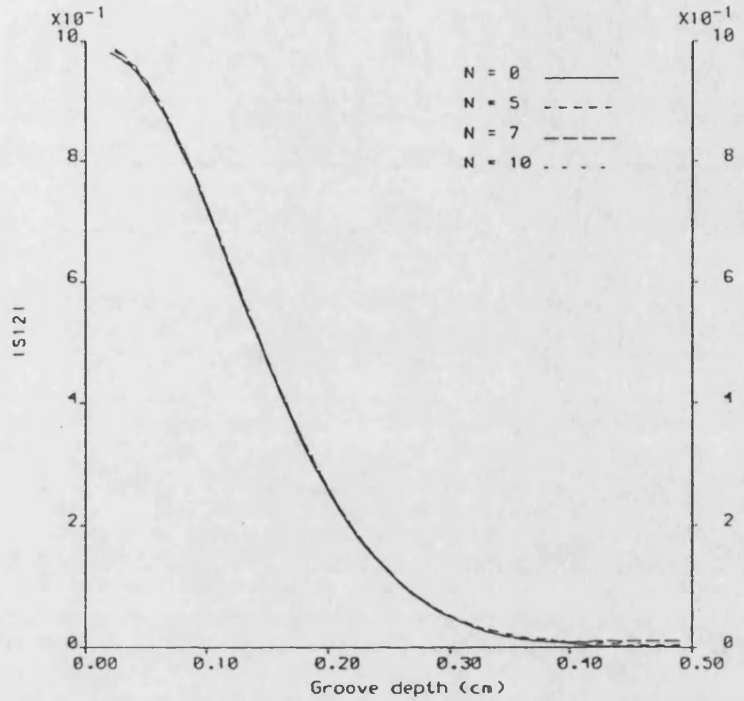

Fig 5.6 Variation of $|S_{12}|$ with groove depths at the Bragg frequency for various order of solution N.

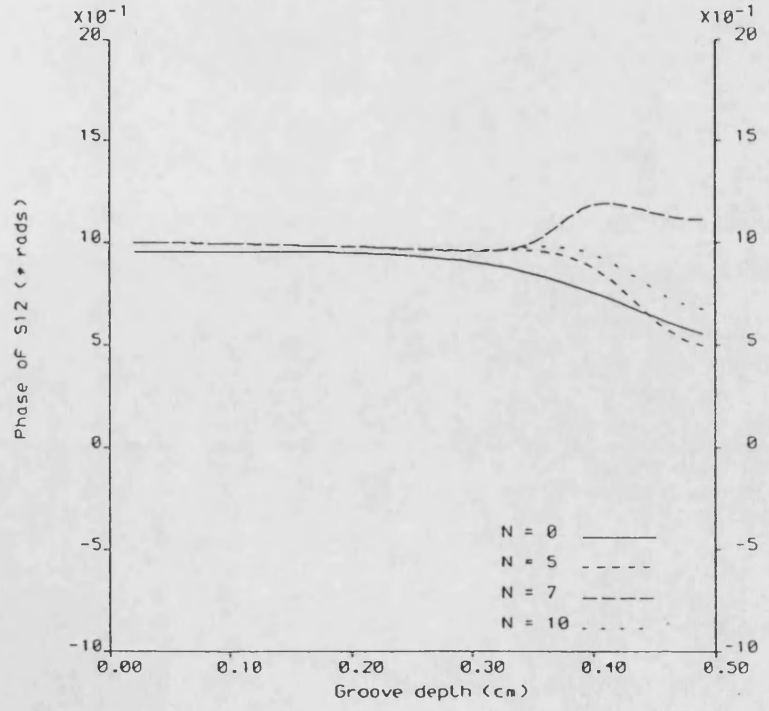

Fig 5.7 Corresponding variation of $\angle S_{12}$ against groove depth for different order of solution N.

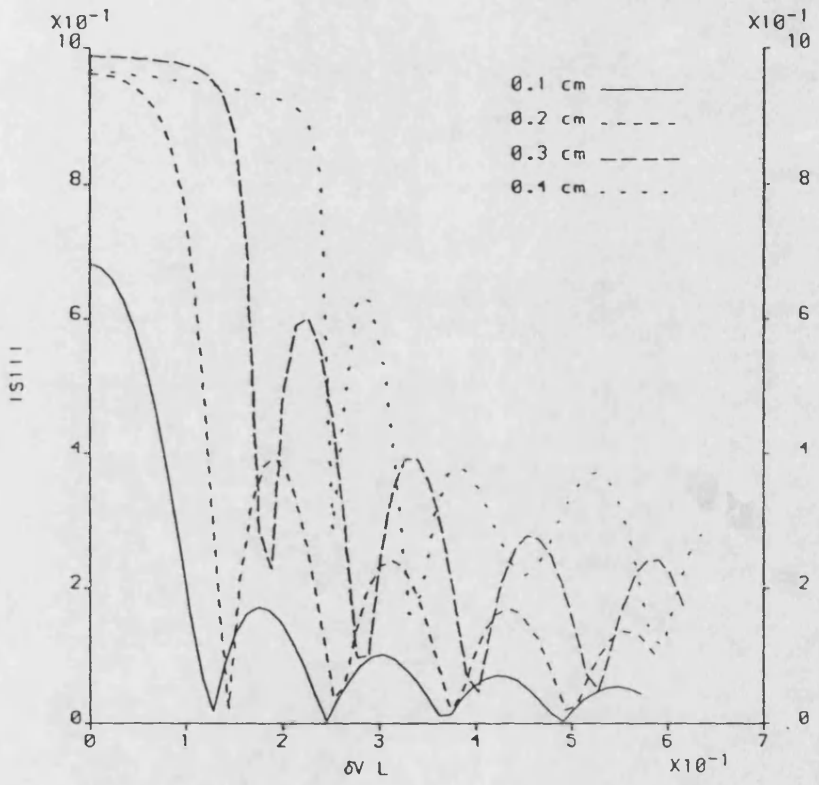

Fig 5.8 Effect of different groove depths on $|S_{11}|$.

δV = $2\pi/c\sqrt{\epsilon_1 - \epsilon_2}(f - f_o)$
f_o = Bragg frequency
f = frequency
c = velocityoflight
L = length of one grating element(0.62cm)
Nc = Number of corrugations 20

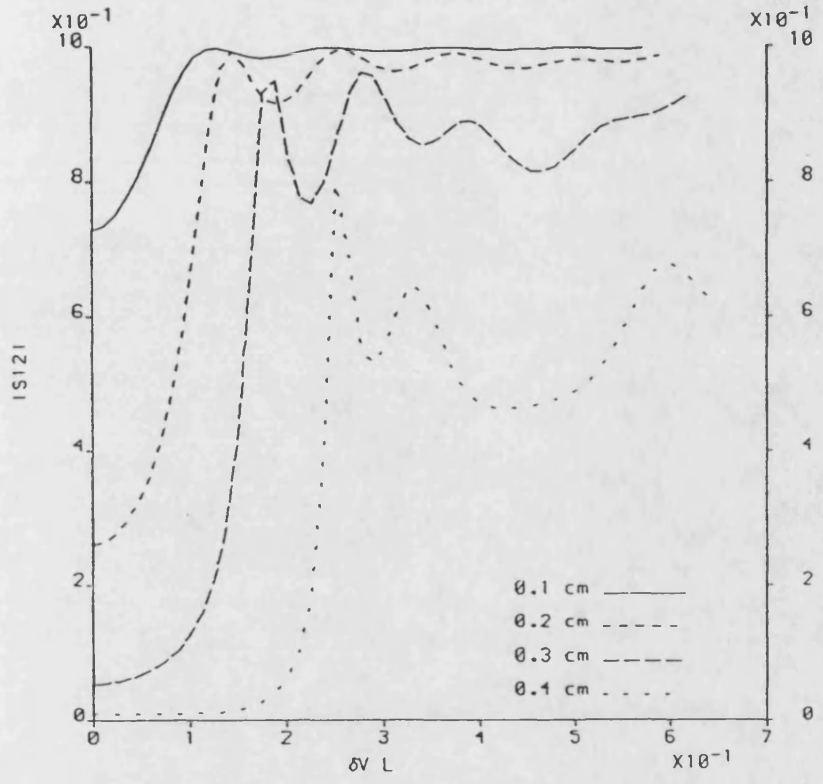

Fig 5.9 Effect of different groove depths on $|S_{12}|$.

δV = $2\pi/c\sqrt{\epsilon_1 - \epsilon_2}(f - f_o)$
f_o = Bragg frequency
f = frequency
c = velocityoflight
L = length of one grating element(0.62cm)
Nc = Number of corrugations 20

is $|S_{11}|$ noticeably levelling off at a value less than unity. The phase of S_{11} is seen to be unchanging for varying groove depth and number of corrugation. The effect of increasing number of corrugation on the stopband of a periodic grating at X-band is shown in Fig 5.13.

5.6.3 Effect of guide thickness

The effect of guide thickness on S_{12} and S_{11} as shown in Figs 5.15 and 5.16 respectively, may best be explained by considering the periodic structure as composed of two layers.

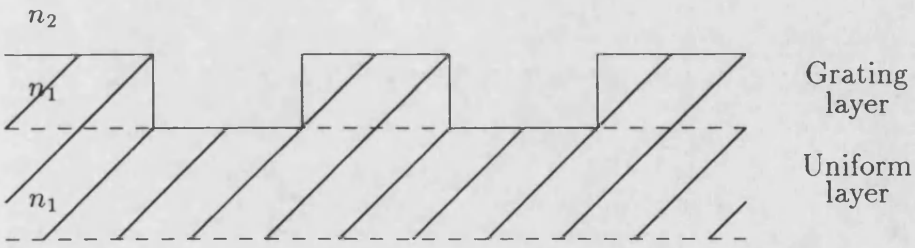

Fig 5.14 Periodic grating as 2 layer slab guide.

A lower layer which represents a uniform waveguide, and a top layer which represents the grating (Fig 5.14). As noted from Figs 5.15 and 5.16, the reduction in S_{11} with the accompanying increase in S_{12}, shows the effect of the grating on the incident field to be reduced for increasing thickness of the lower layer. This results from the field becoming more concentrated in the thicker lower layer. The figures also show the inadequacies of the 1st order (N=0) solution. This is expected since the thick lower layer is about to overmode. The second mode is supported at a thickness of 1.3 cm. The onset of the second mode is clearly evident for the 6th (N=5) order solution. Convergence is just reached at N=10.

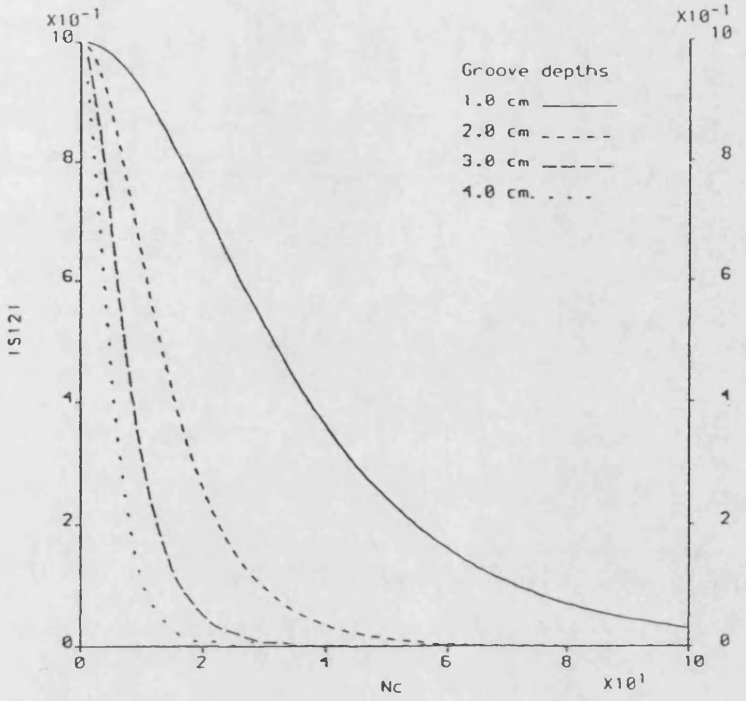

Fig 5.10 Variation of $|S_{12}|$ with number of corrugations (Nc) for several groove depths at the Bragg frequency of 10 GHz

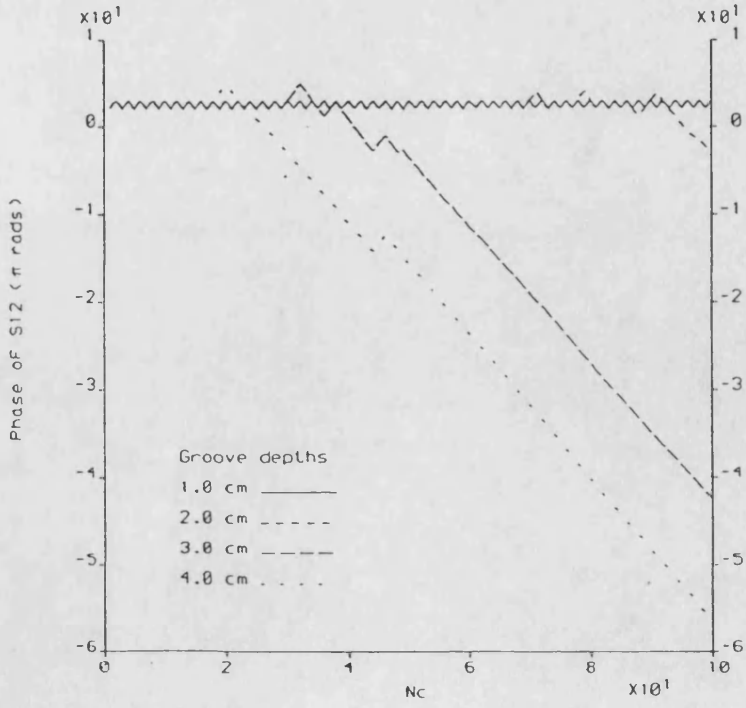

Fig 5.11 Corresponding variation of $\angle S_{12}$ along the structure.

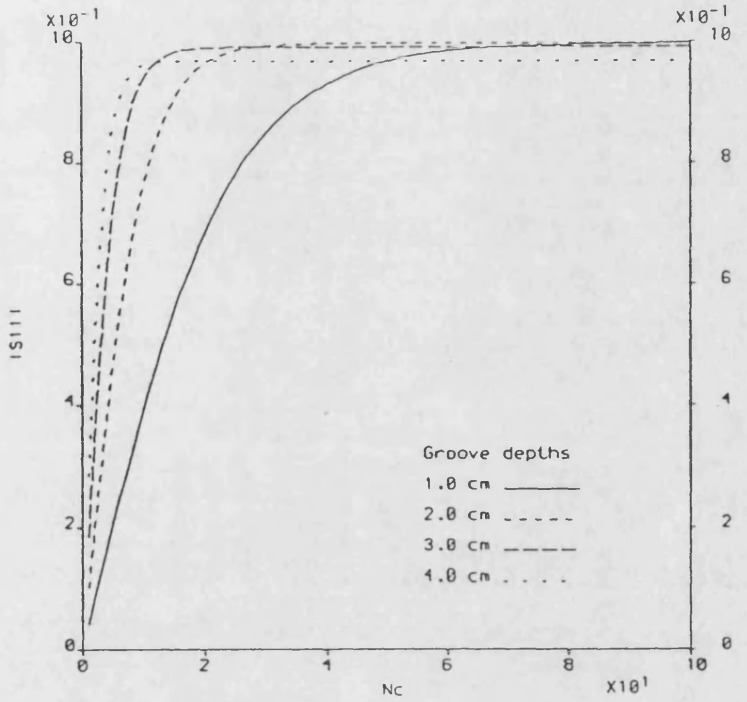

Fig 5.12a Variation of $|S_{11}|$ with number of corrugations (Nc) for several groove depths at the Bragg frequency of 10 GHz

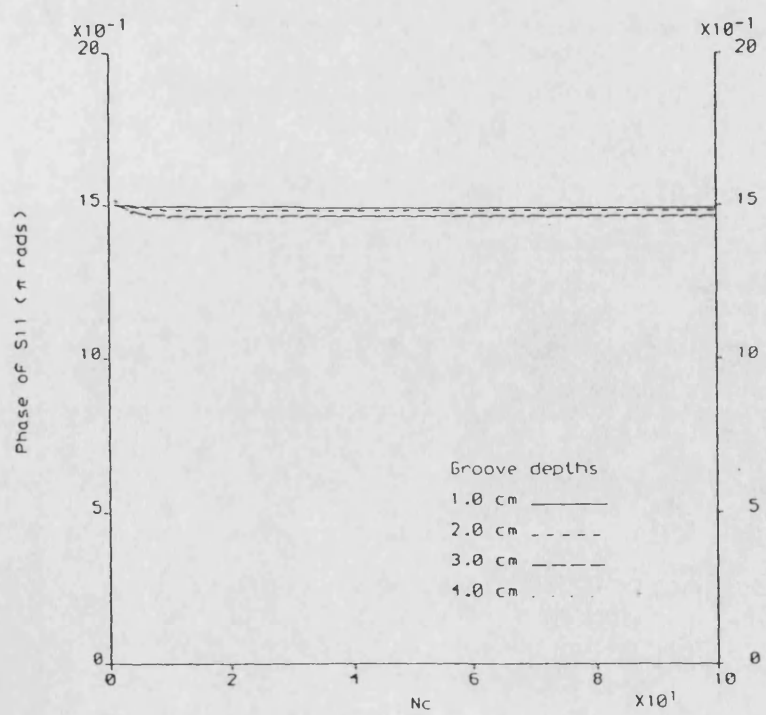

Fig 5.12b Corresponding variation of $\angle S_{11}$.

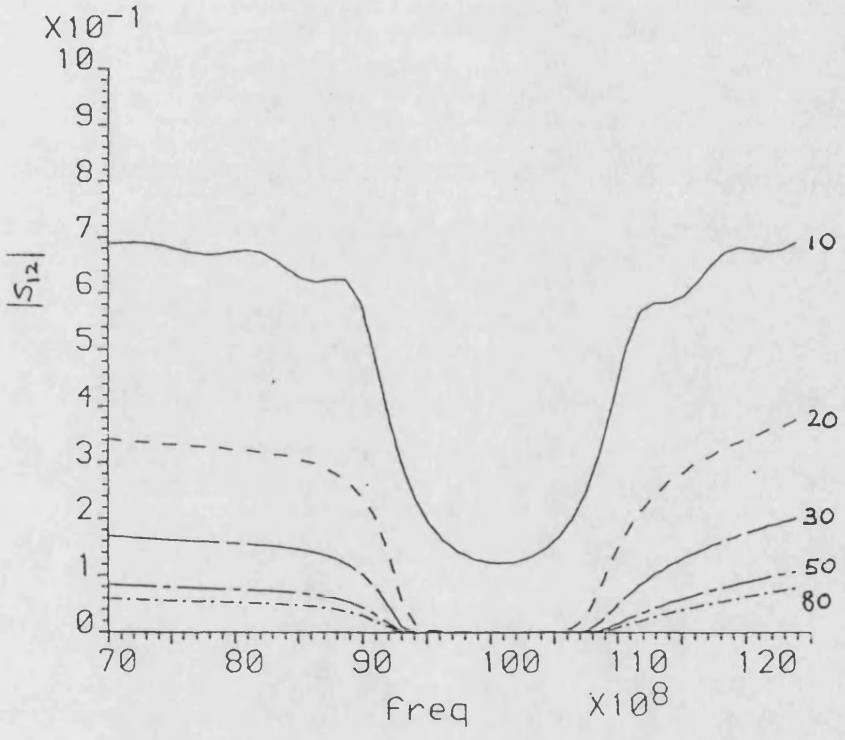

Fig 5.13 Effect of number of corrugations on the stop-band of a periodic grating with groove depth of $d_3 = 0.25$ cm

The poor convergence may be attributed to the use of Laguerre polynomials as the set of basis functions for approximating the modal fields in the thick guide. In our previous discussion of the choice of basis functions in Chapter 3, it was pointed out that the first 5 terms of the Laguerre polynomials are slowly varying functions and are unsuitable for modelling fields with higher order modes. They were used here only because an existing program using them as a basis was adapted for the calculations. Better results should be obtainable by using an appropriate set of mixed basis functions which employ the intermediate modal functions set.

5.6.4 Effect of groove depth

In Sect. 5.6.1 the groove depth variation at the Bragg condition was considered. That involved changing the grating spacing ℓ_1 and ℓ_2 as well for the Bragg condition to be preserved. Here, the change in scattering parameters for varying only the groove depth is considered. The resulting S_{11},S_{12} and radiation loss are shown in Fig 5.17. The periodic structure being considered has a periodicity such that the Bragg condition occurs at the groove depth of 0.3 cm at the operating frequency of 10.0 GHz. We note that the variation of S_{11} and S_{12} with groove depth is very similar to the variation of S_{11} and S_{12} with frequency (refer to Fig 5.8), where several small resonances are seen to occur before the Bragg condition is reached. In open dielectric waveguides, the propagation constant and hence the guide wavelength is directly proportional to the guide thickness, and since changing the groove depth changes the effective thickness of the guide, the similarity in features is then not too surprising.

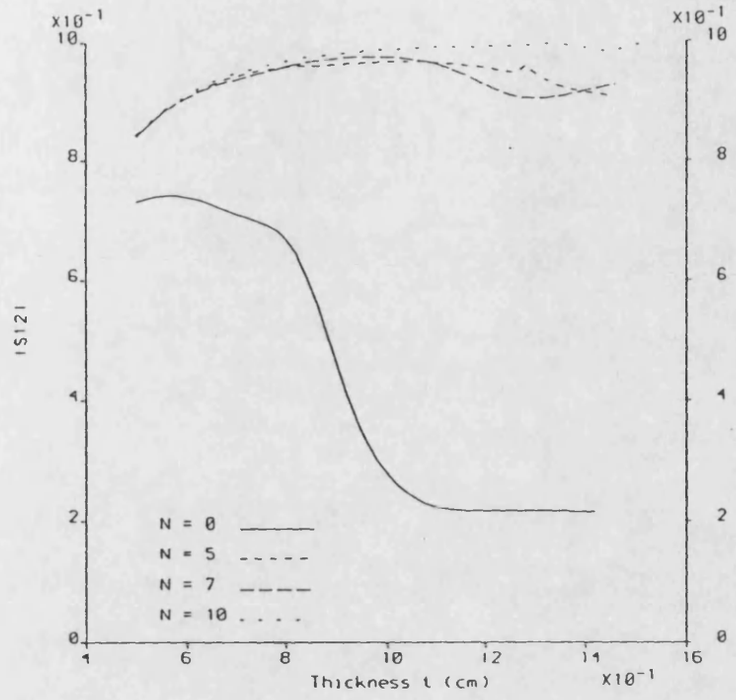

Fig 5.15a Variation of $|S_{12}|$ with the thickness of the uniform layer at the Bragg frequency for various order of solution N. Nc = 20.

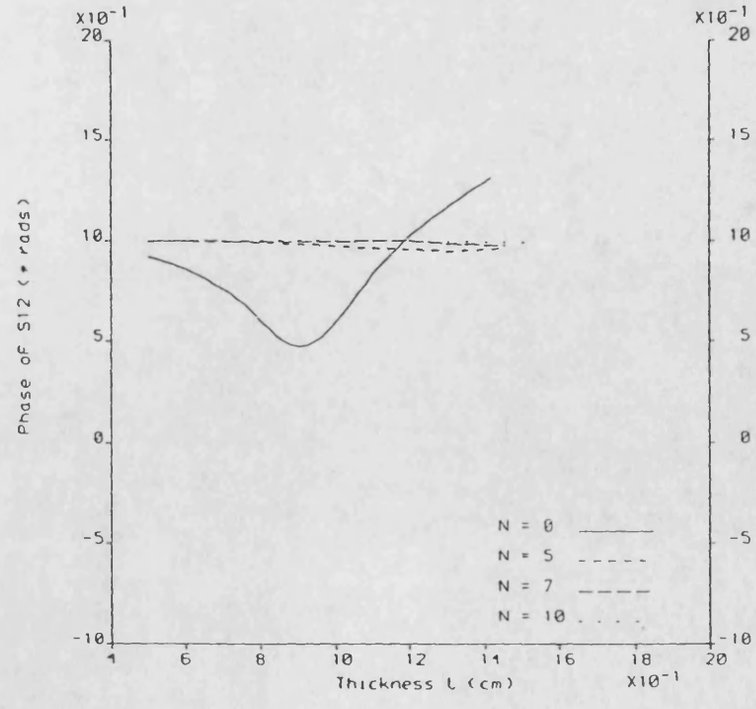

Fig 5.15b Corresponding variation of $\angle S12$.

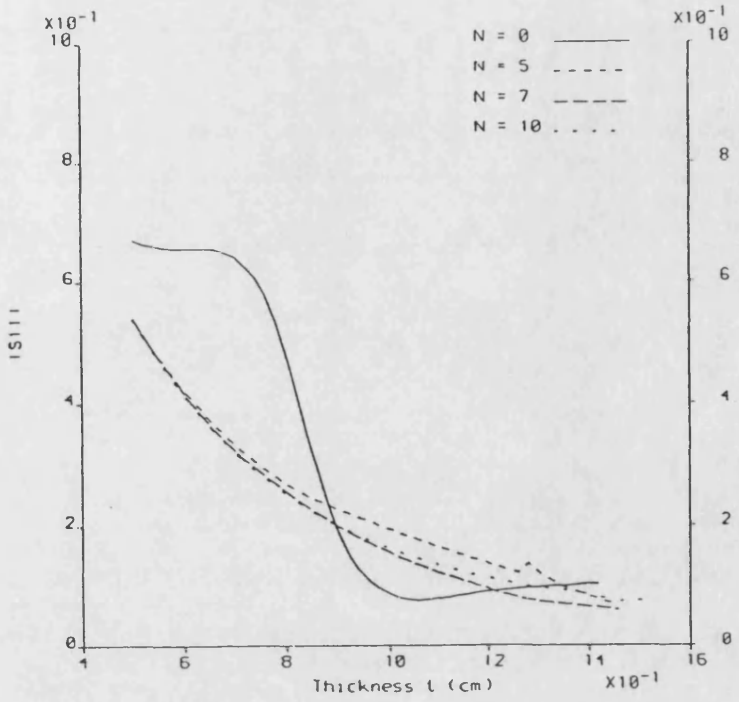

Fig 5.16a Variation of $|S_{11}|$ with the thickness of the uniform layer at the Bragg frequency for various order of solution N. Nc = 20.

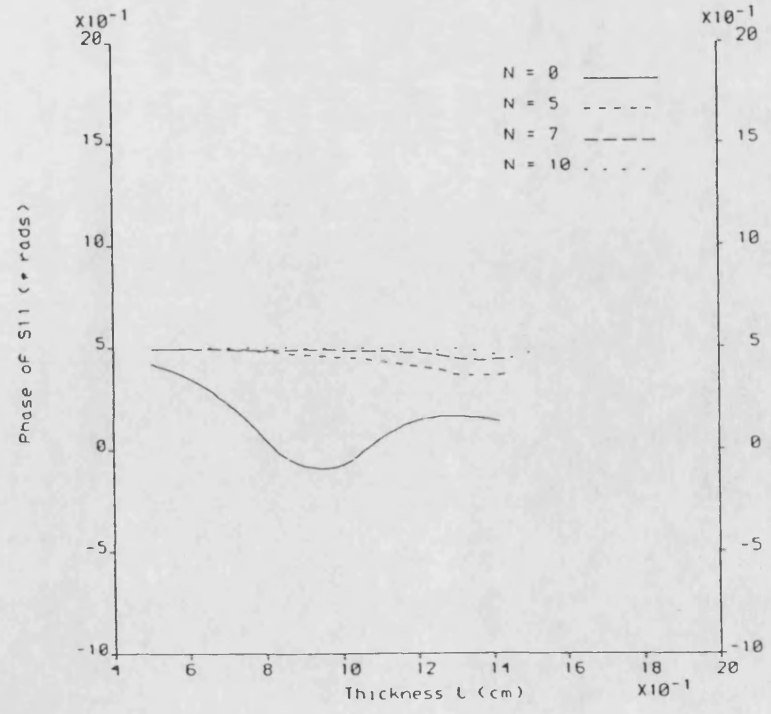

Fig 5.16b Corresponding variation of $\angle S11$.

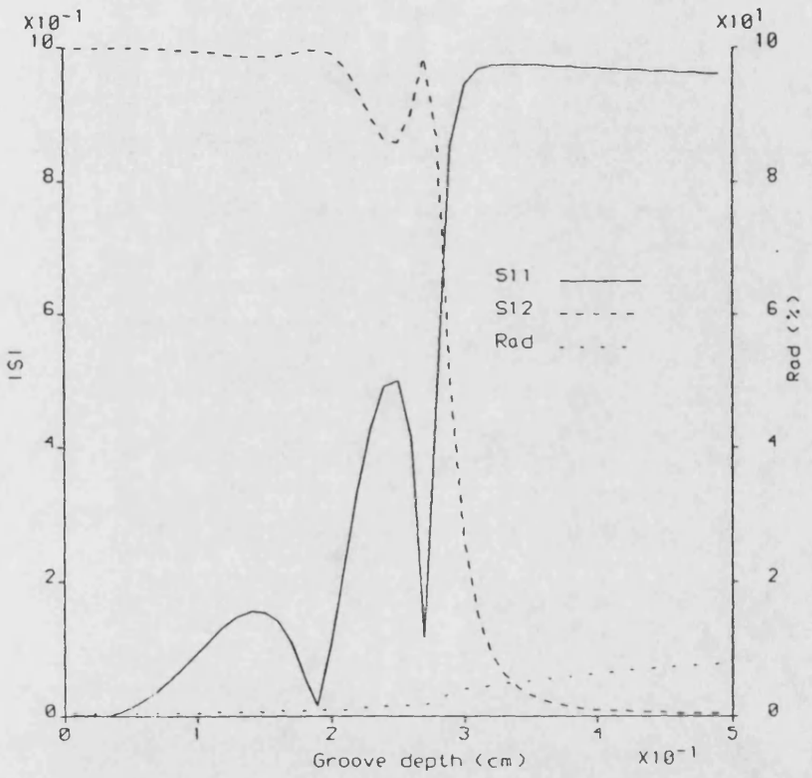

Fig 5.17 Effect of varying groove depth at the Bragg frequency of 10 GHz. Nc = 20.

5.6.5 Effect of number of corrugations on side resonances

As expected, Fig 5.18(a) shows the number of reflection nulls or side resonances is directly proportional to the number of corrugations (Nc), with Nc=50 having 5 times as many resonances as for Nc=10. This is true when corrugation depth is small (d_3 = 0.1 cm) and every element of the corrugation contributes to the resonances of the structure. This behaviour is greatly disturbed at very large groove depths (d_3 = 0.4 cm) shown in Fig 5.18(b) where the effect of radiation takes over. The matched curve in the figure refers to the termination of the finite periodic structure (Nc=50) with a slab guide whose characteristic impedance matches that of the periodic structure. The matched load has the effect of lowering the side resonances of the structure. Fig 5.18(c) shows the effect of large groove depth on $|S_{12}|$ for increasing number of corrugation.

5.6.6 Novel structures

Quarter-wave resonator

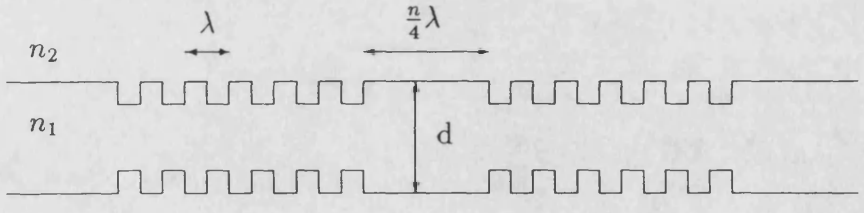

Fig 5.19 High Q n-Quarter-wave Resonator

One of the main uses of periodic structures is their ability to act as a frequency selective reflector, ie, as a stopband filter. It is, however, also possible to make

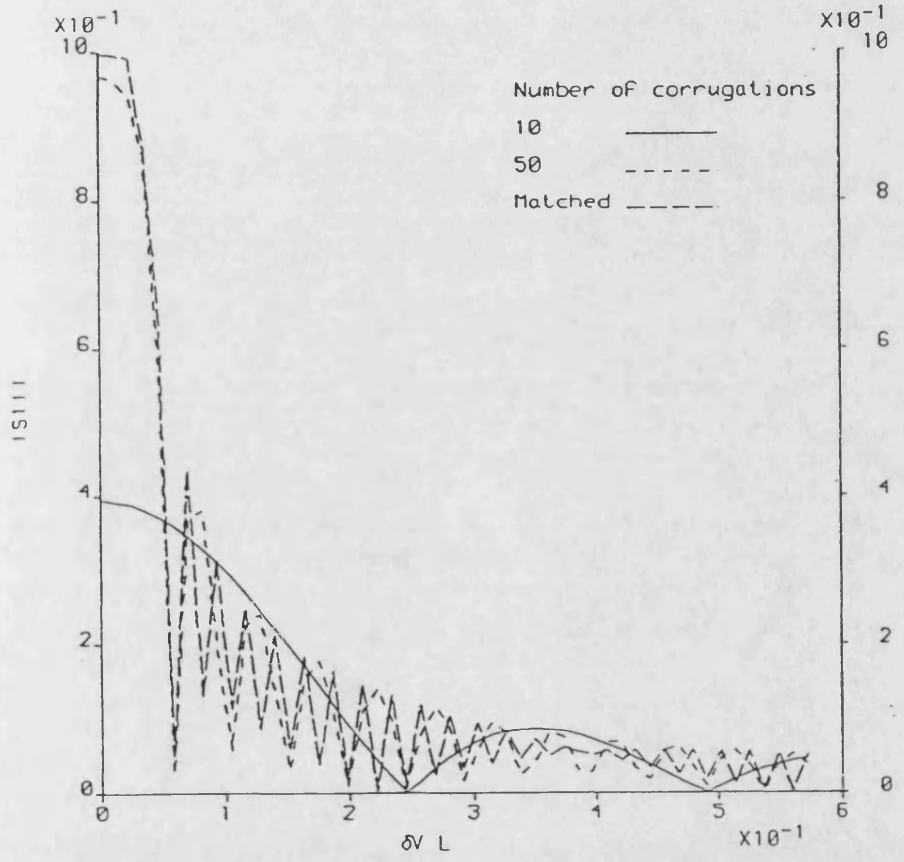

Fig 5.18a Variation of $|S_{11}|$ against δVL for different number of corrugations and for matched load termination at small groove depth of 0.1 cm with slab guide thickness of 0.5 cm.

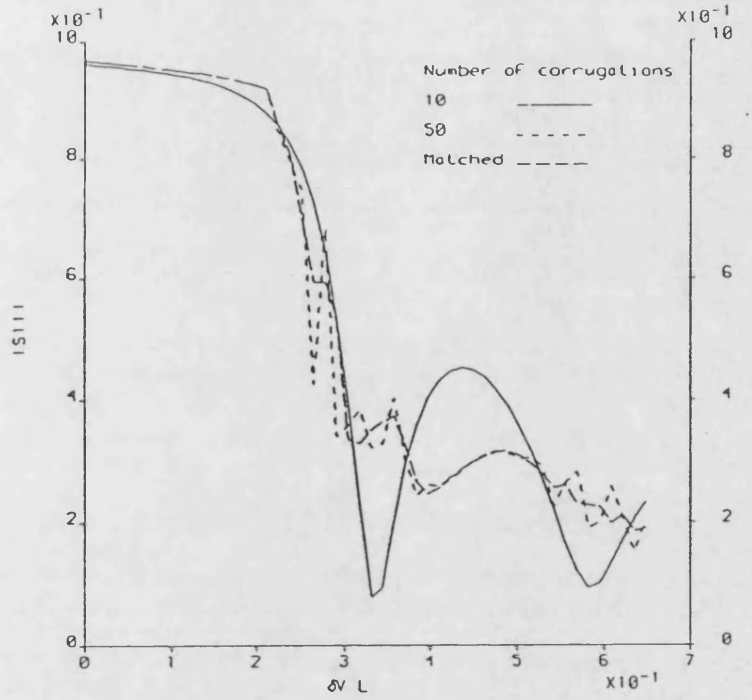

Fig 5.18b Variation of $|S_{11}|$ against δVL for different number of corrugations and for matched load termination at large groove depth of 0.4 cm with slab guide thickness of 0.5 cm.

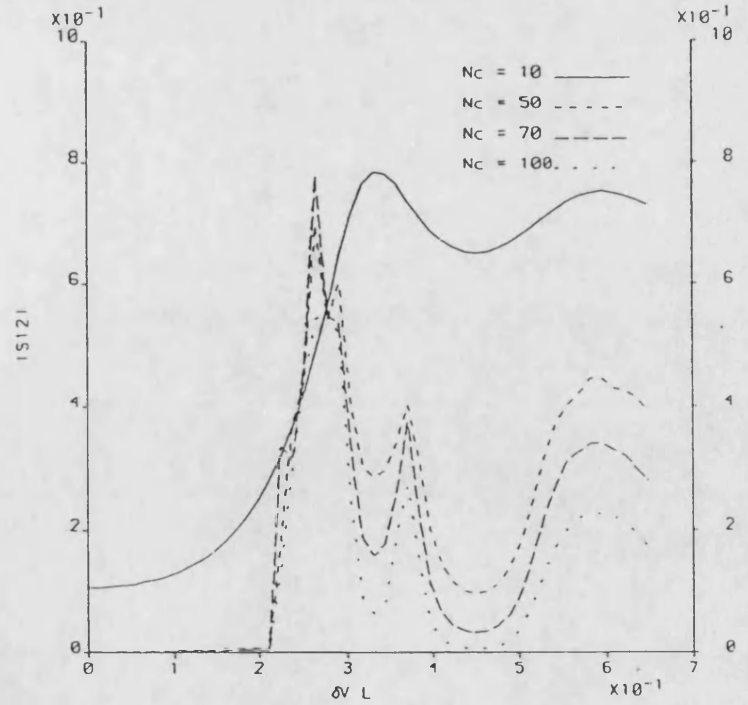

Fig 5.18c Variation of $|S_{12}|$ against δVL for different number of corrugations at large groove depth of 0.4 cm with slab guide thickness of 0.5 cm.

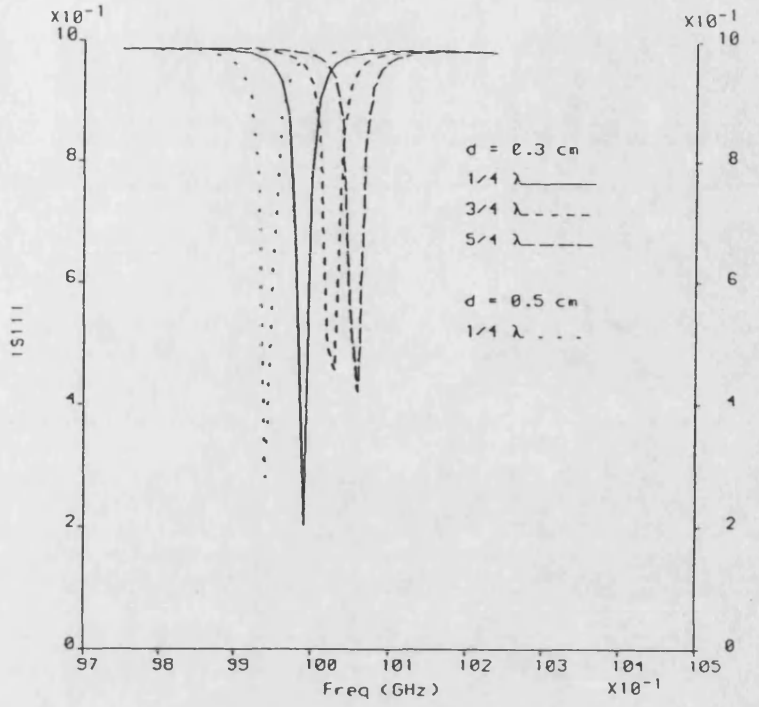

Fig 5.20a Reflection characteristics of the High Q Odd Multiple Quarter Wavelenth Resonator showing the transmission band at the Bragg condition for different lengths ($1/4\lambda$,$3/4\lambda$ and $5/4\lambda$), and for two different thickness d of the resonator.

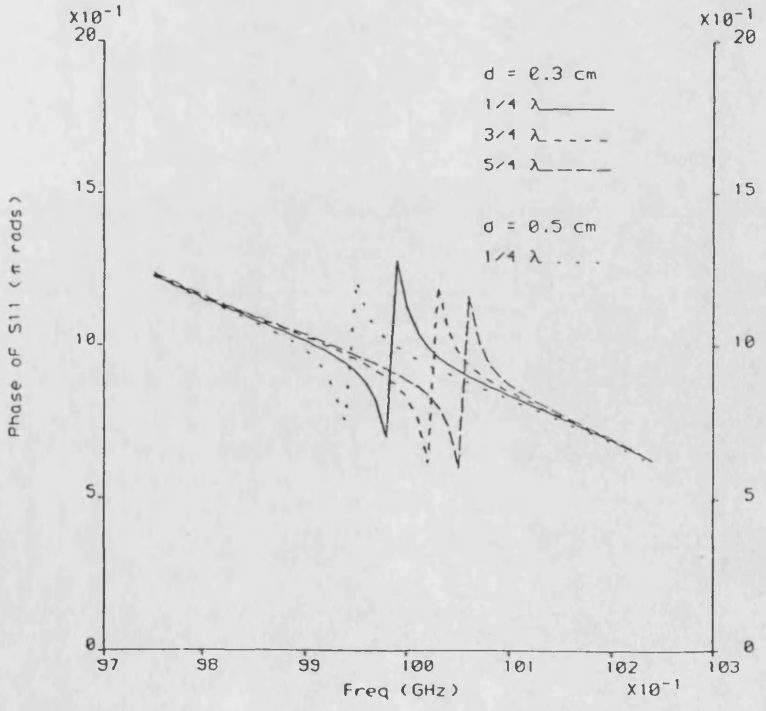

Fig 5.20b Corresponding variation of $\angle S_{11}$ for the High Q Resonator.

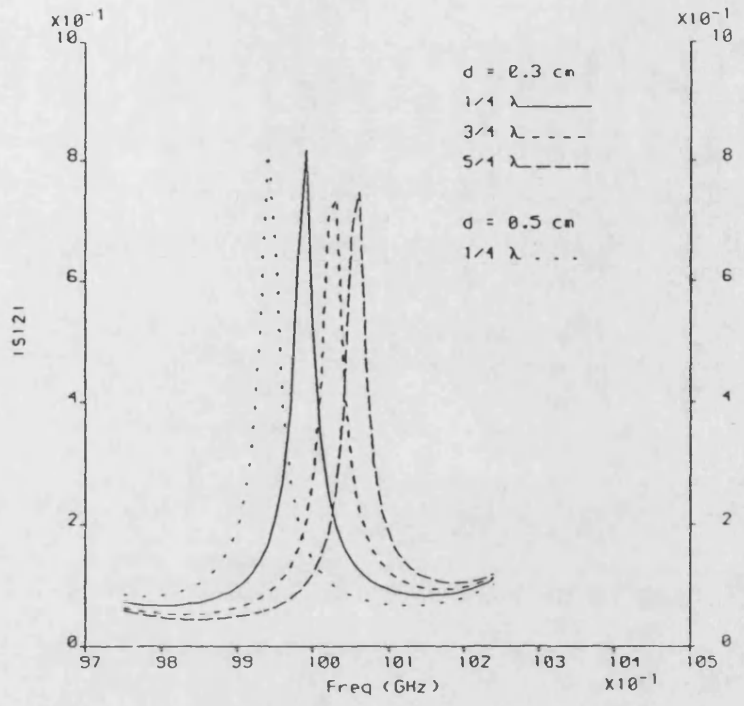

Fig 5.21a Transmission characteristics of the High Q Odd Multiple Quarter Wavelenth Resonator showing the transmission band at the Bragg condition for different lengths ($1/4\lambda$,$3/4\lambda$ and $5/4\lambda$), and for two different thickness d of the resonator.

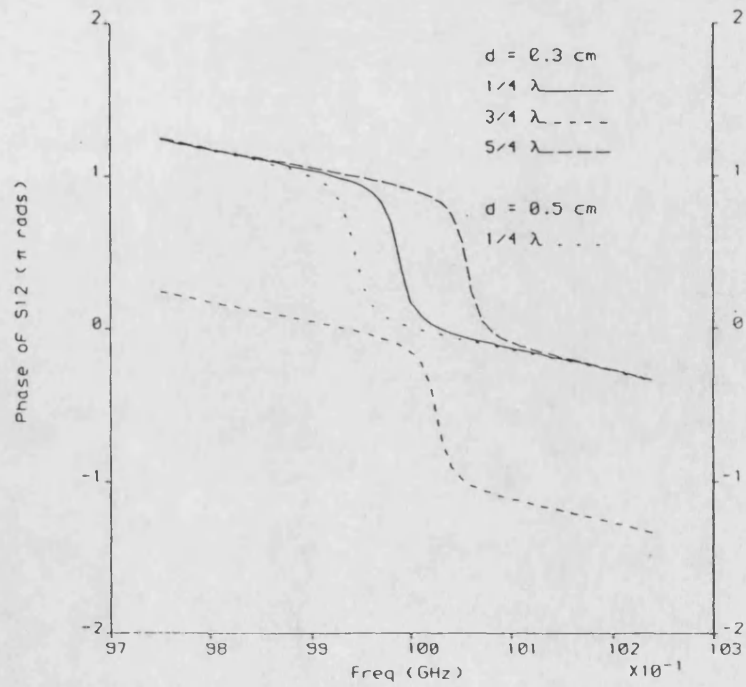

Fig 5.21b Corresponding variation of $\angle S_{12}$ for the High Q Resonator.

them operate as a passband filters. This is achieved by spacing two identical periodic structure by one (or an odd multiple) quarter wavelength apart (Fig 5.19). The result is a very narrow passband created in the canter of the normal stopband of the periodic structure. The Q of the passband is usually very high because the reflectivity of each of the gratings is exploited at the frequency of peak reflection.

By shifting two identical gratings an odd multiple of a quarter wavelength apart the phase of the reflection from one grating is shifted by 180 degrees from the other and thereby in effect, causing a total cancellation of the reflected field at the resonance frequency. Furthermore, by designing the quarter wave resonator to be a quarter wavelength long at the resonant frequency of the periodic gratings the reflection null is produced at the canter of the stopband.

Figs 5.20 and 5.21 shows the effect of various odd multiple of a quarter wavelength long resonators on S_{11} and S_{12} respectively around the stopband region. For the relatively low permittivity of the material used ($\epsilon_1 = 2.57$) and large groove depth (0.2 cm), the Q of the passbands shown in the figures are about 1400.

Log-Periodic grating

The definition of a Log-Periodic transmission line as given by Du Hamel [25] is that the voltage and current at position x and complex frequency f is equal to that at position τx and frequency $\tau^{-1} f$. That is they satisfy the following functional equations,

$$V_n(x, f) = V_{n+1}(\tau x, \tau^{-1} f)$$

$$I_n(x,f) = I_{n+1}(\tau x, \tau^{-1} f)$$

Comparing the above equations with the cascaded network description of a transmission line (Eqn 5.14), the condition for Log-Periodic operation is given as

$$\begin{aligned} A_n &= A_{n+1}(\tau^{-1} f) \\ B_n &= B_{n+1}(\tau^{-1} f) \\ C_n &= C_{n+1}(\tau^{-1} f) \\ D_n &= D_{n+1}(\tau^{-1} f) \end{aligned}$$

Unfortunately, in our present study of open dielectric waveguides, A_n, B_n, C_n and D_n are $N \times N$ complex matrices whose elements depend on the optimised expansion of the guided field by an appropriate set of expanding functions in a complex manner. It is therefore impossible to design a general $2N \times 2N$ transmission matrix that can meet the above requirement exactly. However, we can go some way to meeting the requirements by considering only the 1st order (N=0) solution whereby A,B,C and D are then reduced to a single complex number. This is equivalent to considering only the fundamental mode of each unit cell. It is then quite simple to work out the required electrical length of each unit cell which are related to each other by the factor τ. The values of the parameters for a 20 element Log-Periodic grating (Fig 5.22) is given in Table 5.1. Note that the actual groove depth used is different from $\tau^n d_1$, simply because the relationship between the propagation constant β of the guide and the groove depth is non-linear. The structure is designed to be a wide-band filter, with the resonant frequency of each unit cell different from its adjacent cell by the factor τ. The scattering parameters computed for such a structure is shown in Fig 5.22. Although the stopband achieved is much wider than can be obtained from an ordinary grating, the performance is degraded at the lower frequency end. The effect of a resonant groove for the lower frequencies being much weaker than the effect of a resonant

groove for higher frequencies. Notice that the radiation loss is also greater at the lower frequency end. This is due to the large groove depth at the lower frequency end. From this result we may conclude that a better log-periodic structure with a very wide stopband can be constructed if a value of τ much nearer unity is used enabling more grating elements to be present without reaching large groove depths.

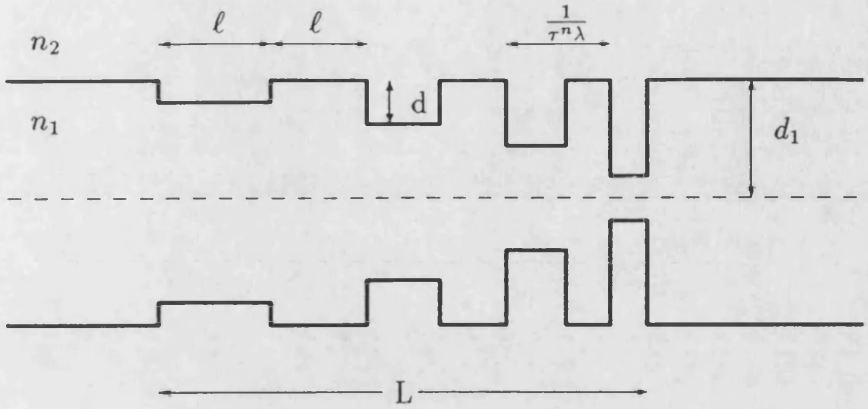

Fig 5.22 Log Periodic grating.

Element number	Resonant Freq (GHz)	Groove Depth d (cm)	Spacing ℓ (cm)	$\tau^n d_1$ (cm)
1	12.00	0.3048	0.4836	0.2333
2	11.74	0.2978	0.4941	0.2276
3	11.49	0.2905	0.5047	0.2217
4	11.25	0.2829	0.5156	0.2157
5	11.02	0.2749	0.5267	0.2096
6	10.78	0.2666	0.5381	0.2033
7	10.56	0.2579	0.5497	0.1970
8	10.33	0.2488	0.5616	0.1904
9	10.11	0.2393	0.5737	0.1837
10	9.90	0.2294	0.5861	0.1769
11	9.69	0.2190	0.5987	0.1699
12	9.49	0.2081	0.6116	0.1628
13	9.29	0.1967	0.6248	0.1555
14	9.09	0.1848	0.6383	0.1481
15	8.90	0.1723	0.6520	0.1405
16	8.71	0.1592	0.6661	0.1327
17	8.53	0.1454	0.6805	0.1248
18	8.35	0.1310	0.6952	0.1167
19	8.17	0.1159	0.7102	0.1085
20	8.00	0.1000	0.7255	0.1000
τ	0.9789			
d_1	1.0 (cm)			
n_1	1.603			
L	22.9 (cm)			

Table 5.1 Design Parameters for a Log-Periodic Grating

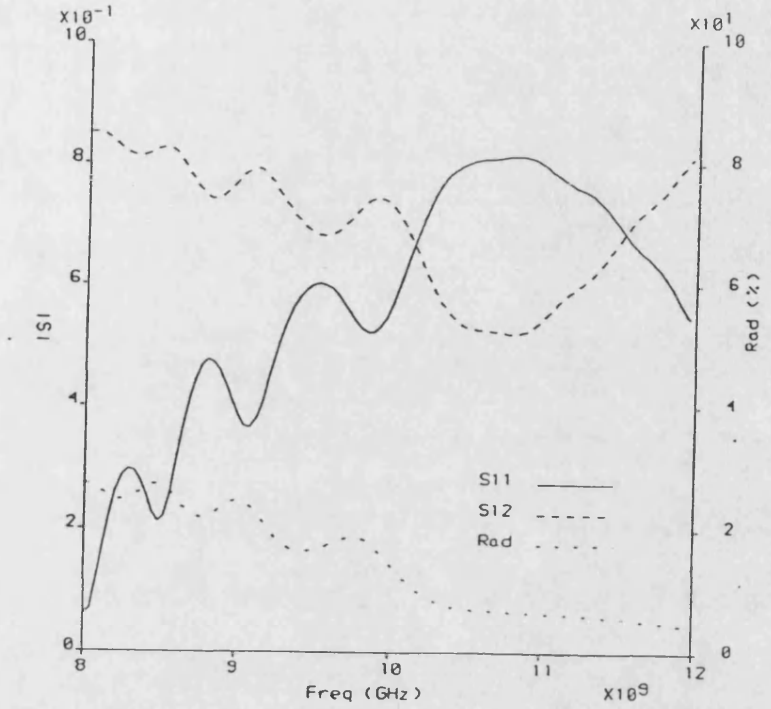

Fig 5.22a Scattering coefficients and radiation loss of a Log-Periodic grating. The structure has 20 elements with groove variation from 0.1cm to 0.305cm with a designed operating stopband of 8.0 to 12.0 GHz.

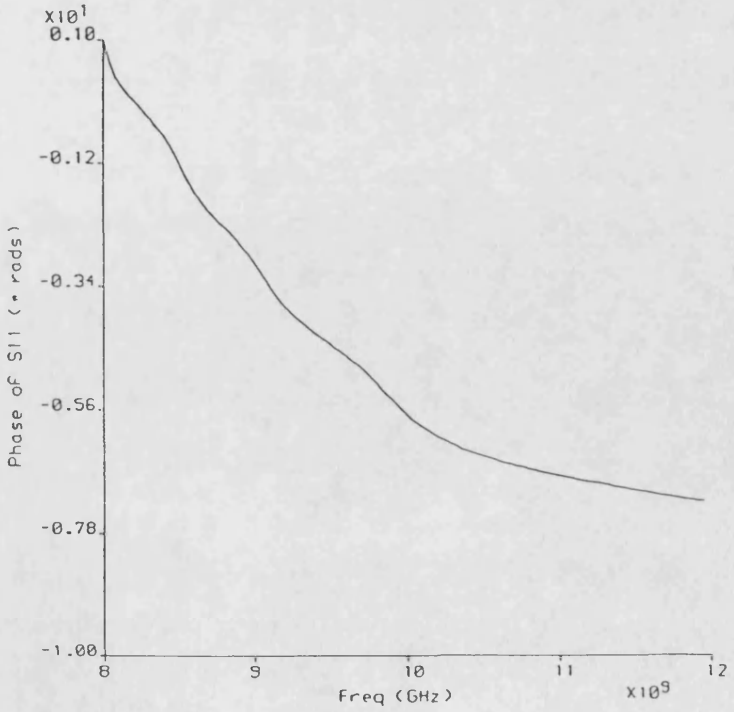

Fig 5.22b Corresponding variation of $\angle S_{11}$ for the Log-Periodic grating.

Blazed grating

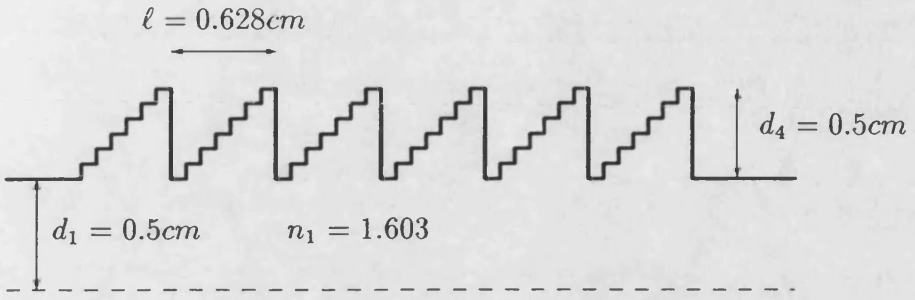

Fig 5.23 Blazed periodic grating approximated using 6 steps.

Periodic gratings with non-square profile can be analysed using the present technique by approximating the non-square grating profile with a succession of small steps. To demonstrate this procedure, a blazed periodic grating is analysed. The blazed grating is approximated with 6 successive steps as shown in Fig 5.23. The scattering parameters for this structure is then calculated by treating the 6 successive steps as one unit cell which is then cascaded twenty times. The structure is thus equivalent to a 20 element blazed grating. The scattering parameters were calculated from 8 GHz to 12 GHz and the results are shown in Fig 5.24. Apart from an expected stopband, the structure is seen to radiate strongly for frequencies above the stopband frequency. Indeed these structures were much studied in the past because they are such good radiators.

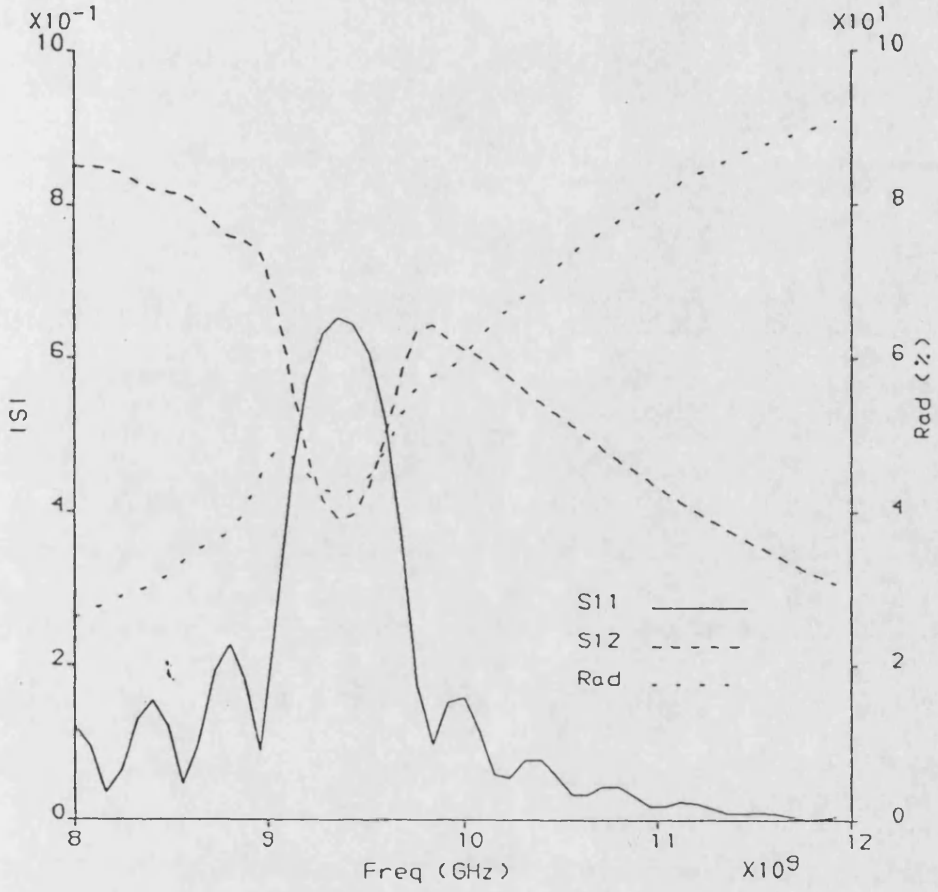

Fig 5.24 Scattering parameters of a 20 element blazed grating approximated using 6 successive steps.

References

[1] T.Itoh,"Applications of gratings in a Dielectric Waveguide for Leaky-wave Antennas and Band-Reject Filters. IEEE Trans Microwave Theory Tech., vol MTT-25 ,pp 1134-1137, Dec 1977.

[2] L.Ogawa,W.S.C.Chang,B.L.Sopori,F.J.Rosenbaum,"A theoretical Analysis of Etched Grating Couplers for Integrated Optics". IEEE Journal of Quantum Electron., vol QE9, pp 29-42, Jan 1973.

[3] F.K.Schewring,S.T.Peng,"Design of Dielectric Grating Antennas for Millimeter-Wave Applications". IEEE Trans Microwave Theory Tech, vol MTT-31, pp 199-208, Feb 1983.

[4] K.L.Klohn,R.E.Horn,H.Jacobs,E.Freibergs,"Silicon Waveguide Frequency Scanning Linear Array Antennas". IEEE Trans Microwave Theory Tech., vol MTT-26, pp 764-773, Oct 1978.

[5] C.Elachi,"Waves in Active and Passive Periodic Structures: A Review. Proc IEEE vol 64, No 12, pp 1666-1698, Dec 1976.

[6] H.Kogelnik,C.V.Shank,"Couple-wave theory of distributed feedback lasers" J. Appl Phys, vol 43, pp 2327-2335, 1972

[7] S.R.Chinn,"Effects of mirror reflectivity in a distributed feedback laser". IEEE J. Quantum Electron., vol QE9, pp 574-580, 1973.

[8] S.Wang,"Principles of distributed feedback and distributed Bragg reflector lasers".IEEE J. Quantum Electron., vol QE-10, pp 413-426, 1974.

[9] W.S.C.Chang,"Periodic Structures and their Applications in Integrated Optics." IEEE Trans. Microwave Theory Tech., vol MTT-21, pp 775-785, 1974

[10] W.Streifer,D.R.Scifres,R.D.Burnham,"Coupled Wave Analysis ofDFB and DBR lasers" IEEE J. Quantum Electron., vol QE-13, pp 134-141, 1977.

[11] T.Tamir,H.L.Bertoni,"Lateral displacement of Optical beams at multilayered and periodic structures.",J. Opt. Soc Amer., vol 61, pp 1397-1413, 1971.

[12] T.Itoh,"Application of gratings in a dielectric waveguide for leaky-wave antennas and band-rejection filters." IEEE Trans. Microwave Theory Tech., vol MTT-25, pp 1134-1138, Dec 1977.

[13] G.L.Matthaei,C.E.Harris,D.C.Park,Y.Kim,"Dielectric waveguide filters using parallel-coupled grating resonators.", Electronics Lett., vol 18, pp 509-510, 1982.

[14] G.L.Matthaei,"A note concerning modes in dielectric waveguide gratings for filter applications." IEEE Trans. Microwave Theory Tech., vol MTT-31, pp 309-312, Mar 1983.

[15] J.N.Polky,J.H.Harris,"Electro-Optic thin film modulators.", Appl. Phys. Lett., vol 21, pp 307-309, 1972.

[16] D.P.Gianrusso,J.H.Harris,"Electro-optic modulation in a thin-film waveguide", Appl. Opt., vol 10, pp 2786-2788, 1971.

[17] T.Itoh,J.Hsu,"Distributed Bragg Reflector Gunn Oscillators for Dielectric Millimeter-Wave Integrated Circuits.", IEEE Trans. Microwave Theory Tech., vol MTT-27, pp 514-518, May 1979.

[18] D.Marcuse,"Exact Theory of TE-wave scattering from Blazed dielectric gratings", Bell Syst. Tech. J., vol 55, pp 1295-1317, 1976.

[19] K.C.Chang,T.Tamir,"Simplified approach to surface-wave scattering by blazed dielectric gratings",Applied Opt. vol 19, pp 282-288, 1980.

[20] A.Katzir,A.C.Livanos,J.B.Shellan,A.Yariv,"Chirped gratings in Integrated Optics". IEEE J. Quantum Electron. vol QE-13, pp 296-304, Apr. 1977.

[21] W.Streifer,R.D.Burnham,D.R.Scifres,"Analysis of Grating-Coupled Radiation in GaAs: GaAlAs Lasers and waveguides - : Blazing Effects. IEEE J. Quantum Electron., vol QE-12, pp 494-499, Aug 1976.

[22] H.Kogelnik,"Filter response of non-uniform Almost-Periodic Structures." Bell. Syst. Tech. J., vol 55, pp 109-126, Jan 1976.

[23] L.Brillouin,"Wave propagation in periodic structures.",Mc Graw Hill, 1946.

[24] E.A.Coddington,N.Levison,"Theory of Ordinary Differential Equations", McGraw Hill, 1955, pp 76-77

[25] R.H.DuHamel,"Log-Periodic Antennas and circuits",in Electromagnetic Theory and Antennas,New York,Pergamon 1963.

[26] C.S.Chang,T.Rozzi,"Rigorous analysis of finite periodic structures in dielectric waveguides", 16th Microwave Conference, Dublin. Sept 1986

[27] L.A.Pipes,S.A.Hovanessian,"Matrix computer methods in engineering" New York,John Wiley & Sons, Inc. 1969

Chapter 6

Conclusion

6.1 Discussion of work done.

In this thesis a rigorous variational technique of general validity was presented for solving step discontinuities in slab waveguides. The basis of this approach is a special adaptation of the *method of moments* which is explained in Chapter 1.

The modal spectrum of open waveguides is discussed in Chapter 2 where a well known mathematical technique for deriving the complete mode spectrum is shown. This approach, based on the consideration of the singularities of the Green's function, delivers the modes in a form which is already normalised. It represents a considerable saving of effort compared to the conventional means of deriving the spectrum by straightforward field matching at each dielectric interface and integrating over the cross-section to determine the normalisation constant. The propagation constant β and the decay constant α (transverse to the slab) of a surface mode are calculated by the above method for a perspex slab guide and the theoretical result show very good agreement with experimental

measurements carried out at X-band.

The problem of a single step discontinuity is rigorously solved in Chapter 3. Here the normalised scattering matrix which completely characterises the single step is formally derived for both TE and TM polarisations. The convergence of the variational solution using different choices of discretization functions is investigated. In particular it is demonstrated that by careful design of the expanding functions which generate the *trial field* for the solution, a good 1^{st} order approximation of the field solution can be obtained. The difficult problem of field singularity at the edges of the dielectric step for the case of TM polarisation is also addressed. In this case we seek to resolve the problem by including the singular behaviour in the trial function itself. This intuitive approach was not only computationally efficient but also give good accuracy for a 1^{st} order solution.

Two basis function sets, namely the Cosine-Laguerre set and the *intermediate mode* hybrid basis function set is shown to give rapid convergence for increasing order of solution. A comparison of the convergence using the different choices of basis functions is given in Table 3.1. Typically, third or fourth significant figure accuracy is achieved with a 5^{th} order solution.

Results are presented for the scattering of incident surface waves for increasing step heights and a comparison of the scattered field coefficients against normalised frequency is made with other published work. It is seen that while guide thickness ratio d_2/d_1 is small the reflection coefficient for a wave incident from either side of the step discontinuity is about the same but start to differ when guide thickness ratio gets more than 2. The case of TE and TM polarisation incident on the step is also investigated. The scattering coefficients are calculated for increasing

frequency until both guides becomes overmoded. The TM polarised field was shown to radiate strongly at the step at low frequencies but not the TE field. At the lower frequencies, the surface modes are poorly guided and because the discontinuous edge of the step effect the TM field more (because only the TM polarisation is singular at the edges), a greater amount of the guided energy will be scattered. These results seem to agree well with those published by Brooke & Kharadly. From this observation it is clear that in the design of radiating structures such as leaky wave antennas, the TM polarised field will give more useful radiation.

The extension of our approach to the case of a double step discontinuity, where the scattered field from both steps interact is given in Chapter 4. The analysis remains rigorous as the field interactions by both the surface modes and the continuous modes are is built into the model. Moreover, by using a circuit network analogy we have shown that it was possible to obtain a normalised scattering matrix formulation for the interacting double steps which is very similar in form to that of the single step. The same basis functions that were used for the analysis of the single step apply equally well for the double steps and convergence of the variational solution is shown to be achieved very quickly. There is, however, one major difference. While we were dealing with an $N \times N$ impedance matrix for the single step, the equivalent impedance matrix for the double step has become a $2N \times 2N$ matrix for an N^{th} order solution. This is not a serious difficulty since an accurate solution is often achieved with N=5; hence matrix sizes generally remain small. The convergence test carried out using the intermediate guide mode set shows that very good approximation is already achieved with just one term of the basis functions (ie. the 1^{st} order solution) provided that both the semi-infinite guide and the region between the double steps are not about to be overmoded.

However, there is disadvantage with this approach which is not so easily resolved. By representing the entire section of the guide between the two steps as an equivalent $2N \times 2N$ network port the modal fields of the region between the double step are no longer accessible. It is therefore not possible to recover the fields in that section. This limitation is not important since there are few situations which require the detailed knowledge of the near fields in that area.

Finally, the method of dealing with interactive double steps is applied to the case of general cascaded steps. As was the usual practice in dealing with cascaded network, the impedance matrix of the double step is transformed to the ABCD matrix of the transmission network form. The cascaded steps may then be represented by the cascade multiplication of the transmission matrices. Once this is solved the impedance matrix is recovered by an inverse transformation and the scattering parameters can then be calculated in a manner similar to that for the double step.

However a straightforward application of the above procedure will lead to numerical difficulties particularly if we need to cascade a large number of steps while employing a high order variational solution. The reason for this is that the eigenvalues of the transmission matrix consist of terms like $e^{\gamma_N \ell}$ and $e^{-\gamma_N \ell}$. These terms represent the forward and backward waves of the field in the periodic structure with a propagation constant of γ. It is a common interpretation as used in coupled modes theory to describe the fields in a periodic structure. In our analysis using a high order solution, we always encounter very large γ for large N. While this may mean that the higher order terms represented waves which are highly attenuated in one direction, there is always an equivalent term which grows with the same magnitude in the other direction. These terms not only make it difficult

to evaluate the eigenvalues, they also frequently cause computation overflow. We have developed a technique whereby the cascaded transmission matrix need not be evaluated numerically. The impedance matrix is recovered from the canonical form of the transmission matrix which can be achieved analytically. This process allows us to cascade structures of unlimited length.

However the strength of the technique lies in its ability to model grating structures of finite length. In addition the structures that can be analysed need not be periodic at all. It was to this end that we seek to demonstrate the method by analysing a High Q Bragg reflection resonator grating and a Log-Periodic grating. The results show the High Q resonator to posses very sharp passbands when operated at the Bragg frequencies of the reflection gratings. This is encouraging results since the reflection gratings consists of only 20 elements. It is worthwhile to note that in optics, the number of gratings used for a typical DBR laser is normally of the order of several thousand. Clearly at microwave frequencies this would mean that a similar structure would be impractically long. We have shown that as long as the modulation depth of the gratings is sufficiently high, a much smaller number of grating elements can be used.

The results obtained for the Log-Periodic grating shows that it too may have promising application. Although multi-octave bandwidth was not demonstrated, the design of the structure was based on crude approximations. (ie. ignoring hider order interactions) While a proper design is not easy, we are confident that a structure with much wider bandwidth can be built. From this initial study it is clear that the large groove depths caused unwanted radiation loss at the low frequency end. This can be avoided by having a structure with the scaling factor τ much closer to unity. This would mean a longer grating with shallower grooves.

We may conclude that with the present theory a large variety of periodic or aperiodic structures may be analysed. The computational work involved is not great although it does involves a certain degree of analytical complexity.

6.2 Future work.

In the development of the theory, the analysis was kept simple by considering only symmetric (in the transverse direction) structures. The extension to asymmetric structures however will not present any difficulties as only the functional form of the field modes need to be changed. The new modal forms can be speedily derived using the method described in Chapter 2. It is acknowledge that many dielectric waveguide structures in microwave are essentially asymmetric in nature since most devices require a metal backing plane. It will therefore be extremely useful to develop programs for asymmetrical guides.

Another area that needs to be addressed is problem of calculating the far field radiation pattern of finite cascaded structures. So far we have only calculated the scattering parameters at either end of a cascade. By that information alone it is not possible to evaluate the far field. However, the present approach had naturally provided the equivalent impedance of the grating structure. Effectively it means that an equivalent semi-infinite guide can be devised with the same impedance as the periodic or aperiodic structure under study and use it as a matched load. By this way a matched load for any point within a periodic structure can be generated. Since it is possible to calculated the total field at the point of the match load, the field within the periodic structure at the boundary of each element may then be found by repeated application of this technique.

The far field can then be calculated as a superposition of all the scattered field at the boundary of each grating element. The assumption here of course is that by attaching a matched load at a particular point the original field at that point have not been disturbed. The effect of using this matched load on a finite grating has already been demonstrated in the results presented in Chapter 5. Essentially it has been shown that by terminating a finite grating structure with a load that has the same characteristic impedance as the periodic grating the effect of the end termination on the periodic structure was removed.

The problem of periodic structures with grating profiles that are non-square requires further study. Although a non-square profile can be approximated by successive steps of matching height, the process is laborious.

Appendix A

Derivation of the surface wave modes.

A close examination of the transcendental equation [Eq.(2.51)]

$$j\,k_{x_1} \;=\; k_{x_2}\tan k_{x_2}d \tag{A.1}$$

will show that a finite number of discrete solutions exist for real k_{x_2} and imaginary k_{x_1}. A graphical solution of this may be found in Collins [8,pp 299]. Let

$$\kappa \;=\; Re\,\{k_{x_2}\} \tag{A.2}$$

and

$$\gamma \;=\; -Im\,\{k_{x_1}\} \tag{A.3}$$

such that from Eq.(2.57), the conservation of wavenumber (for lossless case, $\gamma_z = j\beta$) becomes

$$\beta^2 \;=\; n_1^2k_o^2 \;-\; \kappa^2 \;=\; n_2^2k_o^2 \;+\; \gamma^2 \tag{A.4}$$

Then the surface waves are solutions of the transcendental equation

$$\gamma \;=\; \kappa\tan(\kappa d) \tag{A.5}$$

From Eq.(2.49) one obtains

$$\vec{Y}(x_o) = \frac{1}{j\omega\mu_o}\left[\frac{-\kappa\tan\kappa d + \gamma}{1 + \frac{\gamma}{\kappa}\tan\kappa d}\right] = 0 \quad , \quad \overleftarrow{Y}(x_o) = 0 \qquad (A.6)$$

and $\overleftrightarrow{Y}(x_o) = \overleftarrow{Y}(x_o) + \vec{Y}(x_o) = 0$

Then

$$\frac{\partial}{\partial\lambda_m}\overleftrightarrow{Y}(x_o) \equiv \frac{\partial k_x}{\partial\lambda_m}\frac{\partial\overleftrightarrow{Y}(x_o)}{\partial k_x} \qquad (A.7)$$

$$= \frac{-\frac{1}{\gamma} - d - \tan\kappa d\left[\frac{1}{\kappa} + d\tan\kappa d\right]}{2\left(1 + \frac{\gamma}{\kappa}\tan\kappa d\right)}$$

$$= \frac{-\frac{1}{\gamma} - d - \frac{\gamma}{\kappa}\left[\frac{1}{\kappa} + \frac{d\gamma}{\kappa}\right]}{2\left(1 + \left(\frac{\gamma}{\kappa}\right)^2\right)}$$

$$= -\frac{1}{2}\left(\frac{1}{\gamma} + d\right)$$

Hence the surface modes are given by Eq.(2.64) to be

$$\psi_\nu(x) = A\cos\kappa x \qquad : 0 < x < d \qquad (A.8)$$

$$= A\cos\kappa d\ e^{-\gamma(x-d)} \qquad : d < x < \infty$$

with

$$A = \left(\frac{2}{d + \frac{1}{\gamma}}\right)^{\frac{1}{2}}$$

Appendix B

Derivation of the continuum modes.

The continuum modes owe their existence to the branch cut in the complex $\hat{\lambda}$ plane. As such, they are not solutions of the transcendental equation (A.1). †

Since the branch cut integral [Eq.(2.61b)] is along the real axis of the $\hat{\lambda}$ plane and on the branch where $Im\sqrt{\hat{\lambda}} < 0$, we may set

$$\sigma = Re\{k_{x_2}\} \tag{B.1}$$

$$\rho = Re\{k_{x_1}\}$$

such that $\beta^2 = n_1^2 k_o^2 - \rho^2 = n_2^2 k_o^2 - \sigma^2$.

Similarly, we then have

$$\overleftarrow{Y}(x_o) = 0 \ , \ \overrightarrow{Y}(x_o) = \frac{1}{j\omega\mu_o}\left[\frac{-\sigma \tan \sigma d + j\rho}{1 + \frac{j\rho}{\sigma}\tan \sigma d}\right] \tag{B.2}$$

and from Eq.(2.64), we may write

†Besides the surface wave solutions of Appendix A,there are other solutions. If k_{x_1} and k_{x_2} are allowed to take complex values, there are in fact an infinite number of solutions. These solutions corresponds to the leaky-waves discussed in Section 2.1.

$\underline{0 < x < d}$

$$\int_0^\infty \phi_1(x,\rho)\phi_1(x',\rho)d\rho = -\frac{2}{\pi} Im \int_0^\infty \frac{\rho \overleftarrow{V}(x,x_o,\rho)\overrightarrow{V}(x',x_o,\rho)}{j\omega\mu_o \overleftrightarrow{Y}(x_o)} d\rho \quad \text{(B.3)}$$

$\underline{d < x < \infty}$

$$\int_0^\infty \phi_2(x,\rho)\phi_2(x',\rho)d\rho = -\frac{2}{\pi} Im \int_0^\infty \frac{\rho \overleftarrow{V}(x',x_o,\rho)\overrightarrow{V}(x,x_o,\rho)}{j\omega\mu_o \overleftrightarrow{Y}(x_o)} d\rho \quad \text{(B.4)}$$

The integrand on the R.H.S of Eq.(B.3) and (B.4) when expanded gives

$$R.H.S = Im\left\{\frac{\cos\sigma x_<[\cos\sigma d\, e^{-j\rho(x_< - d)}]}{(j - \frac{\sigma}{\rho}\tan\sigma d)\,/\,(1 + \frac{j\rho}{\sigma}\tan\sigma d)}\right\} \quad \text{(B.5)}$$

$$= Im\left\{\frac{-\cos\sigma x_<[\cos\sigma d e^{-j\rho(x_< - d)}]\,[j + \frac{(\sigma^2 - \rho^2)}{\sigma\rho}\sin\sigma d\cos\sigma d]}{\frac{\sigma^2}{\rho^2}\sin^2\sigma d + \cos^2\sigma d}\right\}$$

$$= Im\left\{\frac{-\cos\sigma x_<\, e^{-j\rho(x_< - d)}(j\cos\sigma d + \frac{\sigma}{\rho}\sin\sigma d)}{1 + \frac{v^2}{\rho^2}\sin^2\sigma d}\right\}$$

$$= \frac{-\cos\sigma x_<[\cos\sigma d\cos\rho(x_< - d) - \frac{\sigma}{\rho}\sin\sigma d\sin\rho(x_< - d)]}{C^2}$$

with

$$v^2 = \sigma^2 - \rho^2 \quad \text{(B.6)}$$

$$C^2 = 1 + \frac{v^2}{\rho^2}\sin^2\sigma d$$

where from Eq.(B3) and (B4) we may deduce

$$\phi_1(x,\rho) = \sqrt{\frac{2}{\pi}}\frac{1}{C}\cos\sigma x \qquad : 0 < x < d \quad \text{(B.7)}$$

$$\phi_2(x,\rho) = \sqrt{\frac{2}{\pi}}\frac{1}{C}\left[\cos\sigma d\cos\rho(x-d) - \frac{\sigma}{\rho}\sin\sigma d\sin\rho(x-d)\right]$$

$$= \sqrt{\frac{2}{\pi}}\cos[\rho(x-d) + \alpha] \qquad : d < x < \infty \qquad \text{(B.8)}$$

where

$$\alpha = \tan^{-1}\left\{\frac{\sigma}{\rho}\tan\sigma d\right\}$$

Appendix C

Design of the dielectric lens

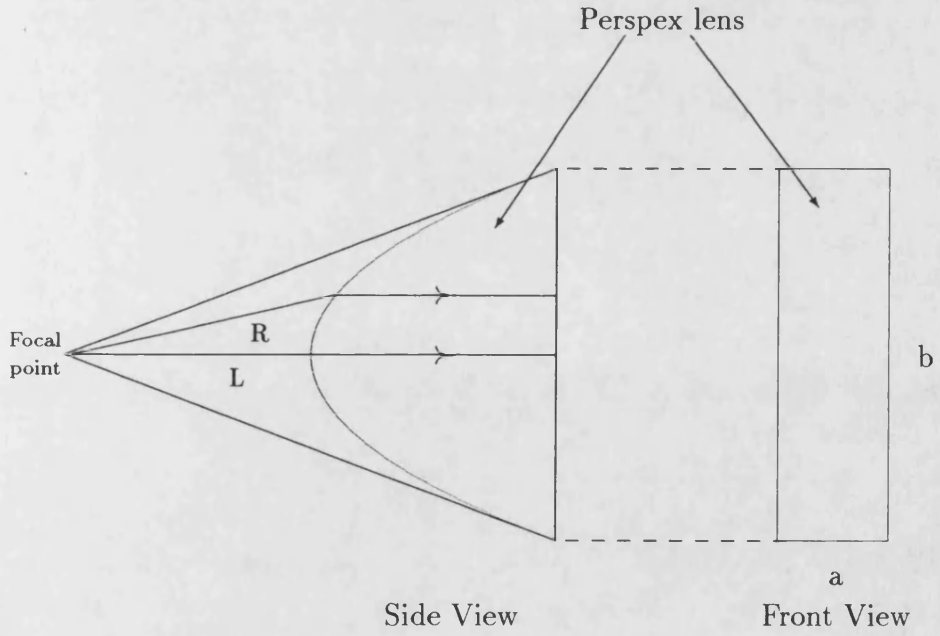

The guide-wavelength inside a rectangular metallic waveguide of cross-sectional dimension a by b meters is given by

$$\lambda_g = \frac{2\pi}{\left(\omega^2\epsilon\mu_o - \left(\frac{n\pi}{a}\right)^2 - \left(\frac{m\pi}{b}\right)^2\right)^{\frac{1}{2}}} \tag{C.1}$$

Therefore the 'effective' refractive index of a dielectric which completely fills a hollow metallic waveguide is

$$n_{eff} = \frac{\lambda_{g_o}}{\lambda_{g_1}} = \left[\frac{\omega^2\mu_o\epsilon_1 - \left(\frac{n\pi}{a}\right)^2 - \left(\frac{m\pi}{b}\right)^2}{\omega^2\mu_o\epsilon_o - \left(\frac{n\pi}{a}\right)^2 - \left(\frac{m\pi}{b}\right)^2}\right]^{\frac{1}{2}} \tag{C.2}$$

From the Principle of Equality of Path Lengths, we require

$$\begin{aligned} R &= n_{eff}(R\cos\theta - L) + L \\ &= \frac{(n_{eff} - 1)L}{n_{eff}\cos\theta - 1} \end{aligned} \tag{C.3}$$

The curve of the lens is a hyperbola.

Appendix D

Coefficients of cosine basis

Surface modes

$$\begin{aligned} Q_m &= \int_0^d \psi(x) C_m(x)\, dx \qquad (D.1) \\ &= \int_0^d a \cos \kappa x \sqrt{\frac{2\eta_m}{d}} \cos \frac{m\pi x}{d}\, dx \\ &= a\sqrt{2d\eta_m}(-1)^m \left[\frac{\kappa d \sin \kappa d}{(\kappa d)^2 - (m\pi)^2}\right] \quad : \kappa d \neq m\pi \end{aligned}$$

For the case when $\kappa d = m\pi$, then we use the form

$$\begin{aligned} Q_m &= a\sqrt{\frac{2\eta_m}{d}} \int_0^d \frac{1}{2}\left[\cos \frac{2m\pi x}{d} + 1\right] dx \\ &= a\sqrt{\frac{d\eta_m}{2}} \quad : \kappa d = m\pi \end{aligned}$$

$$\begin{aligned} \bar{Q}_n &= \int_d^\infty \mathcal{L}_n(x-d)\psi(x)\, dx \qquad (D.2) \\ &= a\sqrt{x_o} \cos \kappa d \left(\gamma x_o - \frac{1}{2}\right)^n \left(\gamma x_o + \frac{1}{2}\right)^{-(n+1)} \end{aligned}$$

Continuous modes

$$P_m = \int_0^d \varphi(x)\, C_m(x)\, dx \qquad \text{(D.3)}$$

$$= \sqrt{\frac{4\eta_m}{\pi d}} \frac{(-1)^m}{C} \left[\frac{\sigma d \sin \sigma d}{(\sigma d)^2 - (m\pi)^2} \right] \quad : \sigma d \neq m\pi$$

$$= \sqrt{\frac{2\eta_m}{\pi d}} \frac{1}{C} \quad : \sigma d = m\pi$$

$$P_n = \sqrt{\frac{1}{2\pi x_o}} (-1)^n \left(\frac{1}{4} + \rho^2 x_o^2 \right)^n \left[e^{j\alpha} \left(\frac{1}{2} - j\rho x_o \right)^{-2n-1} + \right.$$

$$\left. e^{-j\alpha} \left(\frac{1}{2} + j\rho x_o \right)^{-2n-1} \right] \qquad \text{(D.4)}$$

Appendix E

Coefficients of surface modes basis

Surface modes

For the surface modes of the thicker slab guide ($D > d_o$).

$$
\begin{aligned}
Q_{1n} &= a_n \bar{a} \left\{ \frac{1}{2} \left[\frac{\sin(\bar{\kappa} - \kappa_n) d_o}{(\bar{\kappa} - \kappa_n)} + \frac{\sin(\bar{\kappa} + \kappa_n) d_o}{(\bar{\kappa} + \kappa_n)} \right] \right. \\
&+ \frac{\cos \bar{\kappa} d_o}{(\bar{\gamma}^2 + \kappa_n^2)} \left[(\bar{\gamma} \cos \kappa_n d_o - \kappa_n \sin \kappa_n d_o - \right. \\
&\quad \left. e^{-\bar{\gamma}(D - d_o)} (\bar{\gamma} \cos \kappa_n D - \kappa_n \sin \kappa_n D) \right] \\
&+ \left. \frac{\cos \bar{\kappa} d_o \cos \kappa_n D}{\bar{\gamma} + \gamma_n} e^{-\bar{\gamma}(D - d_o)} \right\} \qquad \text{(E.1)}
\end{aligned}
$$

For the case of the thinner slab guide ($d < d_o$) the coefficient of expansion are the same as above except for the following substitutions:

$$
\begin{aligned}
d_o &\longrightarrow d \\
D &\longrightarrow d_o
\end{aligned}
$$

The coefficients for the Laguerre functions are given by

$$Q_{2n} = Q(\bar{\kappa}) - \sum_m Q_{1m}\, Q(\kappa_m) \tag{E.2}$$

with,

$$\begin{aligned} Q(\kappa) = a\sqrt{x_o}\Bigg\{\sum_{k=0}^{n}(-1)^{k+1}\Bigg[e^{-\frac{d'}{2x_o}} L_{n-k}^{k}\left(\frac{d'}{x_o}\right)\times \\ \left(\frac{\cos\left[(k+1)\tan^{-1}2\kappa x_o + \kappa d'\right]}{\left(\frac{1}{4}+\kappa^2 x_o^2\right)^{(k+1)/2} - \frac{\cos\kappa d'}{\left(\frac{1}{2}+\gamma x_o\right)^{k+1}}}\right) \\ - \frac{\cos\left[(k+1)\tan^{-1}2\kappa x_o\right] L_{n-k}^{k}(0)}{\left(\frac{1}{4}+\kappa^2 x_o^2\right)^{(k+1)/2}}\Bigg]\Bigg\} \end{aligned}$$

where d' will take values of d or D depending on whether the coefficients are for the thinner or thicker slab guide respectively.

Continuum modes

For the thicker guide ($D > d_o$),

$$\begin{aligned} P_{1n}(\rho) = \frac{a_n}{C}\sqrt{\frac{2}{\pi}}\Bigg\{\frac{1}{2}\left[\frac{\sin(\kappa_n+\sigma)d_o}{\kappa_n+\sigma} + \frac{\sin(\kappa_n-\sigma)d_o}{\kappa_n-\sigma}\right] + \\ \frac{\cos\kappa_n d}{\gamma_n^2+\sigma^2}\left[(\gamma_n\cos\sigma d_o - \sigma\sin\sigma d_o) - \right. \\ \left. e^{\gamma_n(d_o-D)}(\gamma_n\cos\sigma D - \sigma\sin\sigma D)\right] + \\ \left.\frac{\cos\kappa_o d_o e^{\gamma_n(d_o-D)}}{\gamma_n^2+\rho^2}\left[\gamma_n\cos\sigma D - \sigma\sin\sigma D\right]\right\} \end{aligned} \tag{E.3}$$

For the thinner guide ($d < d_o$),

$$
\begin{aligned}
P_1(\rho) = {} & \frac{a_n}{C}\sqrt{\frac{1}{2\pi}}\left\{\left[\frac{\sin(\kappa_n+\sigma)d_o}{\kappa_n+\sigma} + \frac{\sin(\kappa_n-\sigma)d_o}{\kappa_n-\sigma}\right] + \right. \\
& \frac{1}{\rho^2-\kappa_n^2}\left[\cos\sigma d_o\left((\rho-\kappa_n)\sin[\rho(D-d_o)+\kappa_n D] + \right.\right. \\
& \left.(\rho+\kappa_n)\sin[\rho(D-d_o)-\kappa_n D] + 2\kappa_n \sin\kappa_n d_o\right) - \\
& \frac{\sigma}{\rho}\sin\sigma d_o\left(2\rho\cos\kappa_n d_o - (\rho-\kappa_n)\cos[\rho(D-d_o)+\kappa_n D]\right. \\
- \quad & \left.\left.(\rho+\kappa_n)\cos[\rho(D-d)-\kappa_n D]\right)\right] \\
+ \quad & \frac{2\cos\kappa_n D}{(\gamma^2+\rho^2)}\left(\cos\sigma d_o\left[\gamma_n\cos\rho(D-d_o) - \rho\sin\rho(D-d_o)\right] - \right. \\
& \left.\left.\frac{\sigma}{\rho}\sin\sigma d_o\left[\rho\cos\rho(D-d_o) + \gamma_n\sin\rho(D-d_o)\right]\right)\right\}
\end{aligned}
\tag{E.4}
$$

The coefficients for the Laguerre functions are similarly given as

$$
P_2(\rho) = P(\rho) - \sum_m Q_{1m}\,Q(\kappa_m) \tag{E.5}
$$

with,

$$
\begin{aligned}
P(\rho) = {} & \sqrt{\frac{2x_o}{\pi}}\left\{e^{-\frac{d}{2x_o}}\sum_{k=0}^{n}(-1)^k L_{n-k}^k\left(\frac{d}{x_o}\right)\left(\frac{\cos[(k+1)\tan^{-1}\rho x_o+\alpha]}{\left(\frac{1}{4}+\sigma^2x_o^2\right)^{(k+1)/2}}\right.\right. \\
- \quad & \left.\frac{1}{C}\frac{\cos[(k+1)\tan^{-1}2\sigma x_o+\sigma d]}{\left(\frac{1}{4}+\sigma^2x_o^2\right)^{(k+1)/2}}\right) \\
+ \quad & \left.\frac{1}{C}\sum_{k=0}^{n}(-1)^k L_{n-k}^k(0)\frac{\cos[(k+1)\tan^{-1}2\sigma x_o]}{\left(\frac{1}{4}+\sigma^2x_o^2\right)^{(k+1)/2}}\right\}
\end{aligned}
\tag{E.6}
$$

Appendix F

Evaluation of the ρ integrals of $\hat{Z}_{11}$ and $\hat{Z}_{12}$.

The continuum integrals of Eq(4.7) is re-written here as

$$I_{11} = \frac{1}{2}\int_{-\infty}^{\infty} \frac{1}{C^2} z_o(\rho) \coth(\gamma(\rho)L)\, \bar{\varphi}(x,\rho)\, \bar{\varphi}(x',\rho)\, d\rho \tag{F.1}$$

$$I_{12} = \frac{1}{2}\int_{-\infty}^{\infty} \frac{1}{C^2} z_o(\rho) \operatorname{cosech}(\gamma(\rho)L)\, \bar{\varphi}(x,\rho)\, \bar{\varphi}(x',\rho)\, d\rho$$

where

$$\bar{\varphi}(x,\rho) = \sqrt{\frac{2}{\pi}}\left[\cos\sigma d \cos\rho(x-d) - \frac{\sigma}{\rho}\sin\sigma d \sin\rho(x-d)\right] \tag{F.2}$$

$$z_o(\rho) = \frac{\omega\mu_o}{\sqrt{n_2^2 k_o^2 - \rho^2}}$$

The limits of integration has been changed from $0 \to \infty$ in Eq (4.7) to $-\infty \to \infty$ in Eq (F.1). This is possible because the integrands are even functions of ρ. The change of limits is a necessary step for the *method of residues.*

On examination of the integrands in Eq (F.1), it is clear that poles occur in the $[z_o(\rho) \coth(\gamma(\rho)L)]$ and $[z_o(\rho) \operatorname{cosech}(\gamma(\rho)L)]$ terms and the zeroes of the C^2 term. The cosech and coth terms are very similar as is evident from the series

expansion of cot and cosec

$$\cot z = \frac{1}{z} + 2z\sum_{m=1}^{\infty}\frac{1}{z^2-(m\pi)^2} \tag{F.3}$$

$$\operatorname{cosec} z = \frac{1}{z} + 2z\sum_{m=1}^{\infty}\frac{(-1)^m}{z^2-(m\pi)^2} \tag{F.4}$$

$$\tag{F.5}$$

hence the residues of the cosec term can be easily infered from that of the coth term. For the coth term we have

$$z_o(\rho)\,coth(\gamma L) = \frac{-2j\omega\mu_o}{L}\sum_{m=0}^{\infty}\frac{\varepsilon_m}{[n_2^2k_o^2-\rho^2]-\left(\frac{m\pi}{L}\right)^2} \tag{F.6}$$

$$\text{where} \qquad \varepsilon = \begin{cases} \frac{1}{2} & m = 0 \\ 1 & m \neq 0 \end{cases}$$

Poles occur at

$$\rho = \pm\sqrt{n_2^2k_o^2-\left(\frac{m\pi}{L}\right)^2} = \rho_m \tag{F.7}$$

The residues of the coth term at these poles are then given as

$$\begin{aligned} \text{Res}_{\text{coth}} &= \lim_{\rho\to\rho_m}(\rho-\rho_m)\left(\frac{-2j\omega\mu_o}{L}\right)\sum_{m=0}^{\infty}\frac{\varepsilon_m\,\bar{\varphi}(x,\rho)\,\bar{\varphi}(x',\rho)}{(\rho-\rho_m)(\rho+\rho_m)} \\ &= \frac{-j\omega\mu_o}{L}\sum_{m=0}^{\infty}\frac{\varepsilon_m}{\rho_m}\bar{\varphi}(x,\rho)\,\bar{\varphi}(x',\rho) \end{aligned} \tag{F.8}$$

The residues due to the cosech term is then inferred from Eq (F.8) as

$$\text{Res}_{\text{cosech}} = \frac{-j\omega\mu_o}{L}\sum_{m=0}^{\infty}\frac{(-1)^m\varepsilon_m}{\rho_m}\varphi(x,\rho)\,\varphi(x',\rho) \tag{F.9}$$

The residues due to the zeroes ρ_n of the C^2 term is similarly derived as

$$\begin{aligned} \text{Res}_{c^2} &= \lim_{\rho\to\rho_m}\frac{(\rho-\rho_m)z_o(\rho)\,\coth(\gamma L)\,\bar{\varphi}(x,\rho)\,\bar{\varphi}(x',\rho)}{C^2} \\ &= \left.\frac{\sigma\rho z_o(\rho)\,\coth(\gamma L)\bar{\varphi}(x,\rho)\,\bar{\varphi}(x,\rho)}{2\sigma + v^2d\sin 2\sigma d}\right|_{\rho=\rho_n} \end{aligned} \tag{F.10}$$

The values of ρ_n are found by solving for

$$C^2 = 1 + \frac{v^2}{\rho^2} \sin^2 \sigma d = 0 \qquad \text{(F.11)}$$

or $$\sigma \tan \sigma d = \pm j \rho$$

The above equation is in fact the eigenvalue equation of the electric field in the dielectric slab. An infinite number of solutions will exist since ρ_n is allowed to take complex values. The real values of ρ_n are the transverse propagation constants of the surface wave modes and the complex values are those of the non-propagating leaky waves which will provide an exponentially decreasing contribution to the residue of the integral.

Using the above results, the integrals in Eq (F.1) are reduced to a discrete sum of residues,

$$I_{11} = j\pi \left[\sum_{m=0}^{\infty} \text{Res}_{\text{coth}} + \sum_{m=0}^{\infty} \text{Res}_{c^2} \right] \qquad \text{(F.12)}$$

$$I_{12} = j\pi \left[\sum_{n=0}^{\infty} \text{Res}_{\text{cosech}} + \sum_{n=0}^{\infty} \text{Res}_{c^2} \right]$$

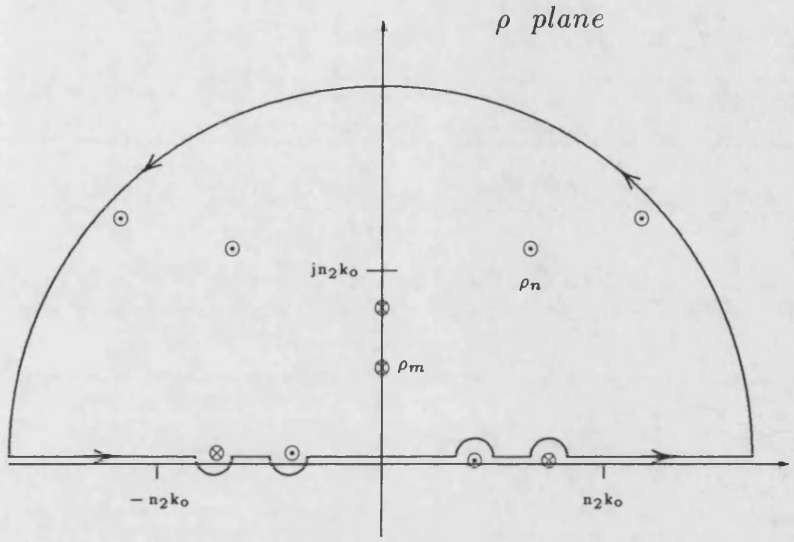

⊙ poles due to $\frac{1}{C^2}\,\bar{\varphi}(x,\rho)\,\bar{\varphi}(x',\rho)$

⊗ poles due to $z_o(\rho)\,\coth(\gamma L)$

Fig 4.10 Integration path around the poles due to various terms in the ρ integrals of Z_{11} and Z_{12}

Appendix G

Derivation of $\mathbf{T}^{-1}$

We want to show that given $\mathbf{T} = \begin{pmatrix} \mathbf{A} & \mathbf{B} \\ \mathbf{C} & \mathbf{A}^t \end{pmatrix}$ then $\mathbf{T}^{-1} = \begin{pmatrix} \mathbf{A} & -\mathbf{B} \\ -\mathbf{C} & \mathbf{A}^t \end{pmatrix}$.

Check,

$$\mathbf{T}\mathbf{T}^{-1} = \begin{pmatrix} \mathbf{AA} - \mathbf{BC} & -\mathbf{AB} + \mathbf{BA}^t \\ \mathbf{CA} - \mathbf{A}^t\mathbf{C} & -\mathbf{CB} + \mathbf{A}^t\mathbf{A}^t \end{pmatrix} \qquad \text{(G.1)}$$

From Eq. (5.6), we have,

$$\begin{aligned} \mathbf{A} &= \mathbf{Z}_{11}\mathbf{Z}_{12}^{-1} \quad , \quad \mathbf{B} = \mathbf{Z}_{11}\mathbf{Z}_{12}^{-1}\mathbf{Z}_{22} - \mathbf{Z}_{12} \\ \mathbf{C} &= \mathbf{Z}_{12}^{-1} \quad , \quad \mathbf{D} = \mathbf{Z}_{12}^{-1}\mathbf{Z}_{22} \end{aligned} \qquad \text{(G.2)}$$

Then,

$$\begin{aligned} \mathbf{AA} - \mathbf{BC} &= \mathbf{Z}_{11}\mathbf{Z}_{12}^{-1}\mathbf{Z}_{11}\mathbf{Z}_{12}^{-1} - \mathbf{Z}_{11}\mathbf{Z}_{12}^{-1}\mathbf{Z}_{22}\mathbf{Z}_{12}^{-1} + I \\ &= \mathbf{I} \end{aligned} \qquad \text{(G.3)}$$

and,

$$\mathbf{A}^t\mathbf{A}^t - \mathbf{CB} = [\mathbf{AA}]^t - \mathbf{CB}$$

$$= [\mathbf{Z}_{12}^{-1}]^t \mathbf{Z}_{11}^t [\mathbf{Z}_{12}^{-1}]^t \mathbf{Z}_{11} - \mathbf{Z}_{12}^{-1} \mathbf{Z}_{11} \mathbf{Z}_{12}^{-1} \mathbf{Z}_{22} + I$$

$$= \mathbf{I} \tag{G.4}$$

since $\mathbf{Z}_{11}$,$\mathbf{Z}_{12}$ and $\mathbf{Z}_{22}$ are all symmetrical. Furthermore,

$$\mathbf{CA} - \mathbf{A}^t\mathbf{C} = \mathbf{Z}_{12}^{-1} \mathbf{Z}_{11} \mathbf{Z}_{12}^{-1} - [\mathbf{Z}_{12}^{-1}]^t \mathbf{Z}_{11}^t \mathbf{Z}_{12}^{-1}$$

$$= 0 \tag{G.5}$$

and,

$$\mathbf{BA}^t - \mathbf{AB} = \mathbf{Z}_{11} \mathbf{Z}_{12}^{-1} \mathbf{Z}_{22} [\mathbf{Z}_{12}^t]^{-1} \mathbf{Z}_{11}^t - \mathbf{Z}_{12} [\mathbf{Z}_{12}^{-1}]^t \mathbf{Z}_{11}$$

$$- \mathbf{Z}_{11} \mathbf{Z}_{12}^{-1} \mathbf{Z}_{11} \mathbf{Z}_{12}^{-1} \mathbf{Z}_{22} + \mathbf{Z}_{11} \mathbf{Z}_{12}^{-1} \mathbf{Z}_{12}$$

$$= 0 \tag{G.6}$$

Appendix H

Derivation of the ABCD matrix

Consider the similarity transform,

$$[\,]\,\mathbf{T}\,[\,]^{-1} = [\,]\,\mathbf{MSM}^{-1}\,[\,]^{-1} = [\,]\,\mathbf{MS}\,[\,]\,\mathbf{M}^{-1} \tag{H.1}$$

where,

$$[\,] = \begin{pmatrix} \mathbf{I}_{m_1}^{-1} & 0 \\ 0 & \mathbf{I}_{m_1}^{-1} \end{pmatrix} \tag{H.2}$$

Then,

$$[\,]\mathbf{M} = \begin{pmatrix} \mathbf{I}_{m_1}^{-1} & 0 \\ 0 & \mathbf{I}_{m_1}^{-1} \end{pmatrix} \begin{pmatrix} \mathbf{V}_{m_1} & \mathbf{V}_{m_1} \\ \mathbf{I}_{m_1} & -\mathbf{I}_{m_1} \end{pmatrix} \tag{H.3}$$

$$= \begin{pmatrix} \mathbf{I}_{m_1}^{-1}\mathbf{V}_{m_1} & \mathbf{I}_{m_1}^{-1}\mathbf{V}_{m_1} \\ 1 & -1 \end{pmatrix} \tag{H.4}$$

and,

$$[\,]\mathbf{M}^{-1} = \frac{1}{2}\begin{pmatrix} [\mathbf{I}_{m_1}^{-1}\mathbf{V}_{m_1}]^{-1} & 1 \\ [\mathbf{I}_{m_1}^{-1}\mathbf{V}_{m_1}]^{-1} & -1 \end{pmatrix} \tag{H.5}$$

Hence,

$$\frac{1}{2}[\,](\mathbf{T} + \mathbf{T}^{-1})[\,] = [\,]\begin{pmatrix} \mathbf{A} & 0 \\ 0 & \mathbf{A}^t \end{pmatrix}[\,]^{-1} \tag{H.6}$$

$$= [\,]\mathbf{M}\begin{pmatrix} \text{diag}\,[\cosh\ \gamma\ell] & 0 \\ 0 & \text{diag}\,[\cosh\ \gamma\ell] \end{pmatrix}[\,]\mathbf{M}^{-1} \tag{H.7}$$

The R.H.S of Eq (H.6) then gives,

$$\begin{pmatrix} \mathbf{I}_{m_1}^{-1}\mathbf{A}\mathbf{I}_{m_1} & 0 \\ 0 & \mathbf{I}_{m_1}^{-1}\mathbf{A}^t\mathbf{I}_{m_1} \end{pmatrix} = \tag{H.8}$$

$$\begin{pmatrix} \mathbf{I}_{m_1}^{-1}\mathbf{V}_{m_1}\text{diag}\,[\cosh\ \gamma\ell][\mathbf{I}_{m_1}^{-1}\mathbf{V}_{m_1}]^{-1} & 0 \\ 0 & \text{diag}\,[\cosh\ \gamma\ell] \end{pmatrix} \tag{H.9}$$

This implies,

$$\mathbf{I}_{m_1}^{-1}\mathbf{A}\mathbf{I}_{m_1} = \mathbf{I}_{m_1}^{-1}\mathbf{V}_{m_1}\text{diag}\,[\cosh\ \gamma\ell]\ \mathbf{V}_{m_1}^{-1}\mathbf{I}_{m_1} \tag{H.10}$$

$$\mathbf{A} = \mathbf{V}_{m_1}\text{diag}\,[\cosh\ \gamma\ell]\mathbf{V}_{m_1}^{-1} \tag{H.11}$$

Similarly,

$$\frac{1}{2}[\,](\mathbf{T} - \mathbf{T}^{-1})[\,] = [\,]\begin{pmatrix} 0 & \mathbf{B} \\ \mathbf{C} & 0 \end{pmatrix}[\,]^{-1} \tag{H.12}$$

$$= [\,]\mathbf{M}\begin{pmatrix} \text{diag}\,[\sinh\ \gamma\ell] & 0 \\ 0 & \text{diag}\,[\sinh\ \gamma\ell] \end{pmatrix}[\,]\mathbf{M}^{-1} \tag{H.13}$$

Again on expanding and equating the expressions on the R.H.S of Eq (H.12), we have

$$\begin{pmatrix} 0 & \mathbf{I}_{m_1}^{-1}\mathbf{B}\mathbf{I}_{m_1} \\ \mathbf{I}_{m_1}^{-1}\mathbf{C}\mathbf{I}_{m_1} & 0 \end{pmatrix} = \tag{H.14}$$

$$\begin{pmatrix} 0 & \mathbf{I}_{m_1}^{-1}\mathbf{V}_{m_1}\text{diag}\,[\sinh\ \gamma\ell] \\ \text{diag}\,[\sinh\ \gamma\ell][\mathbf{I}_{m_1}^{-1}\mathbf{V}_{m_1}]^{-1} & 0 \end{pmatrix} \tag{H.15}$$

which gives,

$$\mathbf{I}_{m_1}^{-1}\mathbf{B}\mathbf{I}_{m_1} = \mathbf{I}_{m_1}^{-1}\mathbf{V}_{m_1}\text{diag}\,[\sinh\ \gamma\ell] \tag{H.16}$$

$$\text{or} \qquad \mathbf{B} = \mathbf{V}_{m_1}\text{diag}\,[\sinh\ \gamma\ell]\ \mathbf{I}_{m_1}^{-1} \tag{H.17}$$

and

$$\mathbf{I}_{m_1}^{-1}\mathbf{C}\mathbf{I}_{m_1} = \text{diag}\,[\sinh\ \gamma\ell]\ \mathbf{V}_{m_1}^{-1}\mathbf{I}_{m_1} \tag{H.18}$$

$$\text{or} \qquad \mathbf{C} = \mathbf{I}_{m_1}\text{diag}\,[\sinh\ \gamma\ell]\ \mathbf{V}_{m_1} \tag{H.19}$$

Appendix I

The determinant of the Matrix Exponential Function.

Let us assume that the matrix **A** has n distinct eigenvalues $\lambda_1, \lambda_2, ...\lambda_n$. Then by Frobeniuis's Theorem, we know that the eigenvalues of $e^{\mathbf{A}z}$ are $e^{\lambda_1 z}.....e^{\lambda_n z}$. We also know that the determinant of a matrix is equal to the product of its eigenvalues. Therefore,

$$\begin{aligned} \det\,[e^{\mathbf{A}z}] &= e^{\lambda_1 z}e^{\lambda_2 z}.....e^{\lambda_n z} \\ &= e^{(\lambda_1 + \lambda_2 + ...\lambda_n)z} \end{aligned} \tag{I.1}$$

However, the sum of the eigenvalues of a matrix is equal to the trace of the matrix, so

$$(\lambda_1 + \lambda_2 + ... + \lambda_n) = \text{trace } \mathbf{A} \tag{I.2}$$

Substituting (I.2) into (I.1), gives the result

$$\det\,[e^{\mathbf{A}z}] = e^{(\text{trace } \mathbf{A})\,z} \tag{I.3}$$

and if **A** is the 2×2 matrix

$$\begin{pmatrix} a & b \\ c & d \end{pmatrix} \tag{I.4}$$

then,

$$\text{trace } \mathbf{A} = a + d$$

$$\text{so that} \quad \det[e^{\mathbf{A}z}] = e^{(a+d)z} \tag{I.5}$$

It is clear then that for the determinant to be unity, we require,

$$a + d = 0 \tag{I.6}$$